Chapter 3
Application of Mössbauer Spectroscopy in Earth Sciences

Robert E. Vandenberghe and Eddy De Grave

Abstract Iron being the fourth most abundant element in the earth crust, ^{57}Fe Mössbauer spectroscopy has become a suitable additional technique for the characterization of all kind of soil materials and minerals. However, for that purpose a good knowledge of the spectral behavior of the various minerals is indispensable. In this chapter a review of the most important soil materials and rock-forming minerals is presented. It starts with a description of the Mössbauer spectroscopic features of the iron oxides and hydroxides, which are essentially present in soils and sediments. Further, the Mössbauer spectra from sulfides, sulfates and carbonates are briefly considered. Finally, the Mössbauer features of the typical and most common silicate and phosphate minerals are reported. The chapter ends with some typical examples, illustrating the use and power of Mössbauer spectroscopy in the characterization of minerals.

3.1 Introduction

The discovery of the resonant absorption of gamma-rays in ^{191}Ir by Rudolf Mössbauer in 1958 was a milestone in nuclear physics because it was formerly assumed that such a phenomenon could never occur due to the large recoil energies involved. The interest for this new finding was nevertheless still limited in the first years, but, a real breakthrough emerged from the fact that many isotopes showed a larger and much more sensitive effect. So, a new technique, called Mössbauer spectroscopy, was born. The most important feature of this spectroscopic method is the extreme sharpness of the emission line which can easily be

R. E. Vandenberghe (✉) · E. De Grave
Department of Physics and Astronomy, Ghent University,
Proeftuinstraat 86, 9000 Ghent, Belgium

Y. Yoshida and G. Langouche (eds.), *Mössbauer Spectroscopy*,
DOI: 10.1007/978-3-642-32220-4_3,

varied in energy by giving the source velocities of the order of cm/s. This enables to study the different hyperfine interactions related to the electronic shells of the Mössbauer active atoms in solids which, in a further stage, yield valuable information about structural and magnetic properties of materials. Up to now, the Mössbauer effect has been observed for nearly 100 nuclear transitions in about 80 isotopes, distributed over 43 elements. Of course, as with many other spectroscopic methods, not all of these transitions are suitable for practical studies and about twenty elements remain for applications. However, it is a gift of nature that the resonant absorption effect is easily achieved in the iron-57 isotope which has an abundance of 2.14 % in natural iron. Considering the importance of the element iron in many branches of science and technology, it is obvious that since 1960, this new spectroscopic technique has proven to be very useful in the study of all kinds of iron-bearing materials. In particular, the abundance of iron in the earth's crust (4th element in wt %) renders this kind of spectroscopy extremely suitable for the characterization of soil materials and minerals. Moreover, a major advantage of Mössbauer spectroscopy is the fact that it probes the influences on the iron nucleus locally. This means that, through the determination of the hyperfine parameters, not only the different iron-bearing components in a sample can be distinguished, but also the different "types" of iron present in a mineral can be detected. This leads to a variety of applications in geology and soil sciences such as the qualitative and quantitative analysis with respect to the various mineralogical compounds and the determination of the oxidation state and coordination of iron in minerals.

From experimental point of view, the equipment for Mössbauer spectroscopy (MS) is nowadays relatively simple and not expensive. Especially, since the data collection can be achieved by a compact electronic unit connected to a PC, the latter not necessarily being of high performance, a complete Mössbauer set-up with low-temperature facilities is cheaper than say, an X-ray diffraction apparatus. However, most of solid-state laboratories or particularly geological institutes in the present case, do not possess Mössbauer spectrometers in their standard equipment. This is often due to the severe rules which are enforced with radioactive source acquisition and handling. Moreover, the relatively serious recurrent cost of sources, having a half-life time of 270 days in the case of ^{57}Fe demands a permanent operation of the spectrometer, which is not evident in case of limited need. Even though the application for the characterization of soils and minerals does not require a deep fundamental physical knowledge, MS is for all the aforementioned reasons not so popular as a standard technique in the community of geologists and soil scientists as it should be. Therefore, a sound and permanent cooperation between Mössbauer laboratories and institutes related to earth sciences is necessary and should still further be promoted.

Another feature that lowers to some extent the general popularity of MS in comparison with other techniques is related to the spectral analysis. Mössbauer spectroscopy is not a so-called push-button technique, yielding directly consistent results after each measurement. As in many techniques, the spectra need to be refined using home-made or commercial computer programs. But, the analyzing

procedure is not always straightforward leading often after trial and error to uncertain results. This is particularly true for complex spectra of minerals and soil materials exhibiting in many cases strongly overlapping absorption lines or showing distributed hyperfine interactions. It is therefore imperative that the Mössbauer spectroscopist uses the appropriate fitting procedures, has a good insight in the various spectra that can occur, and relies if necessary on the results of complementary techniques. This tutorial aims to introduce the reader into those various aspects of the application of MS in earth sciences. Together with a description of the spectral behavior expected for the most relevant minerals, a number of examples shall be given, which illustrates the analytical power of MS.

3.2 Mössbauer Spectroscopy Applied to Earth Sciences

As already mentioned in the introduction, MS leads to applications in earth sciences and particularly in mineralogy, which are very important with respect to qualitative and quantitative analysis of the samples and the determination of the oxidation state and coordination of iron in the involved minerals. Moreover, this technique additionally provides in some cases a crude insight in the morphological and chemical features of the minerals.

3.2.1 Qualitative and Quantitative Analyzing Power of MS

For qualitative analyses of rocks, soils, sediments, ores, etc., MS consists of the recognition of typical "fingerprint" spectra of the various iron-bearing species present in the sample. The standard fingerprint spectra are usually obtained from pure natural or synthetic samples. The appearance of the typical spectra, defined by their specific hyperfine parameters, enables in many cases to assign immediately the unknown components in the sample. The doublet spectra of non-magnetic (paramagnetic or superparamagnetic) materials are defined by two hyperfine parameters, i.e. the isomer shift δ_{Fe} and the quadrupole splitting Δ. The sextet spectra of magnetically ordered materials are defined by three hyperfine parameters, i.e. the isomer shift δ_{Fe}, the quadrupole shift 2ε and the magnetic hyperfine field B. Such spectra are particularly obtained in the case of oxides at RT and of (oxy)hydroxides at lower temperatures. The hyperfine field is then a welcome extra parameter for qualitative phase characterization. The magnetic transition temperature at which the sextet is expected to change into doublet is often also of prominent value.

However, one may not overestimate the direct qualitative analyzing power of Mössbauer spectroscopy. Indeed, many situations occur in which the spectra do not give such a decisive qualitative information. This is particularly true in the cases where merely paramagnetic doublet spectra are obtained. For instance, many

minerals have Fe^{3+} in octahedral environment which all yield similar doublets with a quadrupole splitting in the range 0.4–0.8 mm/s and therefore they cannot be unambiguously identified. Moreover, the hyperfine parameters can slightly be altered by morphological and chemical influences or may show a distributive behavior, which prevents a clear-cut assignment of the spectral components. As will be shown further, many minerals with poor crystallinity or small-particle morphology exhibit a range of hyperfine field values and the sextet spectra often consist of asymmetrically broadened absorption lines. For all those cases it is obvious that a more elaborated Mössbauer analysis combined with results of other techniques are necessary.

Quantitative information is obtained from the spectra through the relative area of each subspectrum. This area is essentially proportional to the concentration of each kind of iron with its valence in a specific environment. So, the distribution of various types of iron among different sites in a mineral or the concentration of different iron-bearing compounds in a multi-phase assemblage can in principle be determined.

The area ratio A_A/A_B of the spectra of two Fe species A and B is given by

$$\frac{A_A}{A_B} = \frac{\Gamma_A R(T_A) T_A}{\Gamma_B R(T_B) T_B} \tag{3.1}$$

where Γ is the width at half maximum of the absorption peaks and R(T) is a thickness reduction function due to saturation effects which depends on the absorber thickness T. The absorber thickness is not a real physical thickness, but a scalar defined by $T = nf\sigma_0$, where n is the number of Mössbauer active atoms per cm^2 in the absorber, f the Mössbauer fraction (recoilless fraction) and σ_0 the cross section at resonance equal to 2.35×10^{-18} cm^2 for ^{57}Fe. If we set $\Gamma_A = \Gamma_B$ and in a first approximation $R(T_A) = R(T_B)$ the ratio N_A/N_B of the amount of iron atoms of both types A an B can then be calculated from

$$\frac{N_A}{N_B} = \frac{n_A}{n_B} = \frac{f_B}{f_A}\frac{A_A}{A_B} \tag{3.2}$$

The Mössbauer fraction f of each kind of iron species is mainly governed by the lattice dynamics in the crystal. Therefore, f is dependent on the coordination and can differ slightly from mineral to mineral. Moreover, the Mössbauer fraction is particularly very sensitive to the valence state of iron and is for Fe^{2+} considerably lower than for Fe^{3+}. Because of the relationship with lattice vibrations, f is also strongly temperature dependent. This means that at RT a large difference in f values is observed and only to a lesser extent at 80 K. The f values for some iron-containing minerals, determined from the temperature dependence of the isomer shift (second order Doppler shift), are listed in Table 3.1.

So far, we did not take into account any thickness effects. The aforementioned formulas are only valid in the case of small thicknesses, because only in that case the transmission integral function, which mathematically describes the spectrum, can be replaced by a sum of Lorentzian lines. The latter profile can be considered

Table 3.1 Mössbauer fractions f at RT and 80 K for some minerals (after Ref. [3])

Mineral	Coord.	f_{RT}	f_{80}	Val.	Coord.		
Oxides and hydroxides							
Hematite	α-Fe_2O_3	Natural[a]		3+	O_6	0.837–0.851	0.923–0.928
		Synthetic[b]		3+	O_6	0.811–0.860	0.914–0.960
Magnetite	Fe_3O_4			3+	O_4	0.889	0.941
2.5+	O_6	~0.80	–				
Maghemite	γ-Fe_2O_3			3+	$(O_4,O_6)_{av}$	0.814	0.915
Goethite[c]	α-FeOOH			3+	$(O,OH)_6$	0.804	0.912
Akaganeite	β-FeOOH			3+	$O_2(OH)_4$	0.877	0.937
	$O_3(OH)_3$	0.835	0.922				
Lepidocrocite	γ-FeOOH			3+	$(O,OH)_6$	0.793	0.908
Ilmenite	$FeTiO_3$			2+	O_6	0.650	0.856
Spinel	$Mg_{0.9}Fe_{0.1}AlO_4$			2+	O_4	0.697	0.875
Silicates							
Ferridiopside	$Ca_{1.03}Mg_{0.77}Fe_{0.20}Si_{1.96}O_6$			3+	O_6(M1)	0.899	0.945
				3+	O_4(Te)	0.862	0.932
				2+	O_6 (M1)	0.747	0.893
Diopside	$Ca_{0.89}Mg_{0.81}Fe_{0.04}Si_{2.12}O_6$			3+	O_6(M1)	0.862	0.932
				2+	O_6 (M1)	0.708	0.879
Hedenbergite	$Ca_{1.00}Mg_{0.15}Mn_{0.3}Fe_{0.76}Al_{0.03}Si_{2.00}O_6$			2+	O_6 (M1)	0.700	0.876

(continued)

Table 3.1 (continue)

Mineral Val.	Coord.	f_{RT}	f_{80}				
Aegerine	$Na_{1.02}Ca_{0.06}Mg_{0.04}Fe_{0.97-}$ $Al_{0.06}Ti_{0.06}Si_{1.84}O_6$			3+	O_6 (M1)	0.874	0.936
Enstatite	$Mg_{1.65}Fe_{0.27}Al_{0.05}Si_{2.02}O_6$			2+	O_6(M2)	0.675	0.882
				2+	O_6 (M1)	0.773	0.902
Olivine[d]	$(Mg,Fe)_2SiO_4$			2+	O_6	0.744	0.893
Some others							
Ankerite	$CaFe_{0.5}Mg_{0.5}(CO_3)_2$			2+	O_6	0.711	0.822
Siderite	$FeCO_3$			2+	O_6	0.743	0.891

[a] Range for 3 samples, [b] Range for 10 samples, [c] Well crystallized [d] Unknown composition

to be reasonably valid up to $T = 2$. Taking $f = 0.8$ and knowing that natural iron contains 2.14 % ^{57}Fe, this thickness corresponds to a n value of 4.6 mg/cm^2 Fe. This value can be a guide for absorber preparation for a single-line spectrum. For a doublet spectrum the area is divided over two lines and this value may be doubled ($\approx$10 mg/cm^2) and for a sextet spectrum with (3:2:1:1:2:3)/12 it may be increased fourfold ($\approx$20 mg/cm^2) if we consider the outer lines. It is worth to remark that the ideal n value for absorber preparation, based on γ-ray absorption [1] or determined from thickness considerations by Rancourt et al. [2] is similar and leads to 5–10 mg/cm^2 of Fe as a rule of thumb.

However, in the case of a thin absorber without appreciable thickness effects, there is still a deviation from the true ratio N_A/N_B which comes from the thickness reduction R(T). This function was called "saturation" function by Bancroft [3], although the original saturation function L(T) was defined by Lang [4]. The latter was the reduced thickness itself, and hence L(T) = R(T)T. Therefore, in our concept, the reduction function R(T) tends to unity when the thickness is zero, but decreases steeply with increasing thickness. If the amount of the different iron species is similar, thus leading to similar thicknesses, the values of the R(T) function are nearly equal and will therefore not lead to a significant error in the value of N_A/N_B. However, if one of the subspectra has a small area relative to the other, the R(T) value for the large area and thus with large thickness will deviate more from unity than the one for the small area. Consequently this leads to a substantial error in the determination of the relative amount of iron. From a thorough numerical analysis based on simulated spectra, Rancourt [5] has calculated the overestimation of the area of a minority line as a function of the area fraction which he represents in a graph for different thicknesses. To give an idea of his results, the true ratio $N_A/N_B = 0.2$ with a nominal thickness $T = 1$ will result in an observed area ratio of about $A_A/A_B = 0.22$ (10 % overestimation) and $N_A/N_B = 0.1$ will result in $A_A/A_B = 0.116$ (16 % overestimation). Using these data it is possible to correct for these effects.

In conclusion, MS has a great potential for determining the relative amount of each kind of iron with its specific valence and with its specific environment if one takes the aforementioned considerations into account. The relative amount of each Fe-bearing mineral in multi-phase assemblages can be similarly calculated from the relative areas. However, the main drawback resides in the analysis of the spectra having strongly overlapping lines in most cases. It is therefore indispensable that an appropriate fitting procedure is used providing the most adequate description of the spectrum. Such a procedure demands often information from other techniques and from Mössbauer measurements at different temperatures or even in applied magnetic fields.

3.2.2 Determination of the Oxidation State and Coordination of Iron

The determination of the valence states of iron in minerals is of extreme importance in geology. In contrast to most of the other abundant elements, iron has in its high-spin state predominantly two valence states which can easily transform from one into another through oxidation or reduction. In this way the valence state may be indicative for the geological history of the minerals (weathering, pressure and temperature changes, …) and even the color can be associated to the valence states or to transitions between them. For the determination of the oxidation states of iron, MS is commonly used because most techniques are not able to distinguish between Fe^{2+} and Fe^{3+}, and chemical analyses often result in unreliable results due to oxidizing or reducing side effects. Among the hyperfine parameters, the isomer shift is very sensitive to the valence and enables to discern readily the various valence states of iron in minerals. Fe^{3+} usually shows a relatively small isomer shift δ_{Fe} in the range 0.3–0.6 mm/s whereas Fe^{2+} covers the range 0.7–1.2 mm/s (Fig. 3.1).

The quadrupole splitting, on the other hand, is generally large for divalent iron, but depends also strongly on the coordination (Fig. 3.2). So, the combination of both the isomer shift and quadrupole splitting values can give some idea about the coordination of iron. Moreover, Δ in the case of Fe^{3+} is merely determined by the lattice contribution, and therefore the quadrupole splitting is also a good measure for the local distortions in the lattice.

An important application in that respect is distinguishing cis and trans configurations of an octahedral $O_4(OH)_2$ (or $(OH)_4O_2$) Fe^{3+} coordination, which quite often occurs in mineralogical systems (Fig. 3.3). Simple point-charge calculations show that the quadrupole splitting should follow the relation $\Delta_{trans} = 2\Delta_{cis}$.

Although the ratio is in practice never exactly 2, due to other effects such as the influences of more distant charges, the measurement of the quadrupole splitting enables the direct determination of those two types of isomers. In the case of Fe^{2+}, the lattice contribution to the electric field gradient is usually opposite to the large valence contribution of the iron cation itself yielding $\Delta_{trans} < \Delta_{cis}$.

In the case of magnetic spectra, the magnetic hyperfine field B is generally also a direct indication of the oxidation state in addition to the isomer shift. Far below the magnetic transition temperature the hyperfine field of Fe^{3+} amounts to 45–55 T

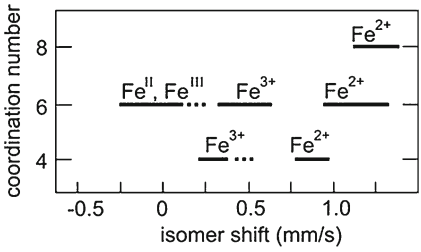

Fig. 3.1 Isomer shift (δ_{Fe}) values at RT versus coordination number for *low-spin* (II, III) and *high-spin* (2+, 3+) Fe in compounds and minerals

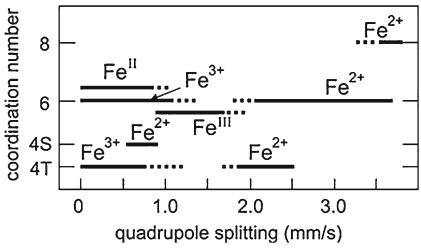

Fig. 3.2 Quadrupole splitting (Δ) values at RT versus coordination number for *low-spin* (II, III) and *high-spin* (2+, 3+) Fe in compounds and minerals

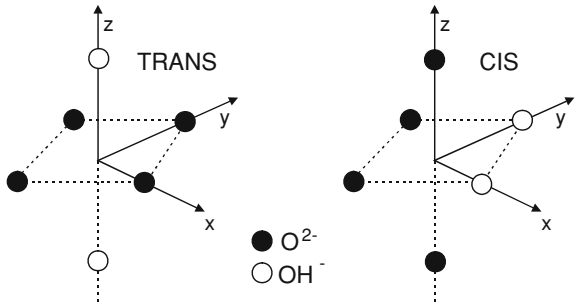

Fig. 3.3 *Trans* and *cis* configuration of a $O_4(OH)_2$ octahedron

whereas it is usually much lower than 40 T for Fe^{2+} due to the reducing effect of the orbital contribution in B which is generally more pronounced for Fe^{2+} than for Fe^{3+}. However, the Fe^{2+} magnetic spectra are often very complex due to the perturbation of a relatively strong quadrupole interaction and/or to structural and magnetic disorder effects.

3.2.3 Morphological Effects and Isomorphous Substitution

In soils, iron oxides and oxyhydroxides are commonly poorly crystallized and as such occurring as agglomerates of ultra fine particles. In various techniques, such a behavior becomes a perturbing factor in the characterization of iron minerals. In X-ray diffraction, for instance, the line width of the reflections may increase considerably, often inhibiting a clear-cut assignment and also hindering an accurate determination of the other well-crystallized components. In MS the poor crystallinity is mainly reflected by a superparamagnetic behavior, which results in a magnetic transition (sextet-doublet transition), that occurs at much lower temperatures than in the well-crystallized material. However, at very low temperatures the small-particle system still reproduces to a large extent the hyperfine parameter values of the bulk compound so that from the point of view of qualitative analysis the compound can still be relatively well determined. The superparamagnetic fluctuations of the particles' magnetic moments are described by a relaxation time given by

$$\tau = \tau_0 \exp(KV/kT) \tag{3.3}$$

where KV is the energy barrier that has to be bridged in order to change the direction of the magnetization, with K the effective anisotropy energy density, V the particle volume and kT is the thermal energy (k Boltzmann's constant). The factor τ_0 is of the order 10^{-9} s and is slightly dependent on the magnetization and the anisotropy. From this relaxation formula, and taking τ to be equal to the Larmor precession time τ_L of the nuclear spin in a local magnetic field, which is approximately 10^{-8} s, the magnetic transition temperature, which is called 'blocking temperature' in this case, can in principle be related to the particle size. However, due to all kinds of uncertainties, in particular regarding the value of the anisotropy constant K, it remains difficult to determine this size quantity accurately from the spectra. Nevertheless, the general spectral behavior observed at a few different temperatures (e.g. room temperature and 80 K) may already be fairly indicative for the degree of crystallinity of the compound. Moreover, the values of the hyperfine parameters, in particular the magnetic hyperfine field, may give similar information as well.

Another important feature of minerals is the isomorphous substitution for iron by another element such as aluminum, calcium, silicon, etc. Such a substitution may alter the hyperfine parameters to some extent and relationships can then be established enabling an estimate of the degree of substitution from the hyperfine parameters. Unfortunately, it often happens that both morphological effects and substitution concurrently give rise to similar changes in the spectrum, thus leading to ambiguous conclusions. In the next sections the possibilities of the morphological characterization by the Mössbauer effect will be discussed for some particular minerals.

3.3 Characterization of Iron Oxides and Hydroxides

Iron oxides and hydroxides are the most important iron-bearing constituents of soils, sediments and clays. To characterize the samples, i.e. the identification of the different minerals present and the determination of their morphology and chemical composition, a variety of standard techniques are commonly used such as X-ray and electron diffraction, chemical analyses, optical and electron microscopy, infrared spectroscopy and thermal analysis (DTA, DTC,…). Most of these techniques are further applied in conjunction with selective dissolution or other separation methods in order to obtain more specific information about particular components in the complex soil system. In addition to all those characterization methods, MS has proven to be a valuable complementary technique for the study of these kinds of materials and in particular for the characterization of iron oxides and hydroxides which are usually poorly crystallized.

Most oxides and hydroxides in soils are indeed known to be less well or rather poorly crystallized. This feature results in the first place in a lowering of the magnetic transition temperature yielding a doublet at temperatures were normally a sextet is

expected. Therefore, for characterization purposes, it is mostly recommended to measure at different temperatures. For practical reasons, Mössbauer spectra are usually collected at two specific temperatures, i.e. room temperature (RT) and liquid nitrogen temperature (~ 80 K) from which already valuable results can be obtained. The more expensive low-temperature measurements down to 4 K or the time-consuming detailed temperature scanning of the spectra are only necessary in those cases where important additional information can be expected.

Secondly, the magnetic sextet spectra of these materials at lower temperature exhibit usually asymmetrically broadened lines. Several mechanisms have been suggested to explain this behavior, but that discussion would lead us far beyond the scope of this paper. Fortunately, for characterization purposes, such spectra can be adequately fitted by a few sextets or even more accurately by considering a distribution of hyperfine fields [6–8]. In this case the spectra are no longer fitted with a single sextet of Lorentzian lines but by a set of such sextets. A versatile distribution fitting procedure which uses several tens of elemental sextets with the necessary smoothing constraint, has been developed by Hesse and Rübartch [9] and was further improved by Le Caër and Dubois [10] or extended by Wivel and Mørup [11] and has been combined in one analyzing method [12]. In this way a much more accurate description can be obtained of partly overlapping sextets, such as those occurring for goethite-hematite associations as for instance demonstrated by the analysis of a Tunisian soil profile [8].

For characterization purposes, MS studies on natural soil samples usually rely on the results of a variety of systematic studies on pure natural or synthetic compounds. Such systematic studies provide a description of the spectral behavior of the different Fe-bearing oxides and hydroxides and a determination of the hyperfine parameters in relation to morphological and chemical features. Many reviews on this subject are available in literature [13–19]. In what follows a brief survey will be given of the spectral features of the various iron oxides and (oxy)hydroxides in relation to their identification and characterization in natural soil samples.

3.3.1 Goethite (α-FOOH)

Goethite is by far the most encountered Fe-bearing compound in soils, sediments and clays, and has therefore been intensively studied in the past forty years. In its most ideal mineral form it is antiferromagnetic with a Néel temperature $T_N = 400$ K [20, 21]. The magnetic hyperfine field amounts to 38.1 T at RT, 50.0 T at 80 K and saturates to 50.7 T at 4 K. However, the well-crystallized form is of rare occurrence and has only been found in particular sites such as the Harz Mountains (Germany) and Lostwithiel (Cornwall, UK) due to the presence of the required extreme hydrothermal formation conditions.

In soils goethite is usually obtained as a weathering product of Fe^{2+} silicates and to a lesser extent of sulfides, carbonates, oxides, etc. This results in a poorly crystalline

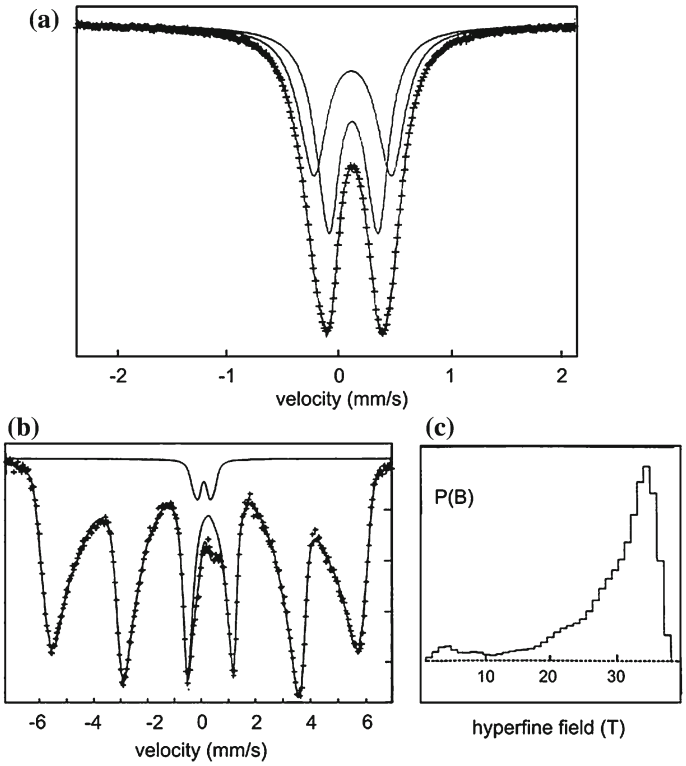

Fig. 3.4 RT Mössbauer spectra of poorly crystallized goethite fitted with two doublets (**a**) and a relatively well crystallized goethite (**b**) with corresponding hyperfine field distribution (**c**)

form, consisting of conglomerations of small, usually needle-shaped crystallites. Consequently, the spectral behavior is mainly governed by superparamagnetic relaxation (Eq. 3.3) with an anisotropy constant K of the order 10^3 Jm^{-3}. The spectra of goethite exhibit simultaneously a sextet and doublet over a wide temperature range, which can be attributed to the non-uniformity of particle morphology within the goethite sample. A doublet spectrum is obtained at room temperature for mean crystallite sizes smaller than about 15 nm. Such a doublet consists of somewhat broadened lines (Fig. 3.4a) indicating the presence of a distribution in the quadrupole splitting with an average value of about 0.55 mm/s (Fig. 3.8). This doublet resembles that of many other paramagnetic or superparamagnetic Fe^{3+}-bearing species and is therefore practically not useful for identification of goethite. However, the magnetically split spectrum of poorly-crystalline goethite, commonly obtained at lower temperatures, is usually recognized by its asymmetrically-broadened lines (Fig. 3.4b). Moreover, its average hyperfine field B_{av} is usually lower than that of well-crystallized goethite and decreases with increasing temperature in different ways depending on the particle size. Therefore its value at a certain temperature

Table 3.2 Summary of hyperfine parameters for goethite

Crystallinity	T (K)	Spectrum	B_{av} (T)	B_p (T)	2ε or Δ (mm/s)	δ_{Fe} (mm/s)
Very high	RT	S	38.1	38.1	−0.28	0.37
(e.g. Harz)	80	S	50.0	50.0	−0.26	0.48
	4	S	50.7	50.7	−0.26	0.49
Related high	RT	S	30–35	31–38	−0.26	0.37
	80	S	47–49	49–50	−0.26	0.47
Moderate	RT	coll S	20–25	25–33	−0.25	0.37
		+D	–	–	0.55	0.36
	80	S	43–47	48–49	−0.25	0.47
Poor	RT	D	–	–	0.55–0.6	0.36
		+ coll S	<20	–	−0.25(f)	0.36
	80	S	40–43	47–49	−0.25	0.47
Very poor	RT	D	–	–	0.6	0.36
	80	S	35–40	47–48	−0.24	0.46
		+D (Fh?)			0.6	0.46

S sextet, *Coll S* collapsing sextet, *D* doublet, *f* value fixed in the fit

could roughly serve as a measure for the average particle size or crystallinity of the goethite phase in a sample. A summary of the hyperfine parameters for goethite obtained from own research is given in Table 3.2. The remaining doublet at 80 K is in many cases most probably ferrihydrite. Examples of different spectra will be shown in Sect. 3.7.

Unfortunately, similar field-reducing and distributive effects are also caused by isomorphous substitutions which are frequently encountered in natural samples. Because of the high abundance of Al in nature the substitution of Al for Fe in goethite has attracted most attention and has been intensively studied [22–25]. Substitution by diamagnetic Al first of all lowers T_N so that a doublet is obtained at RT for an Al substitution of 12 at % and larger [26]. Secondly, this substitution reduces the supertransferred contribution to B, leading to a reduction and a distribution of B. From systematic studies on synthetic aluminous goethites an average field reduction of about 0.05 T at 4 K and of about 0.14 T at 80 K per at % Al has been derived. Because the degree of crystallinity plays a similar role in the dependence of the hyperfine field, both Al concentration and a crystallinity parameter have been introduced in various linear equations of the type,

$$B = B_0 - \alpha\, C(\%\mathrm{Al}) - \beta\, S\left(\mathrm{m}^2/\mathrm{g}\right) \text{or } \beta/MCD_{111} \tag{3.4}$$

where α and β are given coefficients. Either the specific surface area S from the BET method or the mean crystallite diameter MCD_{111} obtained from XRD broadening of the [27] reflection has been taken as a measure for the crystallinity [22, 24, 25].

These relationships were initially considered as promising complementary means to characterize goethite in natural samples. From the most probable hyperfine field B_p or better, the average hyperfine field B_{av}, either the Al

concentration or a measure for the crystallinity can in principle be determined if the other parameter is known from complementary experiments. Although it has been shown that these equations could be successfully applied to certain series of well-characterized natural goethite samples [22, 24], they completely failed for many other natural and synthetic sample series [28]. Friedl and Schwertmann [29] investigated 33 natural goethite samples from different origins, which according to their formation conditions could be divided into 24 samples from tropical and subtropical soils and 9 samples from lake ores. Comparison of the observed hyperfine fields at 4 K with the respective values calculated from the correlation equations resulted in significant deviations, with a somewhat different general behavior for the goethites occurring in the tropical soils than for those occurring in the lake ores. This was corroborated by the linear regressions separately obtained for the two kinds of samples, resulting in different coefficients for both the Al content C and the crystallinity as reflected by the inverse MCD. From a thorough study on well-defined samples of Al goethite, it has been shown that other structural parameters, such as water content, excess hydroxyl ΔOH and structural defects, all having some influence on the lattice parameters [30, 31], play also a substantial role in the magnitude of the magnetic and electrical hyperfine parameters [32–36]. These additional structural parameters are mainly determined by goethite formation factors such as crystallization rate, temperature, OH concentration, etc., and are to some extent related to each other [30].

The situation becomes even more complicated if other elements are involved in the goethite formation. In view of the similar structure of α-MnOOH (groutite), Mn has also been found to substitute for Fe in goethite to a large extent [37, 38]. Because Mn^{3+} is a paramagnetic ion the hyperfine field is less reduced than in the case of Al [38]. Other elements such as Si and P show the tendency to adsorb to the goethite crystallites rather than to substitute for iron in the structure [39–41]. This surface "poisoning" not only opposes the crystal growth during the formation but may also reduce B due to surface effects [28].

It can be concluded that MS is a very suitable tool with respect to the qualitative and to some extent quantitative analysis of goethite in soils and sediments. However, it is clear that MS is still far from being a "magic" analytical technique that provides an in-depth knowledge of the morphological properties of goethite. For the moment, if one compares goethites from a same soil profile, MS can yield some crude indications with respect to crystallinity if equal isomorphous substitutions are expected. Also, other techniques are not so powerful in that respect because natural soil samples mostly contain goethite in more or less close association with other mineral species, likewise hampering to obtain accurate results.

3.3.2 Akaganéite (β-FeOOH)

Akaganéite as the second polymorph of iron oxyhydroxide is by far less abundant in nature in comparison with goethite. In fact, akaganéite requires a small amount of

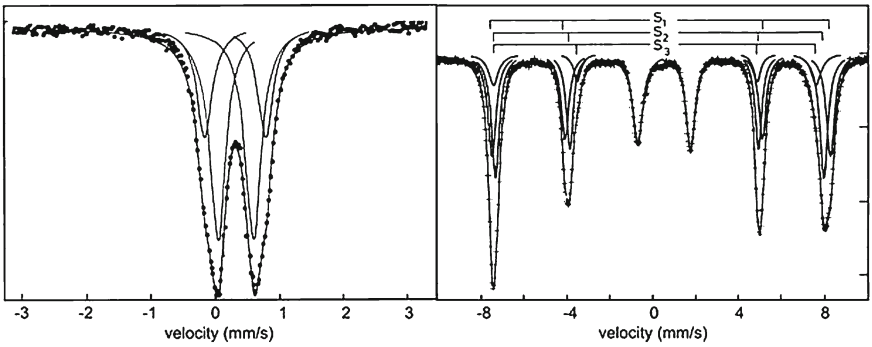

Fig. 3.5 Mössbauer spectrum of a synthetic akaganéite sample at RT with two doublets (*left*) and at low temperature (30 K) with three sextets (*right*) (after Ref. [306])

Table 3.3 Representative hyperfine parameters of oxyhydroxides, other than goethite

Mineral	T (K)	Spectrum	B (T)	2ε or Δ (mm/s)	δ_{Fe} (mm/s)
Akaganeite	RT	D1	–	0.51–0.56	0.37
β-FeOOH		D2	–	0.91–0.96	0.38
	80	S1	∼47	∼−0.1	∼0.46
		S2	∼44	∼−0.5	∼0.47
	4	S1	49.2	−0.10	0.49
		S2	47.7	−0.18	0.48
		S3	47.2	−0.72	0.50
Lepidocrocite	RT	D1	–	0.55–0.70	0.37
γ-FeOOH		D2	–	1.0–1.2	0.36
	4	S	44–46	∼0.02	0.48
Feroxyhite	RT	D	–	0.69	0.37
δ'-FeOOH	4	S1	52.5	0.17	0.48
		S2	50.8	0.07	0.48

chloride or fluoride ions to stabilize the structure. The mineral is an antiferromagnet with a Néel temperature of about 290 K, the latter being often lower, depending on the crystal water content [42]. The RT spectrum consists of a broad doublet with typical asymmetric line shapes (Fig. 3.5). It can be considered as being composed of two discrete doublets, one with $\delta_{Fe} = 0.37$ mm/s and Δ varying between 0.51 and 0.56 mm/s and the second one with $\delta_{Fe} = 0.38$ mm/s and Δ varying between 0.91 and 0.96 mm/s [43, 44]. At 80 K the spectrum exhibits a somewhat broad-lined asymmetric sextet, which for analytical purposes should at least be adjusted with two sextets whereas at lower temperatures three sextets are needed in order to adequately describe the spectrum of akaganéite [45]. The hyperfine parameters are summarized in Table 3.3.

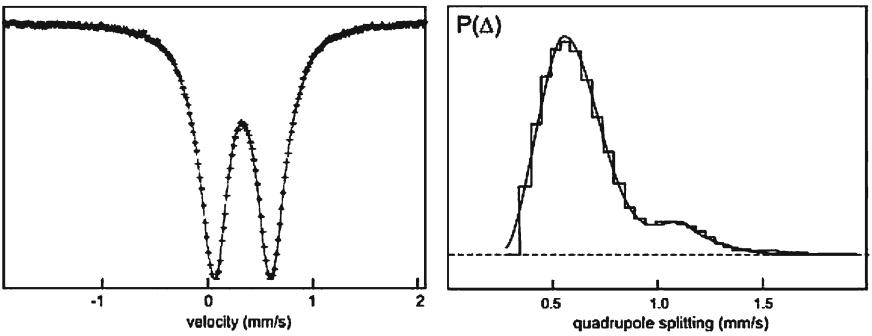

Fig. 3.6 RT Mössbauer spectrum of a lepidocrocite sample (*left*) and corresponding quadrupole distribution (*right*)

3.3.3 Lepidocrocite (γ-FeOOH)

The third oxyhydroxide, lepidocrocite, is an antiferromagnet with a magnetic transition temperature T_N of about 73 K [46]. The magnetic transition is usually not sharp and exhibits a temperature range, often larger than 10 K, in which a sextet and a doublet spectrum coexist. Although this would imply a superparamagnetic behavior [47], similar to other iron oxides and oxyhydroxides, a study of synthetic lepidocrocites of various particle sizes revealed that surface effects play in this case a more significant role, leading to a variety of Néel temperatures which causes the broad transition range [48]. This behavior is probably associated with the typical morphological features of lepidocrocite, which consists of small very thin, raggedly structured platelets [47, 48].

The RT spectrum exhibits a somewhat broadened doublet (Fig. 3.6) with an average quadrupole splitting between 0.55 and 0.7 mm/s, depending on the particle morphology. A more detailed analysis of the doublet yields quadrupole splitting distributions which have more or less two maxima (Fig. 3.6) [47]. The first maximum with $\Delta \sim 0.52$ mm/s is attributed to the bulk part whereas the second with $\Delta \sim 1.1$ mm/s is believed to result from the surface species. At 80 K both distributions are more broadened, so that the second maximum is less pronounced. From diagnostic point of view, these features are not specific enough to discern lepidocrocite from other oxides or oxyhydroxides and one has to rely on magnetically split spectra far below 80 K. At 4 K the magnetic spectrum yields a magnetic hyperfine field of about 44–46 T and a very small quadrupole shift 2ε of about 0.02 mm/s. This hyperfine field is somewhat lower than that of the other iron oxides and oxyhydroxides, which makes lepidocrocite relatively well discernible in complex iron oxide samples. However, a distinction between lepidocrocite and ferrihydrite is much more difficult in view of the broad lines of the latter at low temperatures. The range of the hyperfine parameter values are given in Table 3.3.

Similarly to goethite, lepidocrocite can also contain Al [49]. From a Mössbauer study on a series of synthetic Al-substituted samples [50] it could be confirmed

that Al replaces Fe in the structure to a small extent. A reduction of the maximum-probability hyperfine field B_m with about 0.06 T per at %Al was observed.

3.3.4 Feroxyhite (δ-FeOOH or δ′-FeOOH)

δ-FeOOH, which is isostructural with $Fe(OH)_2$, is the fourth polymorph of iron oxyhydroxide and had initially no mineralogical name because it was not found in nature. On the other hand, δ′-FeOOH, which can be considered as a poorly ordered variant of δ-FeOOH with a somewhat different Fe^{3+} arrangement, has been identified as a rare mineral known as feroxyhite (originally written 'feroxyhyte' by Chukhrov et al. [51]). Showing a typical Fe^{3+} doublet at RT with $\delta_{Fe} = 0.37$ mm/s and $\Delta = 0.69$ mm/s this mineral cannot be distinguished from other oxyhydroxides. This is particularly true in soils where biogenic δ′-FeOOH is often associated with ferrihydrite [52], the latter possessing a similar doublet. Feroxyhite orders magnetically only at very low temperatures and shows at 4 K a broad-lined sextet [53, 54], which in fact is composed of two overlapping sextets (Table 3.3).

Nowadays, both the delta-oxyhydroxides are being called feroxyhite, because δ′-FeOOH is considered to be nothing else than the poorly crystallized (superparamagnetic at RT) variant of δ-FeOOH, the latter being magnetic at RT.

3.3.5 Ferrihydrite

Ferrihydrite is an iron oxyhydroxide with a high surface water content having an approximate composition $Fe_5O_{12}H_9$ written as $Fe_5O_3(OH)_9$ or $Fe_5HO_8.4H_2O$. The most important feature of this mineral is its poor crystallinity, with particle sizes in the range 2–7 nm. XRD patterns consist of 2–6 broad peaks which are not always discernible due to the presence of broad lines of poorly crystalline goethite that often accompanies ferrihydrite in soils. Different models have been proposed for the structure [55–62] and the subject is still under discussion.

Both poor crystallinity and structural disorder lead to a very broad temperature range in which the magnetic order develops and the nature of magnetic order is still in doubt. For a so-called 6-XRD-line ferrihydrite sample the magnetic transition spans a temperature region from 35 to 110 K [63]. Ferrihydrites with less than 6 XRD lines are still paramagnetic at 80 K. It is now believed that these low magnetic transition temperatures result from a kind of superparamagnetic behavior from interacting particles [64], whereas the real antiferromagnetic-paramagnetic transition temperature of ferrihydrite is estimated to be of the order of 500 K [65].

It is obvious that the high degree of structural disorder in such a poorly crystalline system causes broad distributions of hyperfine parameters resulting in broad-lined doublets and sextets. At RT a broad doublet is obtained (Fig. 3.7) with average Δ in the range 0.7–0.9 mm/s. Though the spectra reflect in fact a broad

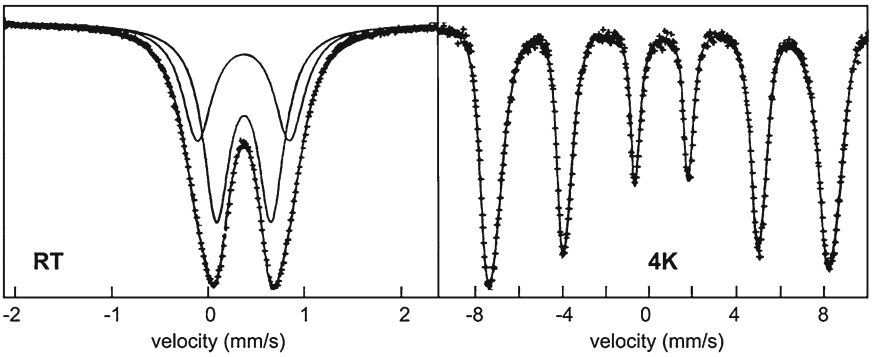

Fig. 3.7 Mössbauer spectrum of ferrihydrite at RT fitted with two doublets (*left*) and at 4 K fitted with a δ-correlated hyperfine field distribution (*right*)

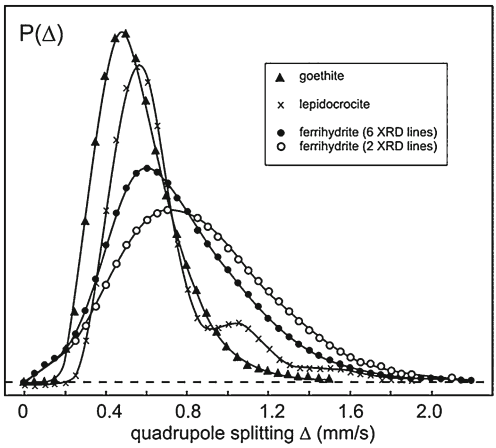

Fig. 3.8 Quadruple distribution in a poorly crystalline sample of goethite and lepidocrocite, and in ferrihydrite

distribution of quadrupole splittings (Fig. 3.8), they are usually satisfactorily described by two doublets (Fig. 3.7) with parameters of about $\delta_{Fe} = 0.37$ mm/s, $\Delta = 0.6$ mm/s (FWHM $\Gamma = 0.3$ mm/s), and $\delta_{Fe} = 0.38$ mm/s, $\Delta = 0.9$ mm/s (FWHM $\Gamma = 0.4$ mm/s). The intensity ratio of these doublets is strongly dependent on the crystallinity and varies from 70/30 to about 30/70 for "better" to poorly crystallized ferrihydrite, respectively.

Such a broad doublet is not only characteristic for ferrihydrite, but also for other Fe^{3+} bearing minerals. Paramagnetic akaganéite, for instance, shows also a broad doublet spectrum at RT, although it is in fact composed of two discrete spectral components. Moreover, akaganéite is readily recognized by the appearance of a magnetically split spectrum at temperatures far above the transition temperature of ferrihydrite. Another compound showing the typically broad doublet at RT with similar distribution is fully oxidized vivianite, often called oxykerchenite.

Similarly, as for most of the ferrihydrites, the spectrum of oxykerchenite remains a doublet down to 80 K [66].

At very low temperatures the sextet of ferrihydrite exhibits broad lines with a rather symmetrical lineshape (Fig. 3.7). At 4 K the average hyperfine field amounts to between 46 and 50 T [67], with a small quadrupole shift 2ε between -0.02 and -0.1 mm/s. The spectra are usually slightly asymmetric in which in particular the 6th line is less deep than the first one. This has been attributed to the presence of additional tetrahedral iron sites [68], although this is still in doubt and correlation effects between B in the distribution on the one hand, and Δ and/or δ on the other hand, which are normally expected in largely disordered structures, may similarly produce such an asymmetry.

As in other iron oxyhydroxides, isomorphous substitution for Fe by Al is expected in natural samples. A study of synthetic samples with Al substitutions by [69] revealed an increasing asymmetry of the doublet lineshape at RT, pointing to an increased average quadrupole splitting. At low temperatures, a decrease of the average hyperfine field and a lowering of the magnetic transition temperature region with increasing Al content is reported. All these features are quite similar to crystallinity effects and are therefore not of practical use for characterization purposes. Also silicon seems to play an important role in ferrihydrite. As in the case of goethite, Si species can easily adsorb on ferrihydrite and thus prevents its further growth [70]. Childs [57] claimed that ferrihydrite can contain up to 9 %at Si, but the question remained if it is adsorbed or incorporated in the structure. Campbell et al. [71] suggested that Si is structurally incorporated and demonstrated the ability of Si to inhibit a transformation to more stable Fe^{3+} oxides or oxyhydroxides.

However, several more recent works have resulted in a complete change in the earlier, more-or-less contradictory ideas about ferrihydrite and its XRD and Mössbauer behavior. Berquó et al. [72] report the possibility of synthesizing Si-ferrihydrites with much better crystallinity. One of the authors' ferrihydrites shows even relatively sharp lines in the XRD pattern and its Mössbauer spectrum even consists of a somewhat collapsed sextet at RT, but with no doublet contribution. The spectrum of a natural sample, showing similarly seven, but somewhat broadened lines in the XRD pattern, exhibits a collapsed sextet at 130 K, but remains exclusively a doublet at RT.

On the other hand, it has recently been shown that some ferrihydrite species still exhibit a magnetic-superparamagnetic transition at very low temperatures. In particular, this seems to happen when ferrihydrite is closely associated to organic carbon [73]. These so-called DOM (dissolved organic matter) ferrihydrites have a lower hyperfine field and are even not completely magnetically ordered at 4 K (see also Sect. 3.5.1).

In conclusion, the very poor crystallinity and the low superparamagnetic blocking temperature in natural ferrihydrites hamper to some extent the characterization of ferrihydrite with MS at standard measuring temperatures (RT, 80 K). From the point of view of identification, ferrihydrite can be recognized by MS as long as it represents the main constituent in soil samples. The broad quadrupole distribution (see Fig. 3.8)

with its high average value is already quite indicative for the presence of ferrihydrite, although, clear-cut evidence can only be obtained from the typical sextet spectrum obtained at very low temperatures (<80 K). On the other hand, XRD may provide more direct evidence through the characteristic broad-lines pattern which will be discernible if ferrihydrite is present in sufficient amount in the sample. Unfortunately, in many soils ferrihydrite occurs only as a minor fraction and no technique is able to recognize it directly among the other interfering components such as poorly crystalline goethite. In goethite-ferrihydrite associations, the doublet fraction which persists down to 80 K may account for ferrihydrite as well as for very poorly crystalline and/or highly substituted goethite. However, if the 80 K spectrum exhibit a goethite sextet with rather narrow lines, the remaining doublet can most likely be attributed to ferrihydrite because goethite with two discrete and drastically different crystallinities or substitutions are not commonly expected in the same sample. At very low temperatures (4 K) the hyperfine fields of goethite and ferrihydrite are comparable. Hence, these components cannot be separated merely by their difference in quadrupole shift. Only the broader lines of the ferrihydrite sextet might be indicative.

Another method which is helpful in the characterization of ferrihydrite is selective dissolution in acid ammonium oxalate [74] followed by a so-called differential X-ray diffraction (DXRD) [75], which consists of subtracting the pattern of a treated sample from that of an untreated one, thus isolating and enhancing the typical ferrihydrite diffraction pattern. In MS, this dissolution applied to natural soil samples usually results in a decrease of the doublet at RT and 80 K, and a narrowing of the sextet lines at lower temperatures. However, it has been demonstrated that ammonium oxalate also dissolves organically bound Fe, Fe from magnetite and from poorly crystalline lepidocrocite [76–79], and also attacks vivianite, siderite [66] and even poorly crystalline goethite [80]. So, MS applied in combination with such a treatment is not always decisive unless information about the presence of the above interfering compounds is obtained from other techniques.

3.3.6 Hematite (α-Fe_2O_3)

Hematite is the most abundant iron oxide in soils and sediments. In comparison to other iron oxides and hydroxides, hematite (α-Fe_2O_3) exhibits a non-common magnetic behavior. In addition to the normal magnetic-paramagnetic transition at $T_N = 955$ K, pure and well-crystallized hematite transforms at about 265 K from a low-temperature antiferromagnetic (AF) to a high-temperature weakly ferromagnetic (WF) state, known as the Morin transition. This transition consists in fact of a 90° spin reorientation from an antiferromagnetic spin configuration in the *c* direction into the basal plane (perpendicular to the *c*-axis) in which the spins are slightly canted resulting in a weak ferromagnetism (Fig. 3.9). This magnetic

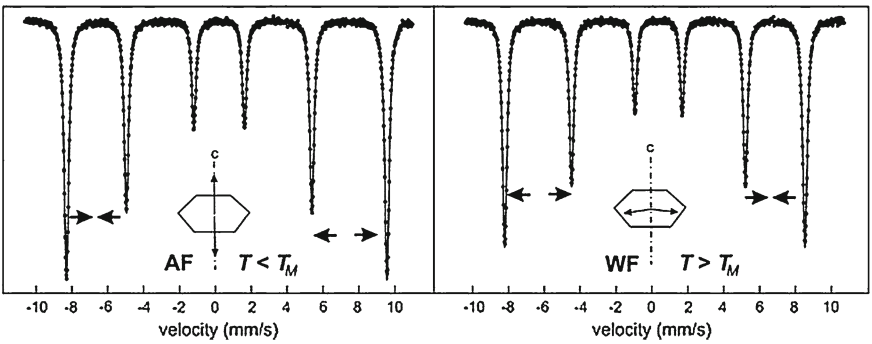

Fig. 3.9 Mössbauer spectra of hematite in the antiferromagnetic state at 80 K (*left*) and in the weakly ferromagnetic state at RT (*right*)

Table 3.4 Representative hyperfine parameters of hematite of various crystallinity

Crystallinity	T (K)	Spectrum	B_{av} (T)	B_p (T)	2ε (mm/s)	δ_{Fe} (mm/s)
High	RT	S(WF)	51.7	$=B_{av}$	−0.19	0.36
	80	S(AF)	54.1	$=B_{av}$	0.38	0.47
	4	S(AF)	54.2	$=B_{av}$	0.39	0.48
Medium	RT	S(WF)	50.0–51.0	$\approx B_{av}$	−0.20	0.37
	80	S(WF)	52.5–53.0	$\approx B_{av}$	−0.19	0.47
		S(AF)	53.5–54.0	$\approx B_{av}$	>0.10	0.47
	4	S(AF)	54.2	$=B_{av}$	0.38	0.48
		S(WF)	53.3	$=B_{av}$	−0.20	0.48
Poor	RT	S(WF)	37.0–48.5	49.5–50.0	−0.21	0.37
	80	S(WF)	52.0–53.0	$\approx B_{av}$	−0.20	0.47
	4	S(WF)	53.2	$=B_{av}$	−0.20	0.48

behavior is well reflected in the Mössbauer spectra. The hyperfine parameters of hematite at different temperatures are given in Table 3.4.

The hyperfine field B in the AF state at 4 and 80 K are nearly equal which is conceivable in view of the high T_N. In the WF state at RT a value of 51.7 T is observed. At the Morin transition temperature T_M, B changes abruptly. The drop of about 0.8 T is explained by the influence of the spin reorientation on the orbital and dipolar contributions to B [81]. The quadrupole shift 2ε, which is only slightly temperature dependent, changes more drastically at T_M. At 80 K a large positive value of 0.38 mm/s is observed whereas the WF state has a negative value of −0.19 mm/s at RT (indicated by arrows in Fig. 3.9). The relation between those two values is consistent with the EFG principal axis lying in the direction of the c-axis. In view of this large difference in 2ε both the WF and AF phase can be separately identified from the fitting, and therefore MS is an extremely powerful tool to study the Morin transition. Moreover, because the latter is very sensitive to microcrystalline effects, lattice imperfections and impurities, it is clear that this technique could offer some possibilities for the characterization of hematite in natural samples.

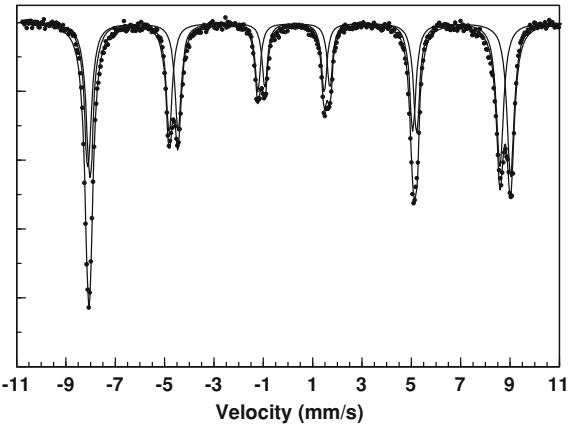

Fig. 3.10 Mössbauer spectrum of a hematite sample showing simultaneously AF and WF phases

Pedogenic hematite consists mainly of small crystallites and, similar to goethite, the spectral features are governed by superparamagnetic relaxation effects. However, the effective anisotropy constant K of hematite is of the order of 10^4 J/m^3 [82], yielding blocking temperatures which are higher than in the case of goethite. Consequently, in most cases the spectra are still magnetically split at RT. Nevertheless, due to microcrystalline effects, the lines may still be asymmetrically broadened. The origin of the field distributive and reducing effects is similar to that of goethite, although, the reduction of B caused by surface effects has been well established in hematite by MS on ^{57}Fe surface enriched hematite [83, 84] and by surface studies with conversion electrons MS [85, 86]. For very small crystallite sizes with particle dimension $D \ll 8$ nm a doublet is observed at RT with a quadrupole splitting Δ in the range 0.5–1.1 mm/s [87], apparently strongly dependent on the particle size.

Morphological effects such as particle size, lattice imperfections and the presence of micro- and macropores have also a pronounced influence on the Morin transition. First of all, the transition temperature lowers with decreasing particle size [88–90] and for particle sizes smaller than about 20 nm the Morin transition is even completely suppressed, resulting in a single WF phase down to 4 K [82]. Further, the normally sharp Morin transition becomes a temperature region with the coexistence of the two phases in which the AF phase diminishes in favor of the WF phase with increasing temperature. A typical spectrum in this transition region is shown in Fig. 3.10.

This region broadens considerably with decreasing particle dimensions and with increasing structural defects [91], and the coexistence of both the AF and WF phase even can extend down to 0 K. Such a case is represented in Fig. 3.11 where the relative areas (RA) and the quadrupole splitting do not change below 150 K. The Morin transition temperature can then be defined as that temperature at which the amount (RA) of AF phase is reduced to half of its initial value at low temperatures.

The influence of the average particle size on the Morin transition temperature has been mainly investigated for synthetic samples and is represented in Fig. 3.12. From

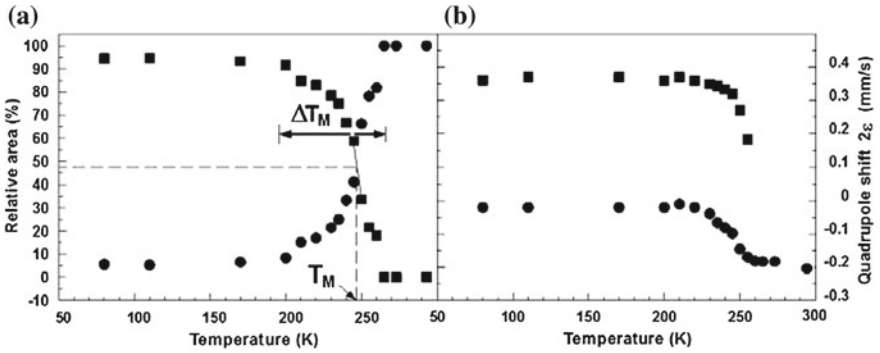

Fig. 3.11 Temperature behavior of the transition region: relative area (**a**) and the quadrupole shift 2ε (**b**) for a small-particle hematite

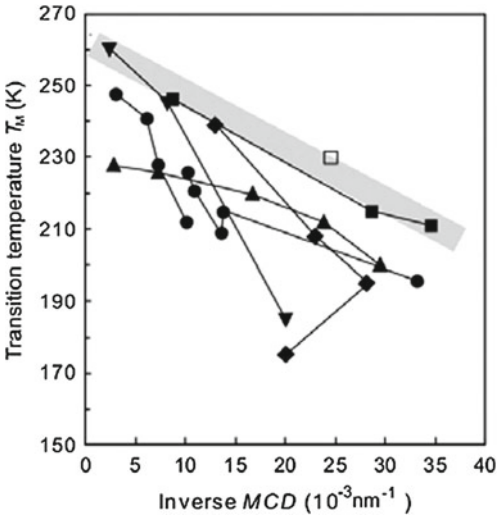

Fig. 3.12 Morin transition temperature vs. inverse average particle size for differently prepared hematite samples (*Black square* prepared from decomposition of lepidocrocite; for the other symbols, see Ref. [99])

that picture it follows that this transition temperature is not solely dependent on the particle size, but also differs according to the preparation method. Large defects and the presence of hydroxyl groups (OH^-) probably cause the large fluctuations in T_M [92–94]. However, hematite samples prepared from lepidocrocite generally show the highest transition temperatures [95–97] and it is believed that natural samples, which are mostly formed from ferrihydrite will possess the same features. The shaded band shown in Fig. 3.12 might be a reasonable analytical guideline for the relation between T_M and the average particle dimensions.

Isomorphous Al for Fe substitution in hematite is also a common phenomenon and has been intensively studied [92, 96, 98–101]. Hematite can contain more than 15 at % Al and, similarly to goethite, this diamagnetic substitution has primarily a

twofold effect on the magnetic properties, i.e. it lowers the magnetic transition temperature and reduces the saturation hyperfine field. However, in view of the high Néel temperature, the sextet-doublet transition still occurs at high temperatures above RT and is therefore not of practical diagnostic use. The reduction of the saturation value of B, which can already be observed at 80 K in view of the very small variation of B between 80 and 4 K, is also rather small. At 80 K a reduction of about 0.04 T per at % Al has been found, whereas at RT it amounts to 0.08 T per at % Al [92, 102].

Similarly as for goethite, a linear relationship of B as a function of Al content and particle size has been proposed [102] which is valid at RT and for concentrations less than 10 %Al. However, all these results are derived from synthetic samples, mostly obtained from goethite. Therefore, particularly at RT, the magnetic hyperfine field will still be largely influenced by morphological effects. Moreover, most preparation methods, based on the decomposition of oxyhydroxides, result in inhomogeneous Al substitution [96]. A more clear-cut picture for the dependence of the hyperfine field on Al substitution is obtained for hematites prepared from oxinates [103] where a reduction of 0.061 at RT and 0.032 at 80 K per at % Al is observed.

Somewhat more pronounced effect of Al substitution is reflected in the behavior of the Morin transition. With increasing Al content the transition temperature T_M decreases and the transition region becomes significantly broader [97]. Moreover the Morin transition is completely suppressed at about 10at % Al in bulk hematite [99] and even at somewhat lower concentrations (8 at %) for less crystalline hematite [100]. On the other hand, the effect of Al on the Morin transition temperature is smaller in the case of more homogeneous Al substitution in samples prepared from oxinates [103]. Using the aforementioned definition, the Morin transition temperature for as-such obtained hematite species decreases by 8 K per at % Al. Because the spectral implications of Al substitution are quite similar to those of morphological effects, the separation of both effects remains a major problem and additional techniques are necessary for the characterization of natural samples.

Another element which is a possibly abundant candidate for substitution of iron in natural hematite samples is manganese [8]. Mn was substituted for iron up to about 18 % in synthetic samples [104], but, it is believed that in natural samples the substitution is much lower (<5 at %) [105]. In a study of some Mn-hematites prepared from Mn-substituted goethites [106] a somewhat smaller decrease for the hyperfine field of the WF phase at RT is observed in comparison with that of similarly prepared Al-hematites, which is expected in view of manganese being a magnetic ion. On the other hand, manganese reduces the Morin transition temperature more rapidly, and already at about 4 at % Mn the transition is completely suppressed [106]. A still more drastic effect on T_M is caused by Ti substitution which is also abundant in nature. Less than 1 at % Ti completely inhibits the Morin transition [27]. However, Ti occurs rather in high concentration tending more to the isostructural ilmenite ($FeTiO_3$). Another important substitution element could be silicon, although little information in that respect is found in the literature. There are indications that silicon increases T_M slightly. For example, an

asymmetric spectrum at RT has been found for a Si-rich hematite sample from Elba, pointing to the presence of the AF phase above 265 K [90].

In conclusion, the characteristic hyperfine parameters and the high magnetic transition temperature T_N and blocking temperature T_B for hematite render MS very suitable for the identification of this material in natural samples. Moreover, when used in conjunction with other techniques, MS yields some indicative information about morphological or substitutional properties through the determination of the magnetic hematite phases present in the sample. Although small-particle effects are not so pronounced as in the spectra of goethite, the spectra of hematite may still show asymmetric lines, particularly at room temperature. Hence, appropriate fitting procedures such as the ones based on a hyperfine field distribution are recommended, especially when the hematite sextet overlaps with other sextets.

3.3.7 Fe–Ti Oxides

Related to hematite, ilmenite, $FeTiO_3$, has a similar rhombohedral structure. Alternating planes are occupied by Ti^{4+} and Fe^{2+}, breaking down the strong magnetic interactions that occur in hematite. It is therefore a weak antiferromagnet with $T_N = 55$ K [107]. Although the whole range between hematite and ilmenite, $Fe_{2-x}Ti_xO_3$ can be synthesized, natural samples of ilmenite possess a relatively high amount of Ti ($0.75 < x < 0.95$). Ilmenite with a higher degree of stoichiometry was found in lunar samples [108]. At room temperature a doublet is observed with a high isomer shift, $\delta_{Fe} = 1.1$ mm/s and a low quadrupole splitting $\Delta = 0.71$ mm/s. These typical hyperfine parameters for ilmenite, make it relatively easy to discern this oxide in the Mössbauer spectrum. At 80 K the quadrupole splitting is larger and amounts to about 1.0 mm/s. At 5 K only a very low magnetic hyperfine field ($\sim$4 T) is observed due a strong opposite orbital contribution of Fe^{2+} [107, 109].

Deviation from stoichiometry implies the presence of Fe^{3+} which is clearly observed in the spectra by an asymmetry, namely the left absorption line is broader and deeper. The spectra can then be analyzed with two doublets: one from Fe^{2+} having hyperfine parameters very close to those of pure ilmenite, and one from Fe^{3+} with typical hyperfine parameters for trivalent iron [110] (see Table 3.5).

Another well-known mineral is pseudobrookite, which consists of a complete solid solution series between ferrous $FeTi_2O_5$ and ferric Fe_2TiO_5. Also in this case, the Mössbauer spectra reveal iron species that vary from Fe^{2+} over mixed valences to Fe^{3+}. However, the structure contains two different sites (8f and 4c) where iron can be present, resulting in two doublets for each iron valence. The hyperfine parameters according to Guo et al. [111] are summarized in Table 3.5.

Table 3.5 Representative hyperfine parameters for Fe–Ti oxides

Mineral	T (K)	Iron	B (T)	2ε or Δ (mm/s)	δ_{Fe} (mm/s)
Ilmenite $FeTiO_3$	RT	Fe^{2+}	–	0.71	1.1
Ilmenite (non-stoichiom)	RT	Fe^{2+}		0.65–0.70	1.0–1.1
$Fe_{1+x}Ti_{1-x}O_3$		Fe^{3+}		0.3–0.5	0.3
Pseudobrookite (ferrous)	RT	Fe^{2+} 8f		1.10	2.16
$FeTi_2O_5$		Fe^{2+} 4c		1.06	3.15
Pseudobrookite (Intermed.)	RT	Fe^{2+} 8f		1.1–1.2	1.6–2.1
$Fe_{1+x}Ti_{2-x}O_5$		Fe^{2+} 4c		1.04–1.06	2.8–3.1
		Fe^{3+} 8f		0.38–0.41	0.54–0.58
		Fe^{3+} 4c		0.34–0.39	0.85–1.00
Pseudobrookite (ferric)	RT	Fe^{3+} 8f		0.38	0.57
Fe_2TiO_5		Fe^{3+} 4c		0.38	0.92

3.3.8 Magnetite

Magnetite (Fe_3O_4) is a ferrimagnetic spinel oxide with a Néel temperature of 858 K. It naturally occurs often in a fairly crystallized form and its presence can readily be recognized in a Mössbauer spectrum. Magnetite has the following structural formula $\left(Fe^{3+}\right)_A\left[Fe_2^{2.5+}\right]_B O_4$ where the octahedral (B-site) ferrous and ferric ions merge into $Fe^{2.5+}$ due to a fast electron hopping in pairs above the so-called Verwey transition (>125 K). Consequently, the RT spectrum of magnetite exhibits two partly resolved sextet patterns (Fig. 3.13) resulting from tetrahedral (A site) Fe^{3+} with $B = 49.1$ T, $2\varepsilon = 0$ mm/s, $\delta_{Fe} = 0.28$, and octahedral (B site) $Fe^{2.5+}$ with $B = 46.0$ T, $2\varepsilon = 0$ mm/s, $\delta_{Fe} = 0.66$ mm/s. The latter sextet possesses a somewhat broader linewidth ($\Gamma \sim 0.5$ mm/s) because it is in fact composed of two B-site sextets with $B = 45.6$ T, $2\varepsilon = 0.18$ mm/s, $\delta_{Fe} = 0.66$ mm/s, and $B = 46.0$ T, $2\varepsilon = -0.05$ mm/s, $\delta_{Fe} = 0.66$ mm/s respectively, as a result of two different possible directions of the magnetic hyperfine field with respect to the local B-site EFG principal axes [112]. However, from the ferric A-site component, magnetite is readily recognized by MS at RT and for characterization purposes a two-sextet fitting is adequate. For ideal magnetite the sextet area ratio $S(B)/S(A)$ has to be 2:1. In practice, this ratio is somewhat lower and amounts to about 1.8:1 at RT. This is related to the Mössbauer fraction f of the $Fe^{2.5+}$ on the B sites being somewhat lower than that of Fe^{3+} on the A sites.

However, deviations from this ideal ratio are often observed. The main reason is that magnetite may partly be oxidized by replacing Fe^{2+} by Fe^{3+} and introducing vacancies. Because the electron hopping occurs in pairs, this oxidation does not result in another intermediate Fe valence on the octahedral sites, but in a decrease of the $Fe^{2.5+}$ component and the appearing of a B-site Fe^{3+} sextet for which the hyperfine parameters do not appreciably differ from those of the A-site sextet. Together with the introduced vacancies, a decrease of the $Fe^{2.5+}$ B-site sextet area and an apparent increase of that of the A-site sextet are observed. Therefore, one cannot speak anymore about one A-site and one B-site sextet—a mistake that is

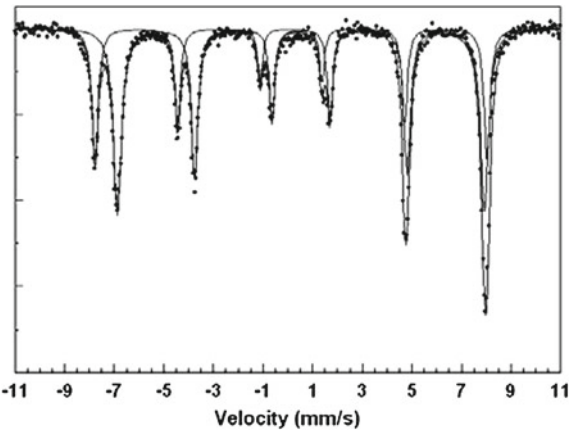

Fig. 3.13 Typical spectrum of magnetite at RT with outer Fe^{3+} and inner $Fe^{2.5+}$ sextet

Table 3.6 Representative hyperfine parameters of magnetite

Magnetite	T (K)	Spectrum	B_{av} (T)	δ_{Fe} (mm/s)
Pure Fe_3O_4	RT	Fe^{3+} A	49.0	0.28
		$Fe^{2.5+}$ B	45.9	0.66
	130	Fe^{3+} A	50.4	0.36
		$Fe^{2.5+}$ B	48.0	0.76
Oxidized $Fe_{3-x}O_4$	RT	Fe^{3+} A	49.0	0.28
		Fe^{3+} B	~50.0	0.36
		$Fe^{2.5+}$ B	45.9	0.66

often made—but instead should speak about one Fe^{3+} sextet and one $Fe^{2.5+}$ sextet (Table 3.6).

The observed value for the $S(Fe^{2.5+})/S(Fe^{3+})$ ratio of a magnetite phase can be used to determine its degree of oxidation. Oxidized magnetite has the general formula $Fe_{3-x}O_4$ with $0 < x < 0.33$. In that case one can expect the following structural formula, $\left(Fe^{3+}\right)_A[Fe^{2.5+}_{2(1-3x)}Fe^{3+}_{5x}\square_x]_BO_4$, where $\square$ stands for the vacancies and where an equal amount of octahedral Fe^{2+} and Fe^{3+} results in $Fe^{2.5+}$. Considering the ratio $R = S(Fe^{2.5+})/S(Fe^{3+})$ to be about 1.8 for pure magnetite at RT, one can write

$$R = \frac{1.8(1-3x)}{1+5x} \tag{3.5}$$

for oxidized magnetite, leading to

$$x = \frac{1.8-R}{5.4+5R} \tag{3.6}$$

On the other hand, it has been claimed that in the case of oxidation of magnetite, the vacancies might be present on both lattice sites [113, 114]. Anyway,

because of the same amount of octahedral $Fe^{2.5+}$ in both cases, the formula for x will not be altered.

However, caution should be taken in using the equation because part of the deviation from the ideal ratio $R = 1.8$ might also be due to isomorphic substitution for Fe by small quantities of other elements such as Al and especially Ti.

Titanomagnetite is the common name for the minerals with general formula $Fe_{3-x}Ti_xO_4$ arising from the solid solution between magnetite and the ulvöspinel, $Fe_2^{2+}TiO_4$. These Ti-magnetites are very common in igneous rocks such as basalts and have been of particular interest in connection with magnetism of the earth. In these magnetites Ti^{4+} substitutes Fe on the octahedral sites creating more Fe^{2+}. Many models have been proposed for the cation distribution (e.g. Pearce et al. [115] and references therein). In most of the models the tetrahedral sites are fully occupied with Fe^{3+} up to $x = 0.2$. This means that, apart from the $Fe^{2+} - Fe3^{+}$ pairs giving $Fe^{2.5+}$ there is an excess of octahedral Fe^{2+}. This results in a two-sextet magnetite-like spectrum with an additional inner shoulder on the $Fe^{2.5+}$ sextet belonging to a Fe^{2+} sextet [116, 117]. However, natural samples which are chemically inhomogeneous and frequently non-stoichiometric show often more complex Mössbauer spectra.

Natural magnetite may also occur with a small particle morphology yielding a Mössbauer spectrum with asymmetrically shaped lines. Due to the increased overlap of the lines of both sextets in that case, it becomes difficult to determine the ratio $R = S(Fe^{2.5+})/S(Fe^{3+})$ accurately.

At low temperatures, the spectrum of pure magnetite is very complex (Fig. 3.14a) and may be described by at least five subspectra [118]. This is due to the 3d electron localization below the so-called Verwey transition at about 125 K leading to discrete Fe^{2+} and Fe^{3+} spectral contributions of the B sites. However, this transition temperature is lowered in the case of substitution or partial oxidation [119–121]. This is illustrated in Fig. 3.14b where oxidized magnetite ($Fe_{2.944}O_4$)

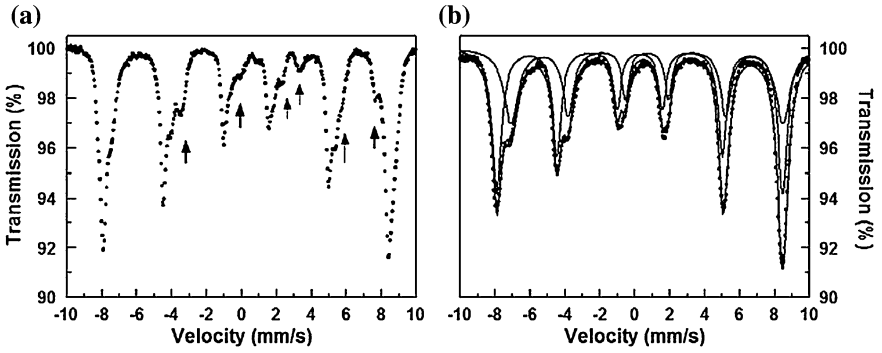

Fig. 3.14 Spectra below the Verwey transition: **a** spectrum of stoichiometric magnetite at 100 K with visible Fe^{2+} lines (indicated by arrows), and **b** spectrum of non-stoichiometric magnetite $Fe_{2.944}O_4$ at 100 K with the two typical Fe^{3+} and $Fe^{2.5+}$ sextets

still shows the typical $Fe^{2.5+}$ and Fe^{3+} sextets at 100 K which is below the normal Verwey transition for stoichiometric magnetite [35].

3.3.9 Maghemite

Maghemite, which is a fully oxidized form of magnetite, has the structural formula $\left(Fe^{3+}\right)_A[Fe^{3+}_{5/3}\square_{1/3}]_BO_4$ where $\square$ represents again the vacancies on the octahedral sites. The corresponding Mössbauer spectrum consists of a somewhat broad-lined Fe^{3+} sextet, which is in fact composed of two non-resolved sextets from Fe^{3+} in tetrahedral and octahedral sites, respectively (Fig. 3.15a). Only by using an external field, the hyperfine field and the isomer shift of both sextets could be accurately determined [125] (see Sect. 3.6.4). Hyperfine parameter values are given in Table 3.7.

Maghemite is commonly formed from oxidation of fine-course lithogenic magnetite, although its abundance in tropical and subtropical regions can also be explained by the conversion of for instance goethite through fires under reducing conditions. Also fine-particle magnetite produced by bacteria may lead to maghemite after spontaneous oxidation. In most of those cases, maghemite possesses a rather small-particle morphology leading to a superparamagnetic behavior. Maghemite can then appear in the Mössbauer spectrum as a doublet at RT. From the effective anisotropy constant of about 10 Jm^{-3} [123] a superparamagnetic doublet is expected at RT for particle sizes smaller than about 5 nm. This

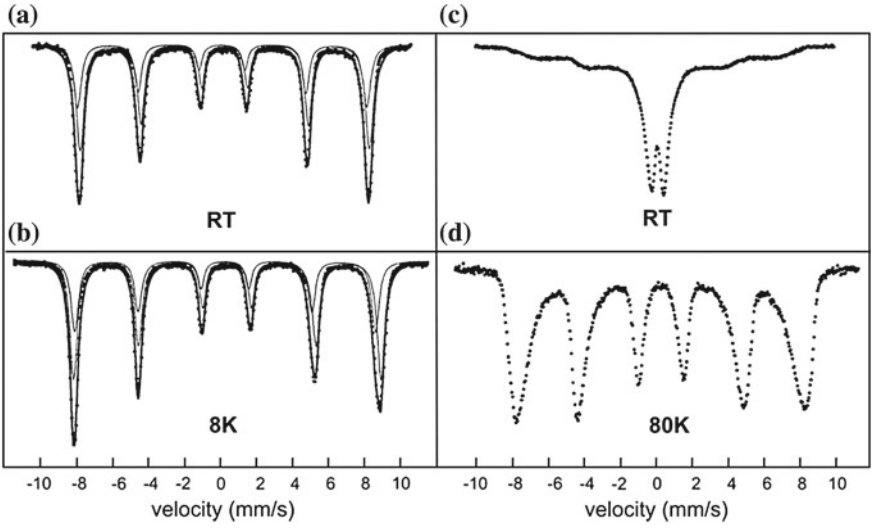

Fig. 3.15 Mössbauer spectra of maghemite: well-crystallized maghemite at RT (**a**) and at 8 K (**b**) fitted with *A*-site and *B*-site sextets according to parameters derived from external-field spectra; poorly crystallized maghemite at RT (**c**) and at 80 K (**d**) (after da Costa et al. [122])

Table 3.7 Representative hyperfine parameters of maghemite

Crystallinity	T (K)	Spectrum	B_{av} (T) or Δ (mm/s)	δ_{Fe} (mm/s)
Good	RT	S Fe^{3+} A	49.9	0.24
		S Fe^{3+} B	49.9	0.36
	80	S Fe^{3+} A	49.9	0.36
		S Fe^{3+} B	52.9	0.48
	4	S Fe^{3+} A	52.0	0.36
		S Fe^{3+} B	53.1	0.48
Medium	RT	S Fe^{3+} av	30–40	0.28
	80	S Fe^{3+} av	45–50	0.45
Poor	RT	D Fe^{3+} av	0.65–0.75	0.35
	80	S Fe^{3+} av	30–45	0.45
		D Fe^{3+} av	0.65–0.75	0.43

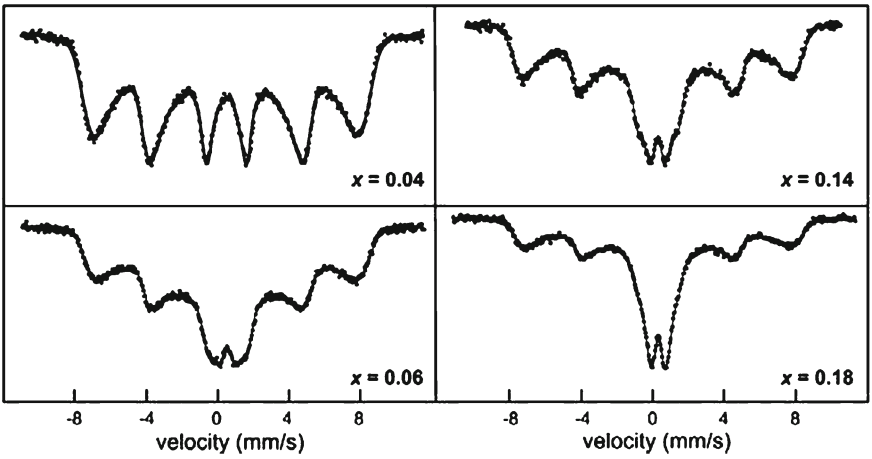

Fig. 3.16 Evolution of the 80 K spectra of poorly crystallized Al-substituted maghemite, γ-$Fe_{2-x}Al_xO_3$ with increasing Al content (after da Costa et al. [126])

doublet exhibits an average Δ in the range 0.65–0.75 mm/s, which is somewhat larger than that of other oxides or oxyhydroxides. At 80 K the spectra of such particles are usually magnetically split (Fig. 3.15) with average hyperfine fields of about 30–45 T (Table 3.7). Pedogenic maghemite occurs often in association with hematite [124]. The spectra of both phases possess a rather similar hyperfine field (in particular when the latter is in the WF state) and differ only in the quadrupole shift. This renders the distinction between both minerals rather difficult.

Al substitution is commonly found in soil-related maghemite. The spectra are somewhat similar to that of Al-free maghemite, but the sextet is often accompanied by a doublet (Fig. 3.16), the contribution of which decreases at lower temperatures. This typical superparamagnetic behavior is a consequence of a combined effect of particle size and diamagnetic substitution [125, 126].

Titanomaghemites originating from oxidation of lithogenic titanomagnetite show similar features in their Mössbauer spectra, i.e. asymmetrically broadened sextet lines accompanied by a central doublet [127, 128]. These maghemites seem to have vacancies on both sites [127, 129].

3.3.10 Green Rust Related Minerals

Green rusts are mixed-valence iron hydroxysalts that have been extensively studied for understanding the corrosion behavior of iron based materials and steels. They are obtained by oxidizing metallic iron or $Fe(OH)_2$ and are intermediate compounds comprising ferrous and ferric ions. Several types have been synthesized incorporating various anions such as CO_3^{2-}, Cl^- or SO_4^{2-} and were studied by MS [130–133]. They all belong to the double layered hydroxide family (HDL) where in the most stable one, i.e. with CO_3^{2-}, positive charged brucite-like layers $\left(Fe_4^{2+}Fe_2^{3+}(OH)_{12}\right)^{2+}$ alternate with $(CO_3.3H_2O)^{2-}$ interlayers, possessing a ferric molar fraction $x = Fe^{3+}/Fe_{total} = 1/3$. Green rusts dissolve usually by oxidation whereas a ferric oxyhydroxide precipitates such as ferrihydrite and/or goethite. However, rapid oxidation under alkaline conditions (in situ deprotonation) keeps the green rust structure essentially unchanged, leading finally to so-called "ferric green rust" which has in fact an orange color [134].

A green rust related mineral in soils was first discovered in a so-called gleysol at Fougères (Brittany, France) and has therefore been named fougèrite [135]. The Mössbauer spectrum, usually measured at lower temperatures (78 K) to avoid oxidation, is typical for green rust, consisting of one or two Fe^{2+} doublets with $\delta \approx 1.25$ mm/s and with $\Delta \approx 2.60$–2.90 mm/s and a Fe^{3+} doublet with $\delta \approx 0.48$ mm/s and with $\Delta \approx 0.50$–0.70 mm/s. The spectrum from the first measured sample is shown in Fig. 3.17a. For different fougèrite samples, the ferric molar fraction x turned out to be between 1/3 and 2/3 [136]. A study in depth with a miniaturized Mössbauer spectrometer showed that fougèrite is more ferric in the upper horizons and variations are consistent with the fluctuations in the water table and thus with aerobic and anaerobic conditions [137]. Those in situ experiments yield spectra and thus hyperfine values close to RT (283 K). They are $\delta \approx 1.05$–1.08 mm/s and $\Delta \approx 2.7$ mm/s, $\delta \approx 0.75$–1.00 mm/s and $\Delta \approx 2.2$–2.7 mm/s both for Fe^{2+}, and $\delta \approx 0.21$–0.30 mm/s and $\Delta \approx 0.6$–0.8 mm/s for Fe^{3+}.

In contrast to the permanently waterlogged soils of a continental aquifer with green rust related minerals with values of x within the (1/3, 2/3) range as firstly extracted in Fougères, similar minerals being still more ferric with x values within the (2/3, 1) range occurs in gley from the schorre of a maritime marsh, as was firstly extracted in Trébeurden (Brittany, France) [138]. The spectrum of a typical Trébeurden sample with $x \approx 0.75$ measured at 78 K and fitted with 3 doublets is shown in Fig. 3.17c. Similar spectra were recorded from samples extracted from

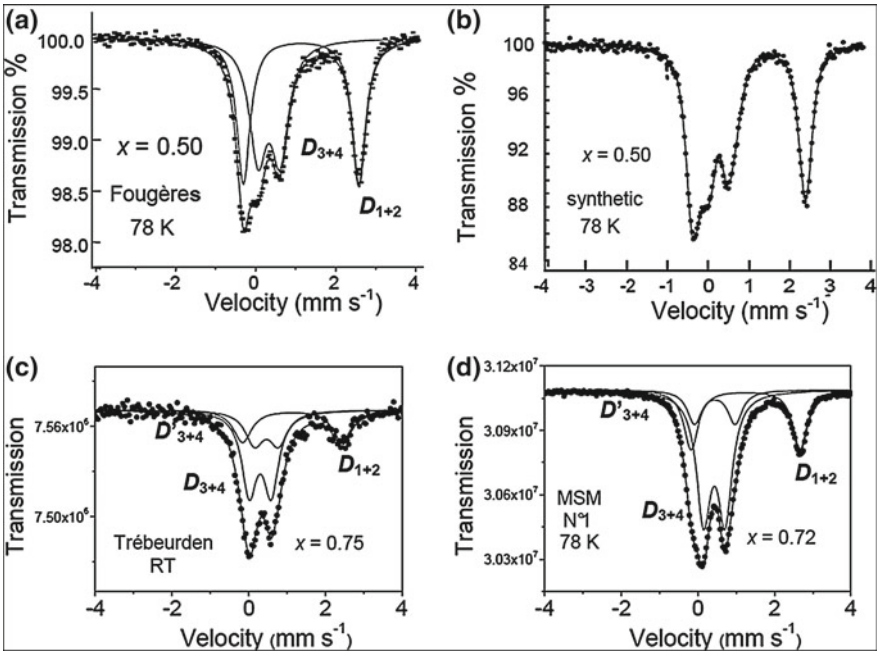

Fig. 3.17 Mössbauer spectrum of a Fougèrite sample at 78 K (**a**) compared with the spectrum of a synthetic oxidized green rust sample with the same Fe^{3+} molar fraction x (**b**) Mössbauer spectrum of a green rust related sample from Trébeurden (**c**) and the spectrum of a similar sample from the Mont Saint Michel (**d**) (adapted from Ref. [307])

the bay of Mont Saint Michel (Normandy, France) [138] as can be seen from the example shown in Fig. 3.17d.

Structural studies on synthetic samples [133] suggest that long ranger order appears for $x = 1/3$, $x = 2/3$ and $x = 1$ which is confirmed by magnetic measurements showing a ferrimagnetic behavior for $x = 1/3$, $x = 2/3$ with Néel temperatures of 5 and 20 K respectively and being ferromagnetic for $x = 1$ with a Curie temperature around 80 K [139]. From these findings together with the appearance of typical doublets in the Mössbauer spectra Génin et al. [138] suggest that the intermediate samples consist in fact of topotaxically mixed domains of the ordered definite compounds. Therefore the natural green rust related minerals must be considered as a mixture of three basic minerals:

$$Fe_4^{2+}Fe_2^{3+}(OH)_{12}CO_3.3H_2O \ (x = 1/3);$$
$$Fe_2^{2+}Fe_4^{3+}(OH)_{10}O_2CO3.3H_2O \ (x = 2/3) \text{ and}$$
$$Fe_6^{3+}(OH)_8O_4CO_3.3H_2O \ (x = 1).$$

They suggest to redefine the first one as fougérite, whereas in the case of $x = 2/3$ and $x = 1$, the new mineral names "trébeurdenite" and "mössbauerite" are respectively proposed [138].

3.4 Sulfides, Sulfates and Carbonates

3.4.1 Sulfides

The most abundant and widespread sulfides are pyrite and marcasite. They both have the formula FeS_2 but the former crystallizes in a cubic structure whereas the latter is orthorhombic. They both contain divalent iron which is in a non-magnetic low spin state (Fe^{II}). Consequently the Mössbauer spectra (Fig. 3.18.) consist of a doublet with low isomer shifts and moderate quadrupole splittings [130].

Although the hyperfine parameters of natural marcasites and pyrites vary somewhat from sample to sample, probably due to chemical impurities, they can be unambiguously distinguished from their spectra. However, more problematic is to recognize the presence of these minerals among Fe^{3+}-containing clay minerals because of the similar range of hyperfine parameter values. Other marcasites exist with S replaced by Se or Te. They show hyperfine parameters comparable to those of the sulfides (Table 3.8). Löllingites ($FeAs_2$ and $FeSb_2$) and mispickel FeAsS, on the other hand, exhibit larger quadrupole splittings. Both the presence of formal Fe^{IV} and the very distorted structure are responsible for the high quadrupole splitting observed.

Another class of iron sulfides is $Fe_{1-x}S$ which crystallize in a hexagonal structure. Stoichiometric FeS, called troilite, is an antiferromagnet with $T_N = 595$ K. At RT the spectrum shows a hyperfine field of about 30.8 T and a positive quadrupole shift of $2\varepsilon \approx 0.3$ mm/s [144].

Most of the monosulfides, however, are not stoichiometric and natural samples consist often of a mixture of compounds with compositions between triolite, FeS and FeS_2, namely $Fe_{11}S_{12}$ ($x = 0.083$), $Fe_{10}S_{11}$ ($x = 0.091$), and Fe_9S_{10}

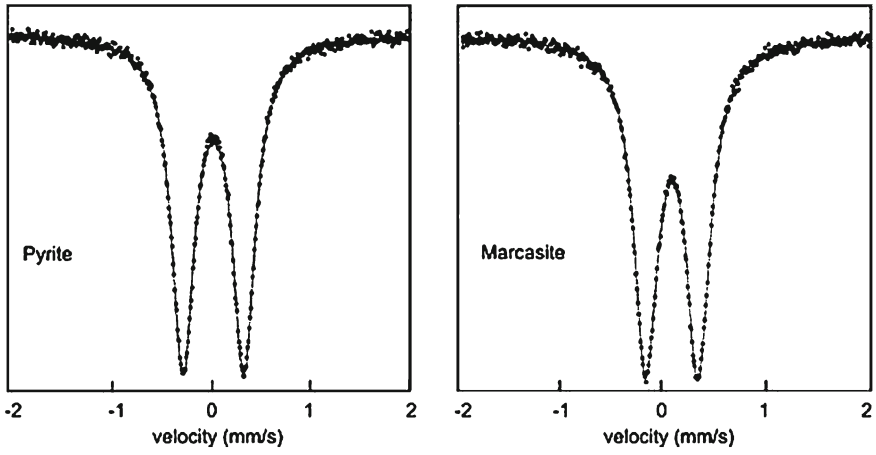

Fig. 3.18 RT spectrum of pyrite and marcasite (adapted from Evans et al. [130])

Table 3.8 RT hyperfine parameters of FeS_2 and related minerals

Mineral	Formula	δ_{Fe} (mm/s)	Δ (mm/s)
Pyrite	FeS_2	0.31	0.61
Marcasite	FeS_2	0.27	0.50
Marcasite (Se)	$FeSe_2$	0.40	0.58
Marcasite (Te)	$FeTe_2$	0.47	0.50
Löllingite (Sb)	$FeSb_2$	0.45	1.28
Löllingite (As)	$FeAs_2$	0.31	1.68
Mispickel	FeAsS	0.26	2.10

Table 3.9 Representative hyperfine parameters at RT of various sulfides

Mineral	Formula $Fe_{1-x}S$	B (T)	2ε or Δ (mm/s)	δ_{Fe} (mm/s)
Triolite	FeS	30–32	−0.3	0.7–0.9
Intermediate pyrrhotite	$Fe_{11}S_{12}$; $Fe_{10}S_{11}$ Fe_9S_{10} ($x = 0.83$; 0.091; 0.100)	22.0–23.5	0.05	0.55
		25.5–26.5	0.05	0.55
		27.5–31.5	0.10	0.55
Pyrrhotite monoclinic	Fe_7S_8 ($x = 0.125$)	22.9	0.08	0.77
		26.7	0.03	0.79
		31.1	0.15	0.79
		34.5	−0.09	0.81
Smythite	Fe_9S_{11} ($x = 0.182$)	22.4	0.33	0.58
		25.9	0.04	0.58
		30.3	0.17	0.47
Greigite	Fe_3S_4 ($x = 0.250$)	31.3	0.0	0.17
		31.3	−0.08	0.42
Mackinawite	$Fe_{1.01}S - Fe_{1.07}S$		(0.02)	(0)
Pentlandite	Fe_9S_8		0.36	0.30–0.37
			0.60–0.68	0

($x = 0.100$), These intermediate pyrrhotites all have a hexagonal structure based on NiAs exhibiting different kinds of ordering of the vacancies [110, 141, 142].

Concerning the magnetic properties the compounds close to FeS still exhibit an antiferromagnetic behavior, but from $x = 0.08$ on the presence of ferrimagnetism has been observed. It has been shown that from about that composition on, these sulfides undergo a 90° spin-flip resulting in a antiferro-ferrimagnetic transition, comparable to the transition in hematite [143, 144]. The Mössbauer spectra are usually complex and mainly consist of three to four overlapping sextets with subsequent hyperfine fields within ranges 22.0–23.5, 25.5–26.5 and 27.5–31.5 T which can be attributed to the various sites in the ordered structure [145, 146].

Pyrrhotite Fe_7S_8 ($x = 0.125$) is normally monoclinic and exhibits a ferrimagnetic behavior. The Mössbauer spectrum consists apparently of three overlapping sextets at RT, but at 80 K four sextets could be well resolved (see Table 3.9) with intensity ratio 2:1:2:2 according to the occupation in the structural model of Bertaut [139]. Similar hyperfine parameter values are obtained for a synthetic and a natural sample by Jeandey et al. [147].

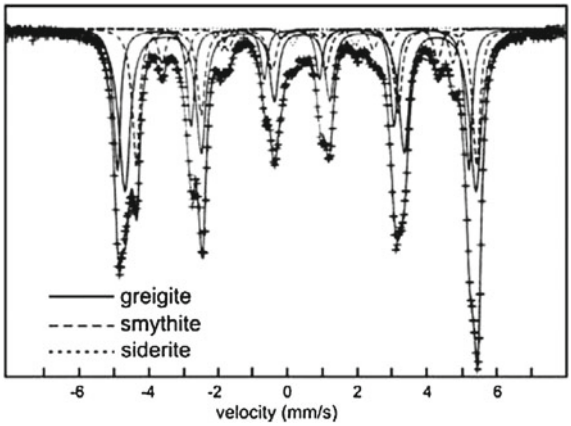

Fig. 3.19 RT spectrum of a natural greigite-smythite sample

Smythite is a hexagonal iron sulfide with composition close to Fe_9S_{11} ($x = 0.182$). There is still considerable doubt about the exact composition and whether it should be included as a separate phase in the iron-sulfur system. The Mössbauer spectra taken for some natural samples, containing other sulfides as well, reveal more or less three sextets [148] for the smythite phase, which are quite similar to three of the four sextets of pyrrhotite. Hoffmann et al. [149] also found three to four sextets but the one with the highest hyperfine field and nearly zero quadruple shift might be a sextet of greigite because the samples were from the same origin.

Greigite (Fe_3S_4, $x = 0.250$) is the sulfide analogue of magnetite and crystallizes in the cubic spinel structure. The RT spectrum exhibits an asymmetric sextet (Fig. 3.19) which is composed of two sextets: one arising from the A sites and one from the B sites with nearly equal hyperfine fields but different isomer shifts [148, 150] (Table 3.9). In contrast to magnetite, greigite does not show a Verwey transition [148, 151]. Because at higher temperature greigite transforms to pyrrhotite and FeS_2 the magnetic transition temperature cannot be determined, but lies above 480 K [148]. However, the magnetic properties are strongly dependent on the grain size [152].

Mackinawite, $Fe_{1+x}S$, with ($x = 0.01$–0.07) is a tetragonal iron sulfide with excess of iron. Morice et al. [153] reported a complex Mössbauer spectrum consisting of at least three sextets with hyperfine fields 29.8, 26.2 and 22.8 T and small quadrupole shifts of about 0.09, 0.06 and 0.09 mm/s respectively. On the other hand, only a singlet spectrum, even down to 4 K, has been observed by Vaughan and Ridout [154]. Probably the concentration of Co and Ni found to be present in the involved natural samples is decisive for the different magnetic behavior.

Pentlandite, $(Fe,Ni,Co)_9S_8$, has a face-centered cubic structure with iron and other metal atoms such as Ni and Co distributed among tetrahedral and octahedral sites. At RT the Mössbauer spectrum appears as an asymmetric doublet consisting of a quadrupole doublet with $\delta_{Fe} = 0.36$ and $\Delta = 0.30$–0.37 mm/s and an additional singlet with $\delta_{Fe} \approx 0.6$ mm/s, which is responsible for the asymmetry [155, 156].

3.4.2 Sulfates

Sulfates are known in nature as a series of minerals that are formed by oxidation of sulfides. Depending on the environment of formation they possess a different stage of hydration. Iron sulfates often accompany coal and are indicative of the weathering of the latter. Recently, a renewed interest for these minerals has been evoked in connection with the mineralogy on Mars, prospected by the Mars Exploration Rovers (MERs).

In recent years, the structural classification of the sulfates has been well established [157]. Sulfates consist predominantly of a polymerization of MO_6 octahedra, where M represents divalent or trivalent cations such as Fe^{2+}, Fe^{3+} and Mg^{2+}, Mn^{2+}, Zn^{2+}, Al^{3+}, etc.) and TO_4 tetrahedra where T stands for hexavalent or pentavalent cations such as S^{6+} and Mo^{6+}, P^{5+}, V^{5+}, etc.

The most common iron sulfate is szomolnokite, $FeSO_4.H_2O$. Other sulfates are the ferrous species rozenite, $FeSO_4.4H_2O$, and melanterite, $FeSO_4.7H_2O$, and the ferric species kornelite, $Fe_2(SO_4)_3.7H_2O$, and coquimbite $Fe_2(SO_4)_3.9H_2O$. Sulfates of mixed valence between ferrous melanterite and ferric kornelite are known as römerite. Another well-known mixed valence sulfate group is voltaite with formula $K_2Fe_5^{2+}Fe_3^{3+}Al(SO_4)_{12}.18H_2O$, but containing a large variety of substituting elements. A diversity of anhydrated sulfate minerals exists with general formula $MFe_3(SO_4)_3(OH)_6$ where $M = Na^+, K^+, \ldots$ being catalogued as jarosites.

Distortions of polyhedra are a common phenomenon in sulfates and result in different stereographic environments. Moreover, natural samples contain a diversity of cations other than iron, which also influences the local environment of the latter. Therefore, the Mössbauer spectra of iron sulfates usually exhibit one or more predominant doublets and some additional smaller doublets. Such spectra can either be fitted with discrete doublets or by quadrupole distributions (Fig. 3.20).

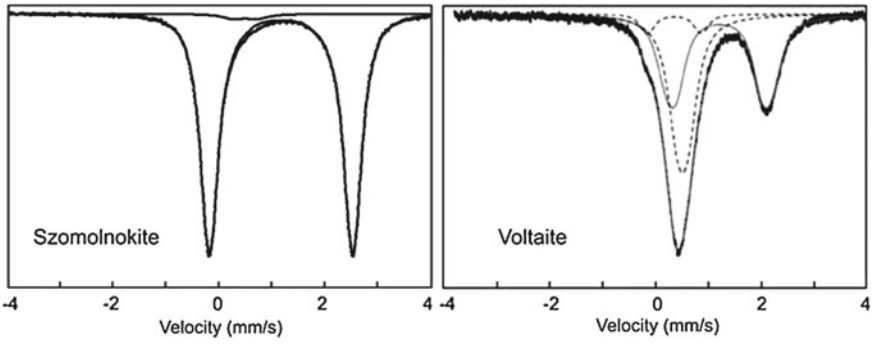

Fig. 3.20 RT spectra of some sulfates: szomolnokite (adapted from Van Alboom et al. 2009 [162]) and voltaite (adapted from Ertl et al. [161])

Table 3.10 Representative hyperfine parameters at RT of some iron sulfates

Mineral	Formula	Fe site	δ_{Fe} (mm/s)	Δ (mm/s)
Szomolnokite	$FeSO_4.H_2O$	Fe^{2+}oct	1.18–1.27	2.67–3.07
		(Fe^{2+} tetr)	0.23	0.69
		(Fe^{3+} oct)	0.55	0.38
Rozenite	$FeSO_4.4H_2O$	Fe^{2+} oct	1.27	3.33
		(Fe^{2+} oct)	0.37	1.15
		(Fe^{2+} tetr)	0.20	0.48
Melanterite	$FeSO_4.7H_2O$	Fe^{2+} oct	1.25–1.27	2.7–3.5
Kornelite	$Fe_2(SO_4)_3.7H_2O$	Fe^{3+} oct	0.47	0.45
		Fe^{2+} oct	1.18–1.32	1.57–1.62
		(Fe^{2+} tetr)	0.21	0.67
Coquimbite	$Fe_2(SO_4)_3.9H_2O$	Fe^{3+} oct	0.46–0.48	0.33–0.36
		(Fe^{3+} tetr)	0.1	0.67
Römerite	$FeSO_4.Fe_2(SO_4)_3.14H_2O$	Fe^{2+} oct	1.27–1.30	3.31
		Fe^{2+} oct	1.25–1.28	2.71–2.75
		Fe^{3+} oct	0.39–0.43	0.35–0.39
		(Fe^{3+} tetr)	0.1	0.66–0.84
Voltaite	$K_2Fe_8Al(SO_4)_{12}.18\ H_2O$	Fe^{2+} oct-M2	1.20	1.56–1.62
		Fe^{3+} oct-M1	0.50	0.13–0.18
		Fe^{3+} oct-M2	0.36	1.06–1.18
Jarosite	$KFe_3(SO_4)_3(OH)_6$	Fe^{3+} oct	0.38	1.23

Table 3.10 summarizes representative hyperfine parameters for a number of sulfate minerals. The data are taken from various authors as collected by Stevens et al. [158] and from others [159–162].

Apparently, four kinds of doublets may be encountered in sulfates: one or two Fe^{2+} doublets with hyperfine parameters in the range $\delta_{Fe} = 1.1–1.3$ mm/s and $\Delta = 2.6–3.3$ mm/s; one Fe^{2+} doublet with $\delta_{Fe} \approx 0.2$ and $\Delta = 0.65–0.70$ mm/s; one Fe^{3+} doublet with $\delta_{Fe} = 0.3–0.5$ and $\Delta = 0.4–0.5$ mm/s and one Fe^{3+} doublet with $\delta_{Fe} = 0–0.1$ and $\Delta = 0.6–0.8$ mm/s.

3.4.3 Carbonates

Siderite, $FeCO_3$, has a rhombohedral structure and contains divalent iron in the high spin state. The magnetic structure is antiferromagnetic with a low Néel temperature of 38 K. At room temperature as well as at 80 K a doublet is observed with hyperfine parameters $\delta_{Fe} = 1.2$ mm/s, $\Delta = 1.79$ mm/s at RT and $\delta_{Fe} = 1.36$ mm/s, $\Delta = 2.04$ mm/s at 80 K. In contrast to X-ray diffraction the Mössbauer spectra are not distinctively influenced by substitution of Mg and Mn for Fe [163], although there are indications that Ca^{2+} provokes an asymmetry in the lineshape, pointing to a second doublet with larger quadrupole splitting [66]. The siderite spectra are mostly asymmetric, namely, one line is deeper than the other one, whereas the widths are the

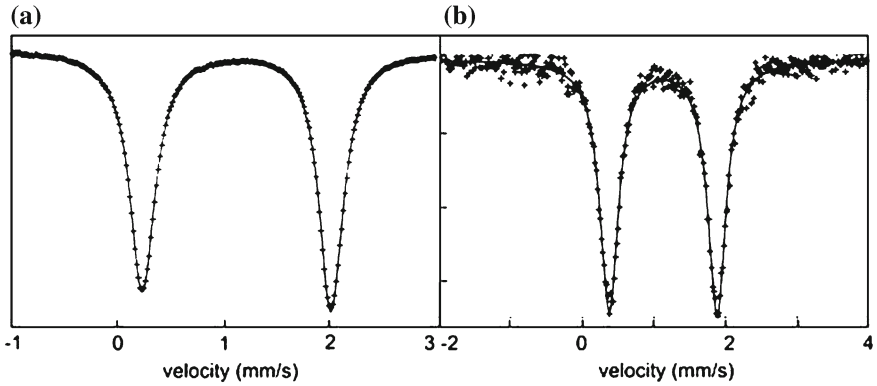

Fig. 3.21 RT Mössbauer spectra of siderite (**a**) and ankerite under the magic angle (**b**) (after De Grave and Vochten [166])

same (Fig. 3.21a). This feature was firstly explained as due to the so-called Goldanskii-Karayagin effect [164] being an anisotropy in the Mössbauer fraction. However, measurements under the so-called "magic angle", i.e. the absorber placed under an angle of 54 degrees with the gamma ray direction [165], yielded nearly equal intensities for both doublet lines pointing to texture effects as the reason for the asymmetry. At very low temperatures the magnetic transition is not sharply displayed in the Mössbauer spectra because of relaxation effects [166].

Ankerite, $CaFe(CO_3)_2$, has a similar rhombohedral structure as siderite but with calcium and iron in alternate positions. In natural ankerites the composition deviates always from the ideal one through the presence of considerable amounts of Mg and Mn. The magnetic transition temperature is much lower than for siderite and in a range of more than 10 K below the transition complicated spectra are observed due to spin–lattice relaxation [167, 168]. Anyway, a long-range order was not observed down to 1.7 K [169]. The spectra at RT and 80 K consist similarly to siderite of a single doublet (Fig. 3.21b), which is mostly asymmetric, most probably also as a result of preferential orientation of the crystallites in the absorber. The isomer shift is about the same as for siderite, but, the quadrupole splitting is somewhat smaller and amounts to 1.44–1.48 mm/s at RT, depending on the composition [170].

3.5 Silicates

3.5.1 Introduction

Silicate minerals are all structurally derived from the tetrahedral bonding of silicon to oxygen. For a relatively small group of these minerals, the structure consists of discrete orthosilicate anions SiO_4^{4-}, but, in the vast majority, the SiO_4 tetrahedra

are joined by oxygen sharing into chains or sheets. Apart from the silicon, they all further contain monovalent, divalent and trivalent metal ions of which a substantial amount of Fe^{2+} and Fe^{3+} can be present. Therefore, Mössbauer studies in silicate mineralogy have already been started in the early days of the application of the Mössbauer effect. The power of the Mössbauer technique resides in the ability to determine qualitatively and quantitatively the iron in the different lattice sites with their specific valence and the distortion of their environments. This has been well demonstrated in the numerous publications of G.M. Bancroft, Roger.G. Burns, M. Darby Dyar, Stefan S. Haffner, Georg Amthauer, Victor A. Drits… and their respective co-workers. Dyar et al. [150] have composed a comprehensive list of the hyperfine parameters of a large variety of silicates.

Commonly, silicates are only magnetic at very low temperatures and hence their MS recorded at RT and at 80 K generally consist of doublets. Moreover, the divalent and trivalent iron cations are in the high spin state yielding comparable hyperfine parameters for a given Fe^{2+} or Fe^{3+} site in various minerals. This means that distinct doublets due to a particular valence, if present in a given spectrum, may strongly overlap and are sometimes difficult to resolve. Furthermore, absorbers from silicates that are crystallized in chains or sheets may be subject to texture effects resulting in a different intensity of the two lines of a given doublet component. All this makes MS not so powerful as far as direct identification of silicates is concerned and one has to rely on the results of other techniques such as X-ray diffraction. Nevertheless, a better resolution for the Fe^{2+} doublets in particular can often be obtained from measurements at several temperatures because of the divergent variation of the quadrupole splitting with temperature for the different ferrous sites. Further, asymmetry in the doublets can be avoided by a suitable absorber preparation eliminating texture effects to a large extent. If necessary, measurements under the so-called “magic angle”, i.e. with the absorber at 54 degrees with respect to the direction of the γ-ray, may also be helpful in that respect.

From the spectral data of silicates some general rules can be put forward:

- the Fe^{2+} and Fe^{3+} oxidation states are usually easily distinguished
- the isomer shift for Fe^{2+} ions in silicates depends both on coordination number and symmetry in the following order: δ (square planar) $\ll \delta$ (tetrahedral) $\ll \delta$ (octahedral) $\ll \delta$ (dodecahedral); δ shows a linear relation with bond distance and bond strength
- the quadrupole splitting of octahedral Fe^{2+} is very sensitive to site symmetry and generally decreases with increasing distortion, due to the lattice contribution being opposite to the dominant valence contribution.

According to the way of stacking the SiO_4 tetrahedra, the silicates are usually divided into different classes (Fig. 3.22): nesosilicates (single tetrahedra), sorosilicates (double tetrahedra), cyclosilicates (tetrahedra joined to rings), inosilicates (tetrahedra joined to single or double chains), phyllosilicates (sheets of tetrahedra) and tektosilicates (three dimensional stacking of tetrahedra). This classification

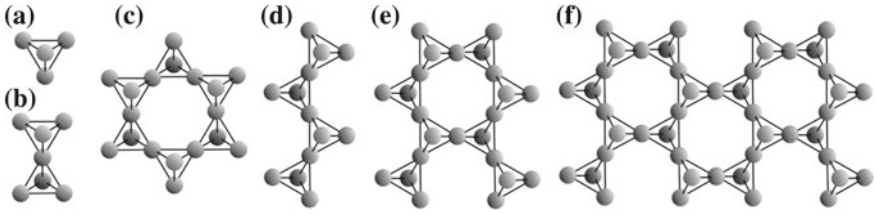

Fig. 3.22 SiO_4 stacking in silicates (only O atoms are shown): **a** Nesosilicates, **b** sorosilicates, **c** cyclosilicates, **d**, **e** inosilicates, **f** phyllosilicates

will henceforward be adopted for further discussion of the specific silicate minerals.

3.5.2 Nesosilicates

Nesosilicates is the class of silicate minerals in which the structure is built up by independent tetrahedra of SiO_4. This class contains some mineral groups like the olivines, the silicate garnets, the epidote group and some separate minerals.

3.5.2.1 Olivines

Olivines consist of independent SiO_4 tetrahedra surrounded by six-coordinated metal cations in two distinct sites M1 and M2. Mössbauer studies of the forsterite-fayalite (Mg_2SiO_4-Fe_2SiO_4) and fayalite-tephroite (Fe_2SiO_4–Mn_2SiO_4) series all revealed at RT a simple doublet with a quadrupole splitting Δ in the range 2.80–3.02 mm/s and an isomer shift $\delta_{Fe} = 1.16$–1.18 mm/s [171]. The doublet is often asymmetric with different line widths and depths indicating the presence of two doublets, one arising from M1 and the other one from M2 sites [172]. However, these doublets overlap to such a large extent that they can hardly be separated in the spectrum analysis. At high temperatures (1000 K) a separation of both doublets can be possible. Fayalite itself orders antiferromagnetically below 66 K, and becomes towards forsterite at a lower composition-dependent temperature a canted antiferromagnet [173–175]. At very low temperatures two distinct magnetic patterns are observed with B of 12.0 and 32.3 T [176, 177].

A mixed-valence iron olivine is laihunite (ferrifayalite) with ideal composition $Fe^{2+}Fe^{3+}(SiO_4)_2$. In this olivine species Fe^{2+} occupies M1 sites, alternated with vacancies, whereas Fe^{3+} occupies the M2 sites. Due to the difference in oxidation state two well resolvable doublets are observed with $\delta_{Fe} = 0.39$ mm/s and $\Delta = 0.91$ mm/s for Fe^{3+} and $\delta_{Fe} = 1.13$ mm/s and $\Delta = 2.75$ mm/s for Fe^{2+} [178]. Ferrifayalite often occurs as an intergrowth of fayalite and laihunite [179] (Table 3.11, 3.12, and 3.13).

Table 3.11 Representative hyperfine parameters at RT for some olivines

Mineral	Formula	Fe site	δ_{Fe} mm/s	Δ (mm/s)
Fayalite	$(Fe^{2+})_2SiO_4$	Fe^{2+} M1,M2	1.17	2.81
Fayalite-forsterite-tephroite	$(Fe^{2+},Mg,Mn)_2SiO_4$	Fe^{2+} M1,M2	1.16–1.18	2.80–3.02
Laihunite	$(Fe^{2+}, Fe^{3+},)_2SiO_4$	Fe^{2+} M1	1.13–1.16	2.75–2.83
		Fe^{3+} M2	0.37–0.43	0.85–0.91

Table 3.12 Representative hyperfine parameters at RT for some garnets

Mineral	Formula	T (K)	Fe site	δ_{Fe} (mm/s)	Δ (mm/s)
Almandine	$(Fe^{2+})_3Al_2(SiO_4)_3$	RT	Fe^{2+} dodec	1.28	3.51
		77		1.43	3.66
Pyrope-almandine	$(Mg,Fe^{2+})_3Al_2(SiO_4)_3$	RT	Fe^{2+} dodec	1.20–1.30	3.47–3.70
		77		1.33–1.44	3.47–3.70
Spessartine	$(Mn,Fe^{2+})_3Al_2(SiO_4)_3$	RT	Fe^{2+} dodec	1.28	3.52
		77		1.42	3.64
Andradite	$Ca_3(Al,Fe^{3+})_2(SiO_4)_3$	RT	Fe^{3+} oct	0.41	0.5–0.6
		77		0.50	0.5–0.6
Almandine-grossular	$(Ca,Fe^{2+})_3(Al,Fe^{3+})_2(SiO_4)_3$	RT	Fe^{2+} dodec	1.20–1.30	3.47–3.70
		77	Fe^{3+} oct	0.35–0.45	0.29–0.75
			Fe^{2+} dodec	1.33–1.44	3.47–3.70
			Fe^{3+} oct	0.42–0.52	0.26–0.64
Titano-andratite	$Ca_3(Fe^{3+},Ti,Si)_2(SiO_4)_3$	RT	Fe^{3+} tetr	0.20	1.15
		77	Fe^{3+} oct	0.40	0.75
			Fe^{3+} tetr	0.30	1.15
			Fe^{3+} oct	0.50	0.75

Table 3.13 Representative hyperfine parameters at RT for some other nesosilicates

Mineral	Formula	Fe site	δ_{Fe} (mm/s)	Δ (mm/s)
Epidote	$Ca_2(Fe^{3+},Al)_3O(OH)(Si_2O_7)(SiO_4)$	Fe^{3+} M3	0.34–0.36	1.9–2.1
Piemontite	$Ca_2(Fe^{3+},Mn,Al)_3O(OH)(Si_2O_7)(SiO_4)$	Fe^{3+} M3	0.34–0.36	2.05–2.10
		Fe^{3+} M1	0.29–0.33	0.9–1.1
Allanite	$(Ca,RE)_2(Fe^{3+},Al)_3O(OH)(Si_2O_7)(SiO_4)$	Fe^{3+} M3	0.37	1.97
		Fe^{3+} M1	0.29	1.33
		Fe^{2+} M3	1.07	1.66
		Fe^{2+} M1	1.24	1.93
Staurolite	$(Fe,Mg,Zn)_2Al_9(Si,Al)_4O_{20}(OH)_4$	Fe^{2+} tetr	0.98 (av)	2.45 (av)
		Fe^{2+} tetr	0.98 (av)	2.10 (av)
		Fe^{2+} tetr	0.97 (av)	1.6 (av)
		Fe^{3+} tetr	0.15 (av)	0.7 (av)

3.5.2.2 Garnets

The most important iron and silicon containing garnet minerals are the pyrope-almandine series $(Mg,Fe^{2+})_3Al_2(SiO_4)_3$ and andradite $Ca_3(Al,Fe^{3+})_2(SiO_4)_3$. When Mg is replaced by Mn the garnet is called spessartine $(Mn,Fe^{2+})_3Al_2(SiO_4)_3$. The garnet structures contain SiO_4 tetrahedra with commonly trivalent cations in 6-coordination and divalent cations in 8-coordination.

Members of the pyrope-almandine series exhibit a doublet at RT with an isomer shift $\delta_{Fe} = 1.2–1.4$ mm/s and a very large quadrupole splitting Δ in the range 3.47–3.70 mm/s [180]. An additional doublet of Fe^{3+} due to the six-fold coordinated Al site is observed with $\delta_{Fe} = 0.35–0.45$ mm/s and $\Delta = 0.29–0.75$ mm/s when going from almandine towards andradite. These intermediate minerals are often called grossular. Pure almandine orders magnetically around 10 and at 4 K an Fe^{2+} octet is observed with a hyperfine field of 23–24. 5 T [181]. The typical large quadrupole splitting in garnets is shown in the spectrum of spessartine in Fig. 3.23.

Andradite possesses at RT the typical Fe^{3+} hyperfine parameters, namely $\delta_{Fe} = 0.39–0.41$ mm/s and $\Delta = 0.5–0.6$ mm/s [180]. The latter is, however, strongly dependent on the composition. It orders magnetically below 11 and at 4 K the hyperfine field amounts to 51.9 T [182]. Actually, the spectrum is asymmetric and can be analyzed with two sextets having different quadrupole shifts $2\varepsilon = 0.32$ and -0.16 mm/s, due to a complex spin structure with different orientations with respect to the EFG principal axis. In some garnets such as titanium andradite, $Ca_3(Fe,Ti,Si)_5O_{12}$, Fe^{3+} also occupies partly the tetrahedral Si sites, exhibiting very low isomer shifts and rather high quadrupole splittings [183].

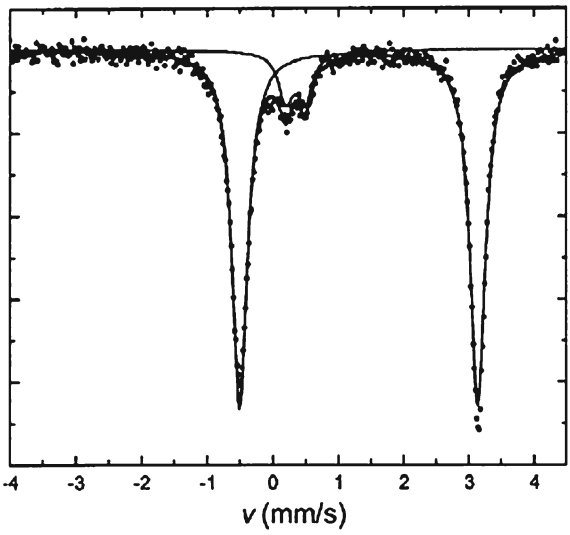

Fig. 3.23 RT spectrum of spessartine showing the predominant Fe^{2+} doublet with the typical large quadrupole splitting for garnets. The spectrum shows an additional small doublet from octahedral Fe^{3+} (after Eeckhout et al. [308])

3.5.2.3 Epidote Group

Epidote has the chemical formula $Ca_2(Fe,Al)_3O(OH)(Si_2O_7)(SiO_4)$. The structure is mainly monoclinic and consists of Al oxide and hydroxide chains linked by single-tetrahedra SiO_4 and double-tetrahedra Si_2O_7. Because of the presence of the latter the epidotes can also be placed under the class of sorosilicates. The Fe^{3+} is mainly located in a very irregular polyhedron called M3 site and hence, unusually large quadrupole splittings in the range 1.9–2.1 mm/s are observed for Fe^{3+}, whereas the isomer shifts 0.34–0.36 mm/s clearly reflects the trivalent state [184–187]. Epidotes have a large variety in chemical composition and trivalent iron has also been found to be present in the more regular octahedral M1 and M2 sites. Also, Ca can partly be substituted by trivalent rare earth elements (RE), such as Ce^{3+}, with simultaneously Fe^{2+} substituting for Al^{3+} to make up the charge balance. Such minerals are called allanites. In the latter some part of Fe^{3+} occupies the M1 sites, whereas also Fe^{2+} is present on both sites yielding four doublets [185].

3.5.2.4 Staurolite

Staurolite belongs to the so-called subsaturate group of nesosilicates because it has in its structure additional oxygen ions to those forming the SiO_4 tetrahedra. The chemical composition is rather complex and can be written as $(Fe,Mg,Zn)_2Al_9(Si,Al)_4O_{20}(OH)_4$. It crystallizes in a monoclinic structure with Fe^{2+} located in different tetrahedral coordinations, having average hyperfine parameters: $\delta_{Fe} \approx 0.98$ mm/s and $\Delta \approx 2.3$ mm/s [184, 188]. Fe^{3+} was found to be present with $\delta_{Fe} \approx 0.20$ mm/s and $\Delta \approx 0.60$ mm/s [188]. However, a more thorough analysis revealed the appearance of up to six doublets in the spectra [189].

3.5.3 Sorosilicates

Sorosilicates consist of double tetrahedral Si_2O_7 units and are relatively uncommon. Representative minerals in this class are the melilites and ilvaite.

3.5.3.1 Melilites

Melilites with chemical formula $(Ca,Na)_2(Mg,Fe^{2+},Fe^{3+},Zn,Al)(Si,Al)_2O_7$ possess a tetragonal structure. It consists of tetrahedral layers with cations (Ca, Na) halfway between adjacent layers. The layer modulation is incommensurate (Seifert et al. 1987). Well-known examples are gehlenite ($Ca_2Al(AlSiO_7)$), åkermanite ($Ca_2Mg(Si_2O_7)$) and hardystonite ($Ca_2Zn(Si_2O_7)$). Calcium occupies a dodecahedral site, whereas the other cations are distributed among two kinds of tetrahedral

sites T1 and T2, the latter being the normal silicon site. Fe^{3+} enters the melilites mainly the T1 site. The hyperfine parameters are $\delta_{Fe} \approx 0.2$ mm/s, $\Delta \approx 0.9$ mm/s for Fe^{3+} and $\delta_{Fe} \approx 1.00$ mm/s, $\Delta \approx 2.3$ mm/s for Fe^{2+}. Although it was suggested that a small amount of Fe^{3+} enters also the T2, it is finally found in ferric melilites that Fe^{3+} actually occupies two differently distorted T1 sites with $\delta_{Fe} \approx 0.19$ mm/s, $\Delta = 0.75$ and 1.04 mm/s [190].

3.5.3.2 Ilvaite

Ilvaite with chemical formula $CaFe_2^{2+}Fe^{3+}(Si_2O_7)O(OH)$ has an orthorhombic structure. Technically spoken, it can be considered as a subsaturated sorosilicate in view of the additional O^{2-} and OH^- groups. The structure can be described as ribbons of double rows of edge-shared octahedra consisting of five oxygens and one hydroxyl anion and designated as M1(8d) sites. Above and below the ribbons are octahedral M2(4c) sites with solely oxygen surrounding. It was later found that low-impurity ilvaite possesses a slightly monoclinic structure with two M1 sites, M11 and M12, and becoming orthorhombic with increasing substitution (e.g. by Mn^{2+}) and temperature [191]. Iron enters all the octahedral sites. The Mössbauer spectra show globally three absorption peaks (Fig. 3.24) which can essentially be analyzed with 3 doublets, one for Fe^{2+} in M11 site, one for Fe^{3+} in M12 site and one for Fe^{2+} in M2 [192, 193]. Representative hyperfine parameters are listed in Table 3.14.

On the other hand, two additional doublets are sometimes introduced to account for Fe^{2+}–Fe^{3+} electronic relaxations [194, 195], in particular for Mn-rich ilvaites [196]. The appearance of only two doublets in Mn-rich ilvaites at higher temperatures indicates a collapse to $Fe^{2.5+}$ in the M1 site, so that in the intermediate temperature region a relaxation process occurs which significantly broadens the central absorption peak [197].

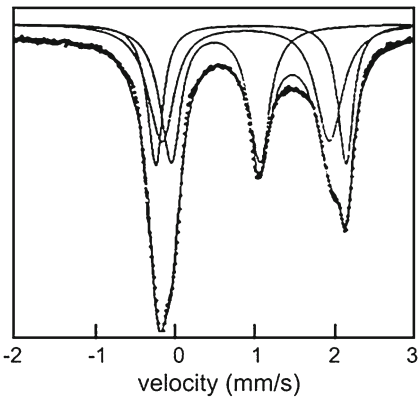

Fig. 3.24 Typical RT spectrum of ilvaite (adapted from Dotson and Evans [193])

Table 3.14 Representative hyperfine parameters at RT for some sorosilicates

Mineral	Formula	Fe site	δ_{Fe} (mm/s)	Δ (mm/s)
Melilite	$(Ca,Na)_2(Mg,Fe^{2+},Fe^{3+},Zn,Al)(Si,Al)_2O_7$	Fe^{2+} T1,T2	≈1.00	2.3
	$(Ca,Na)_2(Mg,Fe^{3+})(Si_2O_7)$	Fe^{3+} $T1_1$	0.19	0.75
		Fe^{3+} $T1_2$	0.19	1.04
Ilvaite	$CaFe_2^{2+}Fe^{3+}(Si_2O_7)O(OH)$	Fe^{2+} M2	≈1.05	2.30–2.50
		Fe^{2+} M11	≈1	2.10–2.20
		Fe^{3+} M12	0.55	1.1–1.3

3.5.4 Cyclosilicates

The most common structural motif in the group of cyclosilicates is the six-membered Si_6O_{18} ring, as been found in beryl and tourmaline. The Mössbauer spectra of these minerals present a number of features that have remained incompletely understood for a long time.

Beryl has a hexagonal structure composed of a stacking of rings forming channels parallel to the *c*-axis. These columns are linked by Al^{3+} and Be^{2+} in six- and four-fold coordination, respectively. The ideal formula is $Be_3Al_2Si_6O_{18}$. The iron contents in these minerals are small and usually less than 1 wt %. In general, the Mössbauer spectrum consists of a broad peak near zero velocity and a sharp line near 2.5 mm/s. This particular spectral behavior has been attributed to an unspecified relaxation process. At low temperatures two well resolved ferrous doublet spectra are observed. At 4 K the hyperfine parameters are $\delta_{Fe} = 1.3$ mm/s, $\Delta = 2.7$ mm/s and $\delta_{Fe} = 1.0$ mm/s, $\Delta = 1.5$ mm/s, respectively [198]. The first doublet has been assigned to octahedral Fe^{2+} whereas the second less intense one represents substitutional Fe^{2+} in the highly distorted Be^{2+} tetrahedral sites. Additionally, small amounts of Fe^{3+} are located in the octahedral Al^{3+} sites. In a sample of deep-bleu beryl a fourth doublet has been resolved and assigned to Fe^{2+} in the channels [199].

Cordierite with ideal formula $Al_3(Fe^{2+})_2(AlSi_5)O_{18}$ is structurally similar to beryl. The principal octahedral cations are Fe^{2+} and some Mg instead of Al. The spectra of both magnesium and iron cordeirites exhibit spectra consisting of a predominant ferrous doublet with $\delta_{Fe} = 1.15$ mm/s and $\Delta = 2.3$ mm/s. A second, much weaker, ferrous component is observed which was attributed to channel iron [200]. However, this second has also been interpreted as being due to Fe^{2+} replacing Al, whereas Na enters the center of the rings [201].

Tourmalines have a complex structure which includes Si_6O_{18} rings, BO_3 groups, spiral chains of $AlO_5(OH)$ octahedral (C) sites and edge-sharing clusters of three $MgO_4(OH)_2$ octahedral (B) sites. The ideal formula would be $X(Y_3Z_6)(Si_6O_{18})(BO_3)_3(OH)_3(OH,F)$ with X = Na, but also K, Ca or vacancies, Y = Mg, but also Fe, Mn, Al, Fe, Cr, Ti and Z = Al, but also Cr, and V. Due to the large variety of cations in this structure a wide variety of spectra have been reported. The most common tourmalines are within the elbaite-schorl series

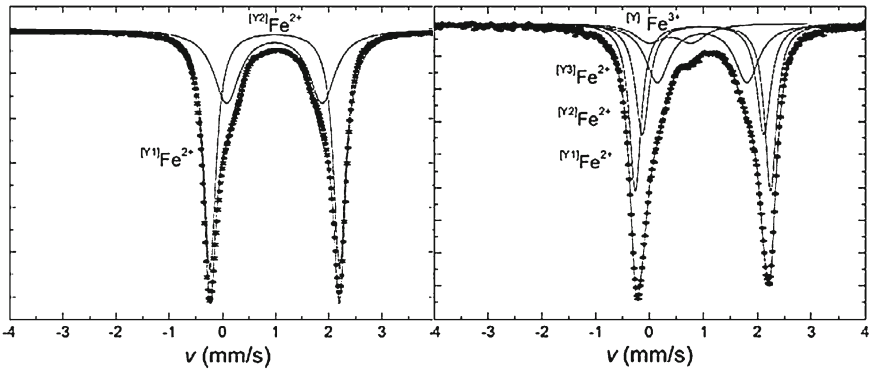

Fig. 3.25 RT spectra of some tourmalines from the English Lake District which needed to be fitted with 2 to 4 doublets (adapted from Eeckhout et al. [207])

Table 3.15 Representative hyperfine parameters at RT for cyclosilicates

Mineral	Formula	Fe site	δ_{Fe} (mm/s)	Δ (mm/s)
Beryl	$Be_3Al_2Si_6O_{18}$	Fe^{2+} oct	1.16	2.70
		(Fe^{3+} oct)	0.59	0.86
Cordierite	$Al_3(Fe^{2+})_2(AlSi_5)O_{18}$	Fe^{2+}	1.15	2.3
Tourmaline (schorl)	$Ca(Fe^{2+})_3]Al6(Si_6O_{18})(BO_3)_3OH)_3(OH)$	Fe^{2+} Y1	1.08–1.10	2.50
		Fe^{2+} Y2	1.07–1.10	2.20–2.35
		Fe^{2+} Y3	1.07–1.10	1.40–1.70
		+ other D		

$[Na(Li_{0.5}Al_{0.5})_3$-$Ca(Fe^{2+})_3]Al_6(Si_6O_{18})(BO_3)_3(OH)_3(OH)$- and the dravite-schorl series $[Na(Mg)_3$- $Ca(Fe^{2+})_3]Al_6(Si_6O_{18})(BO_3)_3(OH)_3(OH)$.

The spectrum of tourmaline consists basically of a quadrupole doublet with $\delta_{Fe} = 1.1$ mm/s and $\Delta = 2.46$–2.48 mm/s originating from Fe^{2+} on the B (Y) sites. Although this doublet is dominant in most of the spectra in tourmalines, other doublets are clearly observed which have been attributed to Fe^{2+}, Fe^{3+} and intermediate Fe^{n+} (from electron exchange processes). Additional iron in C (Z) sites and a cis–trans isomerism in B (Y) sites may render the spectra rather complicated leading up to five or even seven components to be used in the fits [202–207]. RT spectra of some tourmalines are displayed in Fig. 3.25 (Table 3.15).

3.5.5 Inosilicates

The inosilicate minerals are built up by chains of SiO_4 tetrahedra. They can further be divided into two subclasses: the pyroxenes with single-stranded chains, having an overall composition SiO_3^{2-} and the amphiboles with double-stranded chains of $Si_4O_{11}^{6-}$ stoichiometry.

3.5.5.1 Pyroxenes

Pyroxenes have the general formula $X(Y)(SiO_3)_2$. They crystallize in a monoclinic (clinopyroxenes) or orthorhombic (orthopyroxenes) structure. The Y cations are located in the M1 sites which are moderately distorted octahedra whereas X represents cations in highly distorted sites with six-, seven- or eight-fold coordination according to the kind of mineral. Generally, the structure is orthorhombic when X is Mg or Fe^{2+} and is monoclinic when X is Ca or Na.

Orthopyroxenes have compositions close to the enstatite-ferrosilite $MgSi_2O_6$–$FeSi_2O_6$ tie line. The spectra consist of two ferrous doublets, which can be clearly resolved (Fig. 3.25). The one with the small quadrupole splitting (see Table 3.16) can be assigned to the distorted M2 sites [208]. In the $(Mg,Fe)Si_2O_6$ series this doublet remains rather intense evoking the preference of iron for the M2 sites. [209].

A larger variety of crystal chemistry is possible in the clinopyroxenes. Besides the compositions on and close to the diopside-hedenbergite $CaMgSi_2O_6$-$CaFeSi_2O_6$ tie line (augites) there exist sodium pyroxenes such as jadeite $NaAlSi_2O_6$, aegirine $NaFe^{3+}Si_2O_6$ (also called acmite), kosmochlor $NaCrSi_2O_6$ and jervisite $NaScSi_2O_6$, lithium pyroxenes as spodumene $LiAlSi_2O_6$, monoclinic forms of enstatite and ferrosilite (clinoenstatite and clinoferrosilite) and of course all compositions between them of which some received mineral names like omphacites $(Ca,Na)(Fe^{2+},Fe^{3+},Mg,Al)Si_2O_6$ and pigeonites $(Ca,Fe^{2+},Mg)(Fe,Mg)Si_2O_6$. Ca-free clinopyroxenes along the $MgSiO_3$–$FeSiO_3$ tie line only exist under high pressure in the earth crust [210] (Fig. 3.26).

The Mössbauer spectra of the diopside-hedenbergite series are straightforward and predominantly consist of a ferrous doublet (Fig. 3.27a) for which the quadrupole splitting Δ varies between 2.30 and 1.85 mm/s (Table 3.16), decreasing on going from hedenbergite to diopside. [211–213]. Deviations from stoichiometry introduce a small amount of an Fe^{2+} doublet from M2 sites and a weak Fe^{3+} doublet. Because the quadrupole splitting of the M1 doublet is strongly temperature dependent whereas the one of the M2 doublet remains invariant at about 2.0 mm/s, measurements at various temperatures are usually necessary to resolve both doublets. Trivalent iron can also be introduced to some extent in diopside, thus substituting for Mg and Si.

Table 3.16 Table Representative hyperfine parameters at RT for some pyroxenes

Mineral	Formula	Fe site	δ_{Fe} (mm/s)	Δ (mm/s)
Ferrosilite	$Fe_2Si_2O_6$	Fe^{2+} M1	1.17	2.48
		Fe^{2+} M2	1.13	1.93
Enstatite- ferrosilite	$(Mg,Fe^{2+},Mn)_2Si_2O_6$	Fe^{2+} M1	1.15–1.18	2.35–2.69
		Fe^{2+} M2	1.12–1.16	1.91–2.13
Hedenbergite	$CaFe^{2+}Si_2O_6$	Fe^{2+} M1	1.19	2.20
		(Fe^{3+}M1)	0.34	0.68
Diopside-hedenbergite	$Ca(Mg,Fe^{2+})Si_2O_6$	Fe^{2+} M1	1.19	1.85–2.30
Aegerine	$(Na,Li)Fe^{3+}Si_2O_6$	Fe^{3+} M1	0.39	0.30

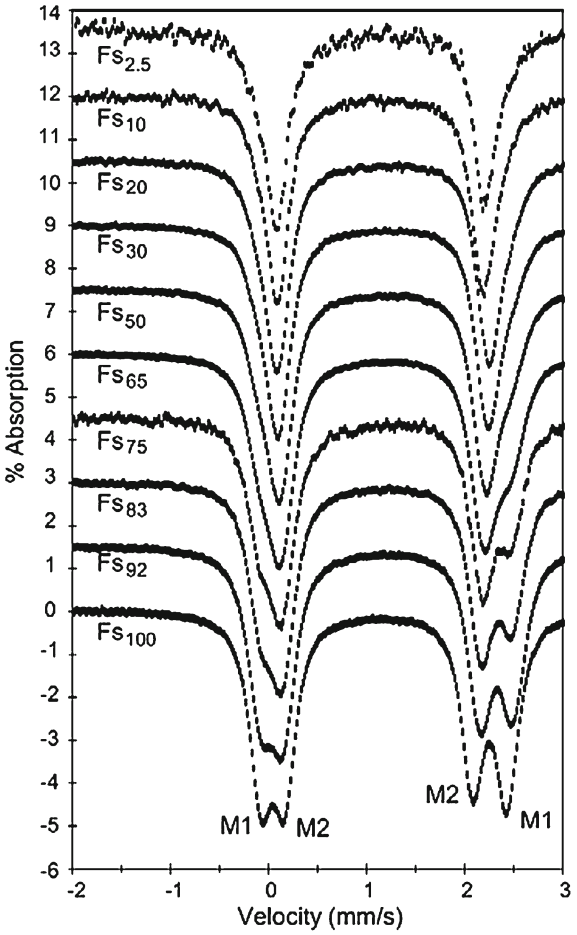

Fig. 3.26 RT Mössbauer spectra of synthetic samples of the enstatite-ferrosilite series showing a gradual increase of Fe^{2+} on M1 sites (from Dyar et al. [209])

Ca–Fe pyroxenes with compositions between hedenbergite and clinoferrosilite $(Ca,Fe^{2+})(Fe^{2+})Si_2O_6$ show structure in their spectra which requires more than two ferrous doublets for an adequate fit [214]. The observed subspectra may arise from the different numbers of iron and calcium neighbors on the three M3 sites. Even a more distinct structure is observed in the omphacites in which the distribution of the charges among the neighboring M2 sites (Ca^{2+} and Na^{+}) has a large effect on the Fe^{2+} located in the M1 sites [215].

Aegirine $NaFe^{3+}Si_2O_6$ shows a ferric doublet with $\delta_{Fe} = 0.39$ mm/s and $\Delta = 0.30$ mm/s (Fig. 3.27b). Replacing Na by Li causes a change in coordination number from eight to six for M2 sites, but has no effect on the hyperfine parameters. Systematic studies of solid solutions of aegirine with diopside, hedenbergite, kosmochlor and $LiFeSi_2O_6$ showed that neither δ nor Δ changes markedly as long as the valences of the neighboring cations of Fe remain unaltered. Whenever ions of different valences are mixed on the same site electron

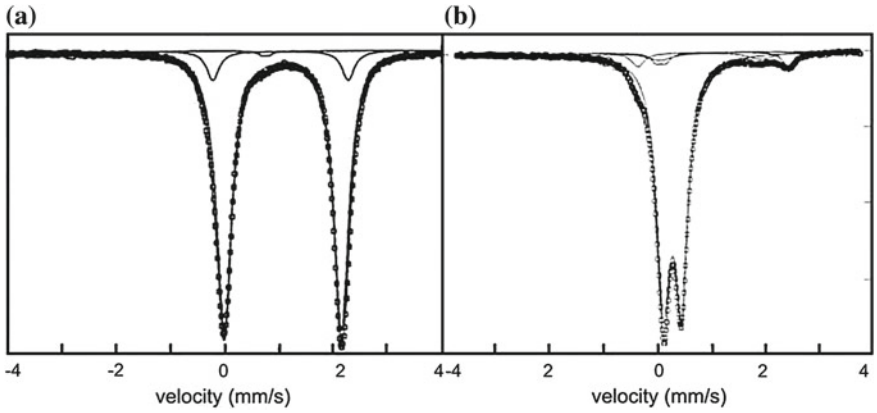

Fig. 3.27 RT spectra of hedenbergite (**a**) and aegirine (**b**)

hopping occurs [197, 216] and consequently the quadrupole splitting depends strongly on the composition.

Beside the clino- and orthopyroxenes there exists a group of minerals with similar chemical compositions of pyroxenes called pyroxenoids. There structures are based on twisted chains of silica tetrahedra. An example is rhodonite $(Mn,X)SiO_3$ (X = Fe, Ca, Mg), which contains five different sites: three moderately and one strongly distorted octahedral sites and one seven-fold coordinated site. Spectra of rhodonite and fowlerite (Zn-rich rhodonite) needed to be adjusted with five doublets showing Fe^{2+} to be present in all the available sites [217, 218].

Other minerals, which are structurally similar to pyroxenes except that the octahedral strips form zigzags, are carpholites, $(Mn, Fe^{2+})Al_2(Si_2O_6)(OH)_4$. In these mineral species the ferrous iron is found to be in a M2 position that is virtually undistorted. Consequently a very large quadrupole splitting of 3.20 mm/s is observed [209, 210].

3.5.5.2 Amphiboles

The amphiboles consist structurally of double Si_4O_{11} chains parallel to the orthorhombic or monoclinic *c* axis. The general formula of the amphiboles is $W_xX_2(Y_5)(Si_4O_{11})_2(OH)_2$ in which Y represents the octahedral M1, M2 and M3 sites, X denotes the cation in the irregular M4 site, similar to the M2 site in pyroxenes, and W is the cation in the ten- to 12-fold coordinated A site which resembles the interlayer sites in micas. The A site is often empty. Similarly to the pyroxenes the M4 site can accommodate Ca, Na, Li, Mg and Fe^{2+} and the M1–M3 sites are occupied by Fe^{2+}, Mg, Fe^{3+}, Al, Mn,… The A site, if occupied, accommodates large monovalent ions such as Na or K. The relative abundances of the various sites M1:M2:M3:M4:A is 2:2:1:2:*x* with $0 \ll x \ll 1$.

The iron end member of the amphiboles is monoclinic grunerite $Fe_7Si_8O_{22}(OH)_2$ with Fe^{2+} filling the M1–M4 sites. The spectra consist of two doublets, an intense one with somewhat broadened lines arising from three non-resolvable doublets corresponding to iron on the M1–M3 sites and the other one to iron on the M4 sites. The hyperfine parameters are $\delta_{Fe} = 1.16$ mm/s, $\Delta = 2.82$ mm/s and $\delta_{Fe} = 1.10$ mm/s, $\Delta = 1.8$ mm/s, respectively [184].

Anthophyllite, $(Mg_2)[Mg_7](Si_8O_{22})(OH)_2$, is orthorhombic and when substitututed with iron shows similarly two resolved doublets for M1–M3 and M4 sites, respectively, with most of the iron occupying the latter. From the degree of Fe/Mg disorder the rock's cooling rate can be determined [219]. The solid solutions between grunerite and anthophyllite are monoclinic up to 70 % anthophyllite. The members of the monoclinic cummingtonite-grunerite series, $(Fe,Mg,Mn)_7Si_8O_{22}(OH)_2$, all show double doublet spectra with hyperfine parameters similar to those of grunerite [220].

Gedrite is an orthorhombic amphibole obtained from anthophyllite by substitution of some Mg and Si by Na and Al. The ideal formula is $Na_{0.5}(Mg_{5.5},Al_{1.5})(Si_6Al_2)O_{22}(OH)_2$ with Na entering the A sites. The spectrum of ferrous iron in gedrites exhibits a broadened doublet because the M1, M2 and M3 sites have no longer similar distortions from octahedral symmetry [221, 222]. The spectra can be fitted with three Fe^{2+} components and a weak Fe^{3+} component, but it remains difficult to assign unambiguously the subspectra to the different sites. Although there is a miscibility gap between anthophyllite and gedrite [223], some Al may substitute in the former and the main effect is to reduce Δ and increase the linewidth of the M1–M3 doublet with increasing Al content.

Holmquistite is another orthorhombic amphibole obtained from anthophyllite by substitution of some Mg by Li and Al, the lithium entering the M4 site. In a sample containing 1.44 iron atoms per formula unit two ferrous doublets could be resolved with $\delta_{Fe} = 1.13$ mm/s, $\Delta = 2.8$ mm/s and $\delta_{Fe} = 1.11$ mm/s, $\Delta = 2.0$ mm/s which were attributed to Fe^{2+} in M1 and M3 sites, respectively. Fe^{3+} and Al enter the M2 sites [224]. Holmquisite has also a monoclinic variant, which has a similar spectrum with comparable hyperfine parameters.

The calcic amphiboles, actinolites, are close to the tremolite-ferroactinolite, $Ca_2Mg_5Si_8O_{22}(OH)_2$–$Ca_2Fe_5Si_8O_{22}(OH)_2$, tie line. Ferrous iron is mainly present in the M1 and M3 sites yielding $\Delta = 2.8$–2.9 mm/s, but is also found in the M2 sites with $\Delta = 1.7$–1.9 mm/s [225]. However, the latter doublet with low Δ value has been assigned by Goldman [226] to Fe^{2+} at the M4 sites, whereas this author introduced an additional doublet with an intermediate $\Delta = 2.0 - 2.4$ mm/s for Fe^{2+} in the M2 sites. Ferric iron, if present, enters also the M2 sites.

Similarly to actinolites a solid solution series of sodic amphiboles exists along the line from glaucophane, $Na_2Mg_3Al_2Si_8O_{22}(OH)_2$, to riebeckite, $Na_2(Fe^{2+})_3(Fe^{3+})_2Si_8O_{22}(OH)_2$. The spectra are rather different from those of the actinolites in that the M1 and M3 subspectra are better separated and that a substantial contribution of an Fe^{3+} doublet is observed. The involved Fe^{3+} is believed to be mainly present in the M2 sites [227, 228] (Table 3.17).

Table 3.17 Representative hyperfine parameters at RT for some amphiboles

Mineral	Formula	Fe site	δ_{Fe} (mm/s)	Δ (mm/s)
Grunerite	$Fe_7Si_8O_{22}(OH)_2$	Fe^{2+} M1	1.16	2.82
		Fe^{2+} M4	1.10	1.8
Cummingtonite-grunerite	$(Mg,Fe^{2+},Mn)_7Si_8O_{22}(OH)_2$	Fe^{2+} M1–M3	1.16	2.81
		Fe^{2+} M4	1.10	1.5–1.8
Anthophyllite	$(Mg,Fe^{2+})_7Si_8O_{22}(OH)_2$	Fe^{2+} M1–M3	1.12	2.6
		Fe^{2+} M4	1.10	1.8
Riebeckite	$Na(Fe^{2+})_3(Fe^{3+})_2Si_8O_{22}(OH)_2$	Fe^{2+} M1	1.14	2.83
		Fe^{2+} M3	1.11	2.32
		Fe^{3+} M2	0.38	0.43
Holmquistite	$(Li,Fe^{3+},Mg,Fe^{2+})_7Si_8O_{22}(OH)_2$	Fe^{2+} M1	1.13	2.8
		Fe^{2+} M3	1.1	2.0
		Fe^{3+} M2	0.38	0.3
Ferroactinolite	$Ca_2Fe_5Si_8O_{22}(OH)_2$	Fe^{2+} M1,M3	1.15	2.81
		Fe^{2+} M2	1.14	1.85–2.1
		(Fe^{2+} M4)	1.10	<1.8

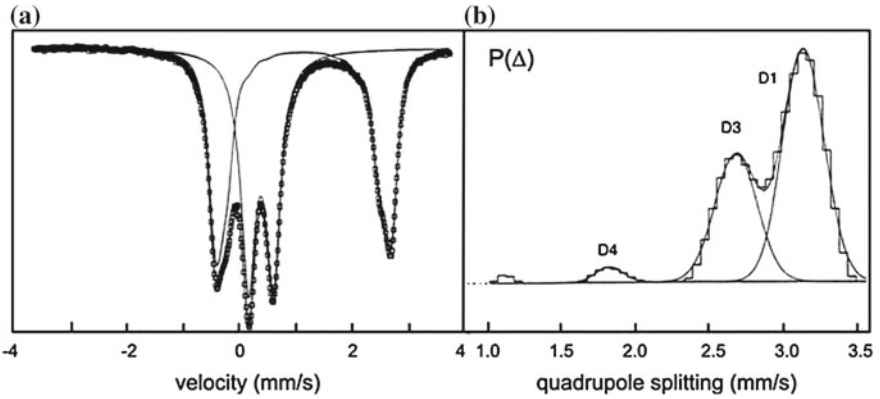

Fig. 3.28 Spectrum at 80 K of a natural riebeckite sample, fitted with quadrupole distributions (**a**); resulting quadrupole distribution for Fe^{2+} showing three peaks (adapted from Van Alboom and De Grave [221])

It is worth to mention that the analysis of the spectra of pyroxenes has not always been successful by using discrete doublets. Already in the early days of Mössbauer investigations of pyroxenes, Bancroft [3] argued that the shortcomings of the until-then commonly applied fitting procedures are the result of the non-uniform chemical environment for both iron sites requiring rather a set of doublets for each site. The use of shape-independent quadrupole distributions seem to be more appropriate in that case [229] and has indeed been successfully applied to the analyses of the spectra of pyroxene minerals such as aluminium diopsides [230] and magnesian hedenbergites [211] and of amphiboles such as riebeckites [231] (Fig. 3.28).

3.5.5.3 Other Chain Silicates

There exist a number of other chain silicates for which the chains are not linked in the way as they are in pyroxenes or amphiboles. A first example is babingtonite in which two chains of SiO_4 tetrahedra are joined by groups of four edge-sharing octahedra. The ideal formula of the iron member is $Ca_2Fe^{2+}Fe^{3+}Si_5O_{14}(OH)$ in which Fe^{2+} and Fe^{3+} each occupy a distinct site. Calcium occupies two types of large interstices. The spectra are consequently quite simple, consisting of narrow ferric and ferrous doublets [232]. Another particular chain silicate is deerite which has a structure based on a hybrid single-double Si_6O_{17} chain. There is a strip of edge-sharing octahedra with nine crystallographically distinct sites, which are classified into three groups of each three sites. The ideal formula is $(Fe^{2+})_6(Fe^{3+})_3O_3Si_6O_{17}(OH)_5$. The spectra are complicated by the effects of electron hopping [233]. There are signs of a preference of Fe^{3+} for M1 and M3 positions and of Fe^{2+} for the others.

3.5.6 Phyllosilicates

Phyllosilicates are the most important minerals of the silicate group. They are either inherited from parent rocks (detrital minerals), reflecting a chemical relation to their environment, or they are secondary minerals. i.e. modified by strong external conditions or transported from other places. Species from the latter group usually show a rather small-particle morphology and are accordingly divided into silt (>2 μm) and clay (<2 μm) fractions. Particularly the clays have ever since ancient times been important minerals for industrial uses. Microcrystalline phyllosilicates were formerly referred to as "clay minerals", but nowadays also fine-grained oxides and oxyhydroxides occurring in soils and sediments are also termed as clay minerals.

The phyllosilicates are composed of sheets of SiO_4 tetrahedra, which can be divided into two groups: the 1:1 layer and the 2:1 layer minerals. The 1:1 layer silicates are composed of alternating tetrahedral Si_4O_{10} and octahedral $Al_4(OH)_{12}$ layers. The octahedra are formed by two oxygen and four hydroxyl anions (Fig. 3.29). The layers themselves are electrically neutral and the stacks are held together by van der Waals or hydrogen bonding. The repeat distance is about 0.7 nm. The general formula is $\left(M_2^{3+}\text{or } M_3^{2+}\right)Si_2O_5(OH)_4$. According to the filling of the octahedra the silicate can either be dioctahedral with 2/3 of the octahedral sites filled or trioctahedral in which all octahedra are filled.

The basic block of a 2:1 layer silicate is a sandwich layer of one octahedral sheet between two tetrahedral ones. The octahedral sheet contains now two apices of two sheets of tetrehedra, so four of the ligands are now oxygen and two are hydroxyl ions (Fig. 3.29). The hydroxyls may be at opposite or adjacent corners of the octahedron, giving trans and cis coordination, respectively, mostly denoted as

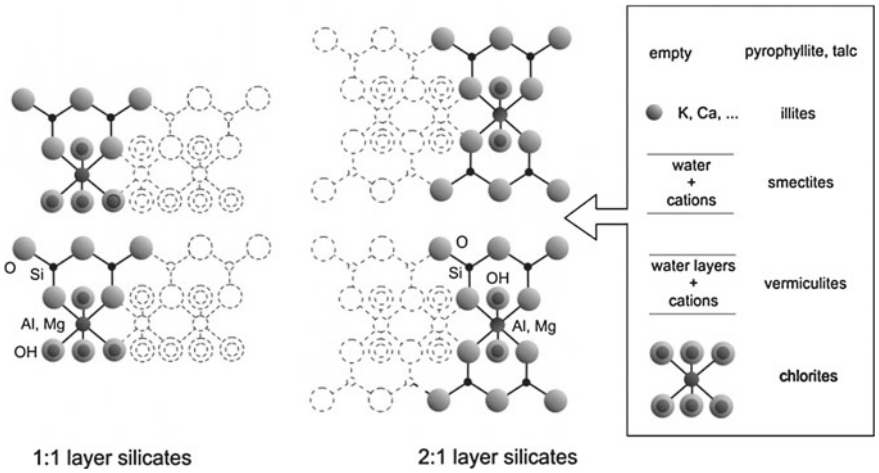

Fig. 3.29 Stacking of octahedra and tetrahedra in phyllosilicates

M1 and M2. The basic blocks may either electrically neutral such as in pyrophyllite or talc, but more frequently there is a charge deficiency which must be compensated. In the micas the substitution of Al^{3+} for a quarter of the Si^{4+} is compensated by a 12-fold coordinated large K^+ ion in the interlayer position. In the so-called brittle micas two silicons are replaced by aluminum and the interlayer cation is divalent. The repeat distance of the layer is close to 1 nm. The smectites and vermiculites contain water or water layers with cations in solution. In the former the repeat distance is variable according to the water content. Because vermiculites are usually better crystallized the charge deficit is higher which makes them difficult to expand. Their normal state is a double layer of water giving the characteristic 1.4 nm spacing. In chlorites the interlayer is occupied by a brucite $(Mg,Al)_3(OH)_6$ sheet which compensates for the charges. The ionic bonding between the brucite sheet and the talc layers also prevents the chlorites to expand. Similar to 1:1 layer silicates, 2:1 layer species can be dioctahedral or trioctahedral.

3.5.6.1 1:1 Layer Silicates

Kaolinite is the basic dioctahedral 1:1 layer silicate. The ideal formula is $Al_2Si_2O_5(OH)_4$. It tends to contain very little iron and it has been shown that ferric iron can substitute for Al to a very small amount. Murad and Wagner [234] summarized the published Mössbauer data giving on the average $\delta_{Fe} = 0.34$ mm/s and $\Delta = 0.52$ mm/s for the ferric doublet. These hyperfine parameters are also representative for superparamagnetic iron oxyhydroxides and oxides which are commonly associated with kaolinite. Therefore spectra at very low temperatures (below the blocking temperatures of the oxides) are necessary to distinguish the

associated oxides from lattice iron. At 4 K kaolinite still shows a doublet with $\delta_{Fe} = 0.48$ mm/s and $\Delta = 0.52$ mm/s. In some cases a small percentage (<10 at %) of Fe^{2+} can be detected with $\delta_{Fe} = 1.1–1.3$ mm/s and $\Delta = 2.4–2.9$ mm/s at RT.

The trioctahedral analogue of kaolinite is the group of serpentine minerals based on antigorite $Mg_3Si_2O_5(OH)_4$ with polymorphs chrystolite and lizardite. Small amounts of iron in those serpentines yield hyperfine parameters of $\delta_{Fe} = 1.14$ mm/s, $\Delta = 2.68–2.76$ mm/s for Fe^{2+} and $\delta_{Fe} = 0.37–0.42$ mm/s, and $\Delta = 0.65–0.85$ mm/s for Fe^{3+} [235, 236]. The iron-rich serpentine is cronstedtite with formula $Fe_2^{2+}Fe^{3+}\left(SiFe^{3+}\right)O_5(OH)_4$. The RT spectrum of cronstedtite is rather complicated due to the electron hopping on the octahedral sites [237]. Tetrahedral and octahedral Fe^{3+} are best distinguished in the magnetically split spectrum at 4 K for which hyperfine fields of 40.6 and 46.7 T are found respectively. The ferrous end member of the serpentines is greenalite with formula $Fe_3^{2+}Si_2O_5(OH)_4$. Its ferrous doublet is well defined with $\delta_{Fe} = 1.15$ mm/s, $\Delta = 2.75$ mm/s [238]. For the intermediate members, the berthierines (not to be confused with chamosite, which is a 2:1 silicate), the quadrupole splitting Δ falls within the range 2.62–2.68 mm/s [239].

3.5.6.2 2:1 Layer Silicates

The basic 2:1 dioctahedral silicate is pyrophyllite with formula $Al_2Si_4O_{10}(OH)_2$. In muscovite, $KAl_2(Si_3Al)O_{10}(OH)_2$, interlayer K compensates electrically for the Al replacement for Si. Illites have a more variable composition with a general formula $(H_30,K)_xAl_2(Si_{4-x}Al_x)O_{10}(OH)_2$. Nontronite is the iron-rich dioctahedral silicate with general formula $M^+Fe_2^{3+}(Si_{4-x}Al_x)O_{10}(OH)_2$.

Although, Mössbauer spectra of the various silicates turned out so far to be reasonably analyzable in a relatively unambiguous way, this is surely not the case for 2:1 layer silicates. In all these silicates Al^{3+} is partly replaced by Fe^{3+} resulting in one or two ferric doublets, which can be interpreted by the Fe-for-Al substitution on trans and cis sites. This is the basic spectrum for all the 2:1 dioctahedral silicates. The quadrupole splitting of the inner doublet (cis) is found to increase in the sequence ferripyrophyllite, nontronite, glauconite, montmorillonite, illite, muscovite (Table 3.18), which in some sense corresponds to increasing distortion of the octahedral [240]. The presence of small amounts of Fe^{2+} possibly introduces two additional doublets similarly attributed to cis and trans arrangements. A third Fe^{3+} doublet with very small quadrupole splitting can be assigned to iron in the tetrahedral sites. (see Johnston and Cardile [241] and references therein). However, in general there is still a lack of common approach for the analysis of the spectra. This is clearly illustrated in the published Mössbauer results for illites and nontronites [242]. Hence, only a fit with two broad-lined doublets or by quadrupole splitting distributions, one for each Fe^{2+} and Fe^{3+}, can provide some straightforward insight in the iron behavior in the structure of these minerals [243]. The iron-rich variants of illite are glauconite and celadonite. In glauconite there is

Table 3.18 Representative hyperfine parameters at RT of some phyllosilicates

Mineral	Site	δ_{Fe} (mm/s)	Δ (mm/s)
Mineral	Site	δ_{Fe} (mm/s)	Δ (mm/s)
1:1 dioctahedral			
Kaolinite	Fe^{3+}	0.48	0.52
	Fe^{2+}	1.1–1.3	2.4–2.9
1:1 trioctahedral			
Antigorite	Fe^{2+}	1.14	2.68–2.76
	Fe^{3+}	0.37–0.42	0.65–0.85
Greenalite	Fe^{2+}	1.15	2.75
Berthierine	Fe^{2+}	1.15	2.62
2:1 dioctahedral			
Muscovite	Fe^{3+}(M2)	0.40	0.72
	Fe^{2+}(M2)	1.13	3.00
	Fe^{2+}(M1)	1.12	2.20
Illite	Fe^{3+}(M2)	0.33	0.59–0.73
	Fe^{3+}(M1)	0.38	1.21
	Fe^{2+}(M2)	1.14	2.75
Nontronite	Fe^{3+}(M2)	0.36–0.39	0.24–0.27
	Fe^{3+}(M1)	0.37–0.40	0.59–0.68
Glauconite	Fe^{3+}(M2)	0.34	0.33
	Fe^{3+}(M1)	0.32	0.69
	Fe^{2+}(M2)	1.1	2.68
	Fe^{2+}(M1)	1.1	1.7–1.9
	Fe^{3+}(interlayer)	0.50	0.5–0.8
Celadonite	Fe^{3+}(M2)	0.35	0.39
	Fe^{2+}(M2)	1.12	2.64
	Fe^{2+}(M1)	1.12	1.76
	Fe^{3+}(DSS)	0.39	1.16
2:1 trioctahedral			
Talc	Fe^{2+}(M2)	1.13	2.6
Biotite	Fe^{2+}(M2)	1.12–1.14	2.57–2.63
	Fe^{2+}(M1)	1.07–1.15	2.12–2.22
	Fe^{3+}(M2)	0.39–0.44	0.37–0.66
	Fe^{3+}(M1)	0.39–0.49	1.16–1.24
Vermiculite	Fe^{3+}(M2)	0.29	0.57
	Fe^{3+}(M1)	0.37	1.10
	Fe^{2+}(M2)	1.11	2.58
Chlorite	Fe^{2+}(M2)	1.12	2.68
	Fe^{2+}(M1)	1.12	2.3–2.4
	Fe^{2+}(brucite)	1.16–1.20	2.67–2.70
	Fe^{3+}(?)	0.38–0.46	0.5–0.75

a much more significant replacement of Si by Al or Fe^{3+} in the tetrahedra than in celadonite, for which the substitution is considered to be 20 at % or less. The Mössbauer spectra of glauconites can be consistently fitted with two ferrous doublets (cis and trans), two ferric doublets (cis and trans) and a third ferric

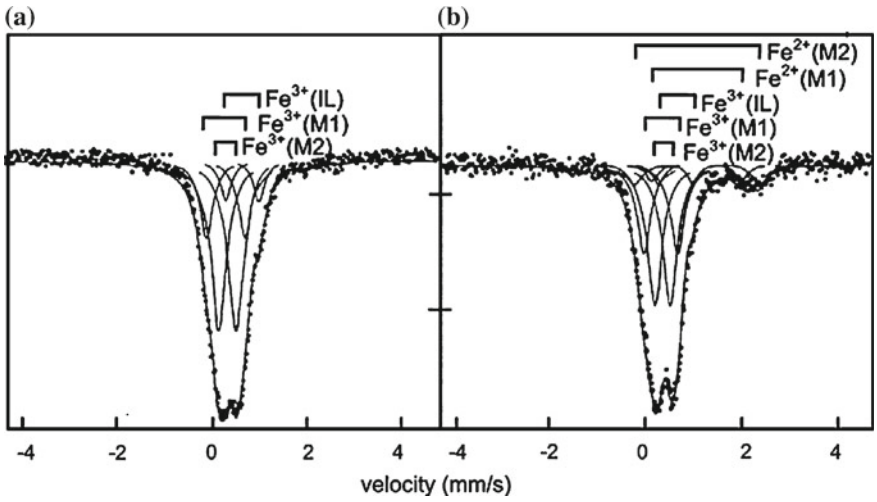

Fig. 3.30 RT spectra of two natural glauconiet samples fitted with three (**a**) or five doublets (**b**) (adapted from De Grave and Geets [309])

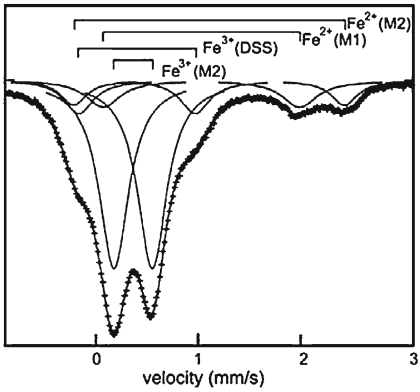

Fig. 3.31 RT spectrum of a natural celadonite sample fitted with four doublets (adapted from Bowen et al. [245])

doublet (Fig. 3.30). De Grave et al. [244] assigned the latter to interlayer Fe^{3+}, whereas Johnson and Cardile [241] analyzed with a third ferric doublet with rather small Δ which they attributed to tetrahedral Fe^{3+}.

The spectrum of celadonite can be adjusted with two ferrous doublets and one ferric doublet, the latter assigned to M2 sites (cis) [245]. A second weak Fe^{3+} doublet with relatively large quadrupole splitting ($\Delta \approx 1.1$–1.2 mm/s) (Fig. 3.31) has been ascribed to iron in dehydroxylated surface sites (DSS) [246, 247].

The basic mineral of the 2:1 trioctahedral silicates is talc with formula $Mg_3Si_4O_{10}(OH)_2$. It is obvious that for this silicate Fe^{2+} will be the most abundant valence of iron and consequently the spectra consist predominantly of ferrous doublets [246, 248]. Similarly, this is also the basic spectral appearance for all

trioctahedral silicates. The spectra of biotites show consistent peak positions for Fe^{2+} in M2 sites and for Fe^{2+} in M1 sites with broader variation in hyperfine parameters for the latter [247, 249]. Additional Fe^{3+} components that appear in the spectra are resolved as two distinct doublets with hyperfine parameters representing the M2 and M1 sites [249, 250].

Chlorites exhibit the main features of biotites. Well-known representatives of the chlorite group are clinochlore, $(Mg,Fe^{2+})_5Al(Si_3Al)O_{10}(OH)_8$ and its iron-rich variant chamosite. The major Fe^{2+} doublet in the spectra of chlinichlore and chamosite has the typical values $\delta_{Fe} = 1.13$ mm/s and $\Delta = 2.70$ mm/s whereas a minor Fe^{3+} doublet gives $\delta_{Fe} = 0.39$ mm/s and $\Delta = 0.67$ mm/s [243]. A third doublet is observed at lower temperatures, but has nearly the same hyperfine parameters as the M2 ferrous iron at RT. This doublet might be attributed to substitutions in the brucite layer [251]. The hyperfine parameters of trioctahedral micas obtained in about fifty studies of these silicates are summarized in a review by Dyar [250].

Finally, Table 3.18 presents a survey of δ_{Fe} and Δ values that have been reported so far in the literature for a number of selected phyllosilicate species. It is obvious from these data that the interpretation of the Mössbauer spectra of micas is not straightforward, the more so nature has provided us with such silicates with an enormous variety in chemical composition.

3.6 Phosphates

3.6.1 Introduction

A large variety of phosphate minerals are found on Earth. Among these, apatite, $Ca_5(PO_4)_3(F,OH,Cl)$, is the most abundant one and consequently serves as the major source from which other naturally occurring phosphates originate by diverse transformational processes. The structure of apatite can accommodate numerous metal cations that substitute for Ca. By far most of the phosphates exhibit a structure that is based on a polymerization of (PO_4) tetrahedra and $(M\phi_6)$ octahedra, with $\phi = O^{2-}$ or OH^-. As such one distinguishes structures with finite clusters of (PO_4) tetrahedra and $(M\phi_6)$ octahedra (e.g. anapaite), structures with infinite chains of tetrahedra and octahedra (eosphorite), structures with infinite sheets of tetrahedra and octahedra (strunzite, vivianite), and finally structures with infinite frameworks of tetrahedra and octahedra (triphylite, heterosite, leucophosphite). Iron, both as a divalent or trivalent cation, is a common substituent and even complete solid solutions may be encountered. As a particular iron phosphate generally occurs in low concentrations and as fine-grained material in association with other mineral species, including other phosphates that may or may

not contain iron, it is often a pain-staking task to collect a sufficient amount of uncontaminated sample to derive a sound and diagnostic Mössbauer-spectroscopic fingerprint for that given Fe phosphate. This drawback is possibly one of the reasons why in the past Fe-bearing phosphates, compared to silicates, have less frequently been studied by the Mössbauer effect. In what follows a few Fe phosphates are selected and their Mössbauer characteristics as observed from their paramagnetic spectra (mostly room temperature) are presented.

3.6.2 Anapaite

The ideal chemical formula of anapaite is $Ca_2Fe^{2+}(PO_4)_2{\cdot}4H_2O$. It has the triclinic structure. The Ca and Fe cations exhibit an eight- and a six-fold co-ordination respectively. The iron is bound to four basal water molecules and two apical oxygen atoms, which belong to a phosphate tetrahedron. The Fe octahedron shares two edges with the Ca dodecahedron. Hence, there is only one type of octahedral site available for the Fe^{2+} cations with coordination $O_2(OH_2)_4$. Consequently, the Mössbauer spectrum (see Fig. 3.32a) consists of a sharp quadrupole doublet with parameters as indicated in Table 3.19. The mineral remains paramagnetic down to a temperature as low as 4.2 K. From the temperature dependence of the quadrupole splitting, combined with external-field spectra, it is concluded that the Fe octahedron is subjected to a tetragonal compression [252]. Oxidation treatments in solutions with various H_2O_2 concentrations up to 20 % and subsequent Mössbauer experiments at room temperature, have revealed that the anapaite structure is unusually highly resistant against oxidation since eventually only a small amount of Fe^{2+} ($\sim$6.5 %) is converted into Fe^{3+} (see Fig. 3.32b). The Fe^{2+} doublet parameters are not affected by this partial oxidation.

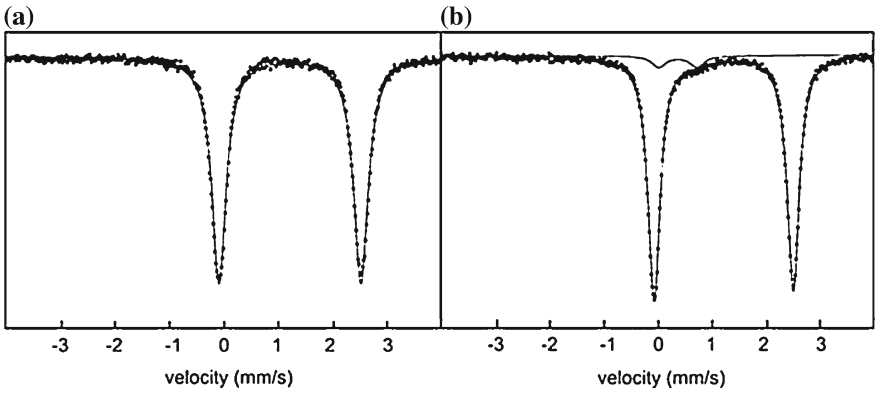

Fig. 3.32 Mössbauer spectra of anapaite at 11 K (**a**) and of oxidized anapaite at 80 K (**b**)

Table 3.19 Representative hyperfine parameters at RT of some iron-bearing phosphates

Mineral	Formula	Fe site	δ_{Fe} (mm/s)	Δ (mm/s)
Anapaite	$Ca_2Fe^{2+}(PO_4)_2.4H_2O$	$Fe^{2+}O_2(OH_2)_4$	1.19	2.49
Eosphorite	$Mn^{2+}AlPO_4(OH)_2.H_2O$	$Fe^{2+}O_4(OH)_2$	1.25	1.74
Manganostrunzite	$Mn^{2+}Fe_2^{3+}(PO4)_2(OH)_2{\cdot}6(H_2O)$	$Fe^{3+}O_2(OH_2)_4$	0.42	0.61
		$Fe^{3+}O_3(OH_2)(OH)_2$	0.41	0.79
		[Fe(1)]	0.41	0.63
		$Fe^{3+}O_3(OH_2)(OH)_2$ [Fe(2)]		
Ferristrunzite	$Fe_3^{3+}(PO4)_2(OH)_2{\cdot}[(H_2O)5(OH)]$	$Fe^{3+}O_2(OH_2)_3(OH_2)$	0.40	0.64
		$Fe^{3+}O_3(OH_2)(OH)_2$ [Fe(1)]	0.39	0.89
		$Fe^{3+}O_3(OH_2)(OH)_2$ [Fe(2)]	0.39	0.74
Ferrostrunzite[a]	$Fe^{2+}Fe_2^{3+}(PO4)_2(OH)_2{\cdot}6(H_2O)$	$Fe^{2+}O_2(OH_2)_4$	1.33	2.65
		$Fe^{2+}O_2(OH_2)_4$	1.33	3.06
		$Fe^{3+}O_3(OH_2)(OH)_2$	0.52	0.85
		[Fe(1)]	0.52	0.64
		$Fe^{3+}O_3(OH_2)(OH)_2$ [Fe(2)]		
Vivianite	$Fe_3^{2+}(PO_4)_2.8H_2O$	$Fe^{2+}O_2(OH_2)_4$ [Fe(1)]	1.19	2.48
		$Fe^{2+}O_4(OH_2)_2$ [Fe(2)]	1.22	2.96
Ox. vivianite	$Fe_{3-q}^{2+}Fe_q^{3+}(PO_4)_2.(8-q)H_2Oq(OH)$	$Fe^{2+}O_2(OH_2)_4$ [Fe(1)]	1.23	2.48–2.39
		$Fe^{2+}O_4(OH_2)_2$ [Fe(2)]	1.22	3.00
		$Fe^{3+}O_2(OH_2)_4$ [Fe(1)]	0.41	0.91–1.01
		$Fe^{3+}O_4(OH_2)_2$ [Fe(2)]	0.42	0.44
Triphylite	$LiFePO_4$	$Fe^{2+}O_6$ [M2]	1.22	2.96
Heterosite	$Fe^{3+}PO_4$	$Fe^{3+}O_6$ [M2]	0.41	1.63
Leucophosphite	$KFe_2(PO_4)_2(OH).2H_2O$	$Fe^{3+}O_5(OH_2)$ [Fe(1)]	0.41	0.84
		$Fe^{3+}O_4(OH)_2$ [Fe(2)]	0.41	0.55

[a] data at 50 K

3.6.3 Eosphorite

The manganese phosphate eosphorite, $Mn^{2+}AlPO_4(OH)_2.H_2O$, has the orthorhombic symmetry. The structure consists of alternating chains of $MnO_4(OH)_2$ octahedra and $AlO_2(OH)_2(H_2O)_2$ octahedra that run parallel to the *c*-axis. The strongly distorted

Mn octahedra share opposite O–O edges, while the more regular Al octahedra share opposite H_2O corners. The two types of chains are linked to one another by sharing their OH corners, thus forming parallel sheets that are held together by phosphorous species in a tetrahedral O_4 co-ordination. Eosphorite is isomorphous with childrenite, $FeAlPO_4(OH)_2.H_2O$, and the two mentioned minerals form the end members of a complete solid-solution series. Naturally occurring eosphotites usually exhibit a substantial Fe-for-Mn substitution. It is generally accepted in the literature that only Fe^{2+} is present in the structure of iron-substituted eosphorite, (Mn,Fe)Al-$PO_4(OH)_2.H_2O$. This belief is corroborated by its Mössbauer spectrum, which consists of a relatively narrow ferrous doublet at temperatures as low as ~ 35 K. At RT the relevant hyperfine parameters are as listed in Table 3.19 [253].

3.6.4 Strunzite

Three distinct variants of strunzite are known to occur in nature: manganostrunzite, $Mn^{2+}Fe_2^{3+}(PO_4)_2(OH)_2{\cdot}6(H_2O)$, ferristrunzite, $Fe_3^{3+}(PO_4)_2(OH)_2{\cdot}\left[(H_2O)_5(OH)\right]$, and ferrostrunzite $Fe^{2+}Fe_2^{3+}(PO_4)_2(OH)_2{\cdot}6(H_2O)$, respectively. Ferristrunzite may be regarded as the fully oxidized form of ferrostrunzite. The strunzite structure is triclinic and consists of infinite chains of octahedral ferric sites along the *c* axis which are linked one another by sharing hydroxyl groups and by PO_4 tetrahedra. The latter also bind adjacent chains, thus forming slabs that are connected to each other by Mn octahedra between remaining PO_4 vertices. Within the chains two ferric sites Fe(1) and Fe(2) alternate, both having an octahedral $O_3(OH)_2(OH_2)$ coordination. The Fe(1) is somewhat more distorted than Fe(2) as indicated by a slight difference in average Fe–O bond length and average O–Fe–O bond angle. The crystallographic unit cell contains two iron octahedra of each type and two Mn octahedra with coordination $O_2(OH_2)_4$. In ferristrunzite the manganese is substituted by Fe^{3+}, in ferrostrunzite by Fe^{2+}. In the first case the charge balance is re-established by substitution of OH by H_2O at a non-bridging vertex of the Mn octahedron. Mössbauer spectra (MS), both for these three mineral species have been reported [254–256]. The spectrum of manganostrunzite recorded at ~ 60 K is reproduced in Fig. 3.33a. It was decomposed into three ferric quadrupole doublets. This model was imposed by the results at 4.2 K at which temperature the sample is magnetically ordered and clearly three distinct sextet components are recognized. Obviously, there is no indication whatsoever that Fe^{2+} would be present in the structure of this manganostrunzite species. The doublet hyperfine parameters observed at RT are included in Table 3.19. The presence of three spectral components implies that the manganese sublattice is partly substituted by Fe^{3+} and from the relative spectral area of the corresponding doublet ($\Delta = 0.61$ mm/s), i.e. ~ 12 %, it is inferred that the Fe-for-Mn substitution is around 25 %, which is in accordance with the results of the chemical analysis [255]. The two other ferric doublet components are assigned to the Fe(1) and Fe(2) sites on the basis that the former sites exhibit a somewhat higher distortion and hence are expected to produce the larger quadrupole splitting. The

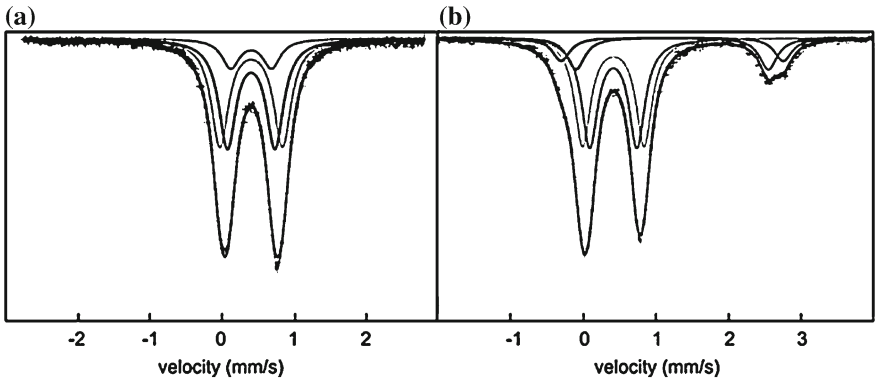

Fig. 3.33 Mössbauer spectra of manganostrunzite at 60 K (**a**) and of ferrostrunzite at 50 K (**b**)

paramagnetic spectra of the ferristrunzite variant are very similar to those of manganostrunzite, the major distinction being the higher relative contribution of the first doublet ($\Delta = 0.64$ mm/s), i.e. ~ 30 %, which is due to Fe^{3+} cations on the Mn sites. The ideal value for a complete Fe-for-Mn substitution would be 33 %. The small deviation is ascribed to the presence of Al cations in the structure to an amount of approximately 0.1 p.f.u., as derived from the chemical analysis. A spectrum of ferrostrunzite is shown in Fig. 3.33b and refers to a temperature of ~ 60 K. Clearly two ferrous components are present in addition to a dominant ferric doublet. The latter was decomposed into two contributions which were assigned to Fe(1) and Fe(2) sites, respectively (see Table 3.19). Rationally, the two ferrous doublets were attributed to the Mn sites. However, the reason why two distinct Mn sites appear has remained unexplained. Moreover, the ferrous-to-ferric concentration range was found to be 0.36, which is significantly smaller than the value 0.5 for ideal ferrostrunzite.

3.6.5 Vivianite

Ideally, the chemical formula of vivianite is $Fe_3^{2+}(PO_4)_2.8H_2O$. As such the mineral is colorless. In soils vivianite species are commonly fine-grained and easily oxidize in the air, the color becoming pale blue. There are no structural changes observed upon oxidation and oxidized vivianite can be represented as $Fe^{2+}_{(3-q)}Fe^{3+}_q(PO_4)_2.[(8-q)H_2Oq(OH)]$. The unit cell of (oxidized) vivianite is monoclinic. The structure consists of single and paired octahedra bound together by PO_4 tetrahedra, thus forming infinite sheets parallel to the (010) plane. The single octahedron has a $O_2(OH_2)_4$ coordination with the oxygens in *trans* position, and is denoted as the Fe(1) site. The paired octahedra form the group $O_6(OH_2)_4$ and share two O^{2-} anions along their common edge. For both octahedra of the

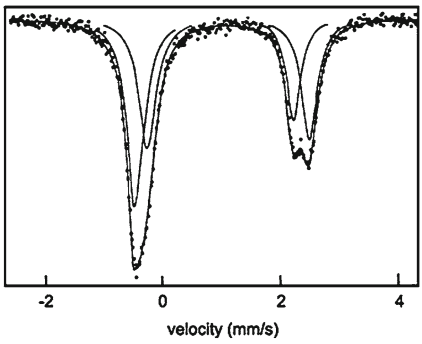

Fig. 3.34 Mössbauer spectra of non-oxidized vivianite at room temperature

paired unit the two other O^{2-} anions are in a *trans* position. The two octahedra are identical and are henceforward referred to as the Fe(2) sites. There are twice as many Fe(2) sites in the vivianite structure than there are Fe(1) sites.

MS for a single crystal of non-oxidized vivianite were reported by [257–259]. The spectrum at RT as presented in the latter work is reproduced in Fig. 3.34 and concerns a species from Anloua, Cameroon. It was recorded under a geometry whereby the incident γ-ray was perpendicular to the crystallographic *ac* plane and had therefore to be analyzed by a superposition of two asymmetric quadrupole doublets arising from Fe^{2+} at the Fe(1) and Fe(2) sites respectively. The asymmetry is due to texture effects as a result of the EFG's principal axis being non-randomly oriented with respect to the incident γ-ray direction. Such a situation leads to a quadrupole doublet of which the two composing absorption lines have unequal spectral areas. Fitting the spectrum of Fig. 3.34 yielded a line-area asymmetry of 0.64 for both doublets, which is consistent with the conclusion of Forsyth (1970) that for both Fe sites the EFG's principal axis is lying in the *ac* plane. The hyperfine parameters are given in Table 3.19. Both Gonser et al. [257] and De Grave [259] observed a significant deviation of the area ratio of the two subspectra from the ideal value of 1:2 and ascribed this feature to the pronounced effective thickness of the single-crystal absorber.

Partly oxidized vivianites, commonly as powders, have been studied by Mössbauer spectroscopy by De Grave et al. [260], McCammon and Burns [261], and Dormann et al. [262]. Various oxidation degrees q have been considered. Two room temperature spectra are reproduced in Fig. 3.35 referring to $q = 0.31$ and $q = 0.14$, respectively, as derived from the analyses of the spectra using two ferrous and two ferric doublets. The assignment of the various doublet components to the Fe(1) and Fe(2) sites is specified in Table 3.19, together with their respective δ_{Fe} and Δ values. It was found that the quadrupole splitting for the Fe^{2+} and the Fe^{3+} cations at the Fe(2) sites is not affected by the oxidation degree q. On the other hand, for the Fe(1) sites both the ferrous and ferric Δ decrease with increasing q. It was further noticed that the oxidation of Fe^{2+} to Fe^{3+} preferably takes place at the Fe(1) octahedra so that the fraction of total iron as Fe^{3+} at the Fe(2) sites does not exceed 0.05 in the range $q \leq 0.32$.

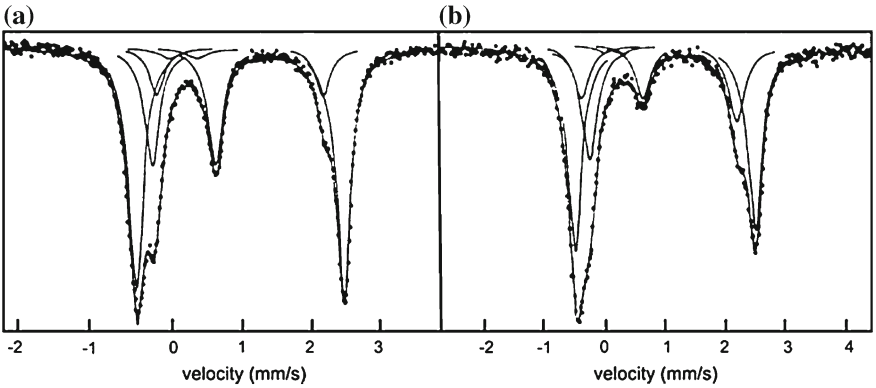

Fig. 3.35 Mössbauer spectra at room temperature of oxidized vivianites, $Fe^{2+}_{3-q}Fe^{3+}_{q}(PO_4)_2.(8-q)H_2Oq(OH)$, with (**a**) $q = 0.31$ and (**b**) $q = 0.14$

3.6.6 Triphylite

Lithium-iron phosphate, $LiFePO_4$, has received ample attention in recent years because of its potential application as electrode active material for rechargeable lithium batteries (see [263] and references therein). It occurs in nature and as such is known as the mineral triphylite. It has an olivine- type crystallographic structure in which the ferrous cations occupy strongly distorted corner-sharing octahedral M2 sites, which form zig-zag chains running parallel to the *c*-axis. A second type of edge-sharing octahedral sites, M1, forms linear chains that are also directed along the *c*-axis and are occupied by lithium cations. Each $M1O_6$ octahedron shares edges with two adjacent $M1O_6$ octahedra, with two $M2O_6$ octahedra and with two PO_4 tetrahedra. The $M2O_6$ octahedron has common edges with two $M1O_6$ octahedra and one PO_4 tetrahedron. Mössbauer spectra of both naturally occurring and synthetic triphylites have been reported by several authors (Van Alboom et al. [264] and references therein). Below $\sim$52 K the material is antiferromagnetically ordered. At higher temperatures the Mössbauer spectrum consists of a narrow doublet with a relatively high quadrupole splitting (see Table 3.19).

3.6.7 Heterosite

This mineral, ideally $Fe^{3+}PO_4$, possesses the same structure as triphylite, however, with all M1 sites being vacant. Actually, the two mentioned minerals are the end members of a complete solid solution. Heterosite also forms a solid solution with purpurite, $MnPO_4$. The Mössbauer spectrum recorded at 80 K for a natural Mn-substituted heterosite species (Buranga, Rwanda) is reproduced in Fig. 3.36 and very similar spectra were observed for all temperature higher than $\sim$60 K

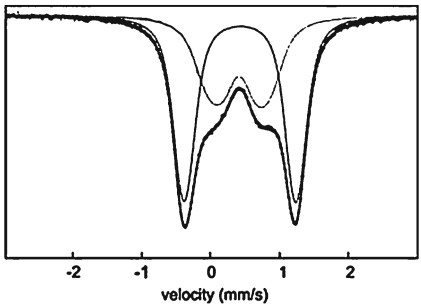

Fig. 3.36 Mössbauer spectrum at 80 K of a natural Mn-substituted heterosite species

(unpublished results). Clearly the spectra consist of an outer doublet component and an inner much broader doublet, and are most adequately analyzed with a superposition of two quadrupole-splitting distributions. The maximum-probability Δ values at RT were calculated to be 1.63 mm/s and 0.40 mm/s, respectively. On the basis of the isomer shifts both doublets are attributable to ferric cations.

A value of 1.63 mm/s for the quadrupole splitting is unusually high for Fe^{3+} species and is ascribed to a strong deformation of the M2 octahedra as a result of the presence of Mn^{3+} cations, which are Jahn–Teller active. The appearance of two distinct spectral components is not consistent with the availability of only one type of site for the cations. Yamada and Chung [265] reported MS at RT for synthetic $(Mn_yFe_{1-y})PO_4$ compounds, showing indeed only one doublet with Δ increasing with increasing Mn content from 1.53 mm/s for $y = 0$, to 1.65 mm/s for $y = 0.5$. Therefore, it is likely that the inner doublet in the MS of the Buranga heterosite is due to a second Fe-bearing phase. This suggestion is corroborated by the observation that the inner doublet remains to be present at temperatures as low as 15 K, at which the heterosite is magnetically ordered and produces a well-resolved sextet (unpublished results).

Considering the substantial fraction of total iron that is present in this second phase ($\sim$40 %), it is puzzling that this phase was not detected in the X-ray diffractogram. A possible explanation could be that the involved impurity concerns an amorphous iron phosphate. It should be noted that recently Fehr et al. [266] reported the Mössbauer spectrum of a naturally occurring Mn-substituted heterosite (Sandamab, Namibia). In addition to the heterosite doublet with $\Delta = 1.63$ mm/s, the authors found an inner doublet having $\Delta = 0.69$ mm/s. They concluded that this inner doublet is due to an associated iron-phosphate mineral.

3.6.8 Leucophosphite

Leucophosphite is an iron-potassium phosphate with ideal composition given as $KFe_2(PO_4)_2(OH).2H_2O$. It is often found in guano deposits, in pegmatite deposits and in lateritic crusts. The crystal structure of leucophosphite is triclinic. The atomic arrangement is based on an octahedral tetramer involving an edge-sharing

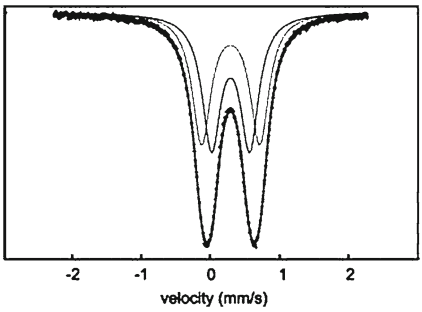

Fig. 3.37 Mössbauer spectrum at room temperature of synthetic leucophosphite

dimer (hereafter called Fe(2) sites) which further links by corner sharing to two other octahedrons (Fe(1) sites). The edge-sharing octahedrons possess two OH^- groups in *cis* position along the shared edge. The two other octahedrons each have a water molecule at the corner that is in *cis* position with respect to the shared corner. The K ions and one water molecule per formula unit are located in channels that run parallel to the [010] and [001] crystallographic axes.

The Mössbauer spectrum for a synthetic leucophosphite at RT is reproduced in Fig. 3.37 [267]. It is adequately fitted with two ferric quadrupole doublets, which are assigned to the Fe(1) and Fe(2) sites (see Table 3.19) on the basis that the Fe(1) are expected to exhibit the largest ΔE_Q value since the ferric species in these sites experience the largest charge asymmetry for their closest co-ordination shell. Within error limits the area ratio of the two doublets is 1:1, but the Fe(1) doublet has a slightly broader linewidth.

3.7 Examples

3.7.1 Goethite-Hematite-Ferrihydrite Associations

Most weathered mineral or soil-related samples contain simultaneously goethite, hematite and ferrihydrite. As a general rule, hematite occurs more frequently in places below 40° latitude whereas ferrihydrite is mostly found above that latitude [124]. In such composite samples, hematite exhibits nearly always a sextet with asymmetric lines at RT and remains predominantly weakly ferromagnetic down to 80 K. On the other hand, the spectrum of goethite is strongly dependent on the crystallinity and at RT can vary from a doublet for poorly crystallized goethite over a largely collapsed spectrum to a sextet with strongly asymmetric lines for relatively well-crystallized goethite. Due to the asymmetry of the absorption lines in the latter case, the involved subspectrum was often fitted with a few sextets with consecutively decreasing intensity. However, an adequate fit is only obtained if a distribution of hyperfine fields is considered.

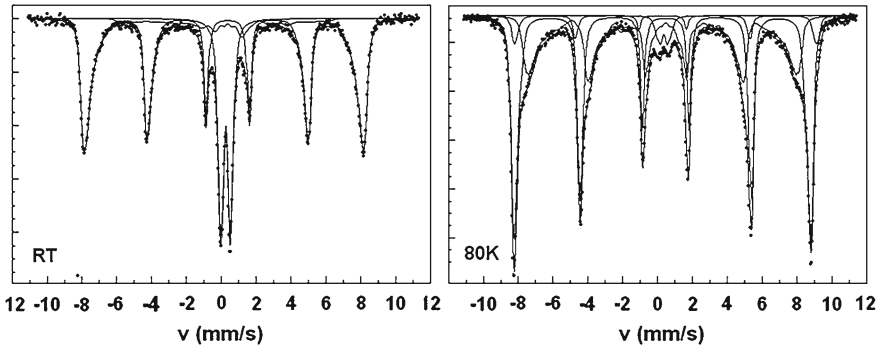

Fig. 3.38 Mössbauer spectrum at RT and at 80 K of a hematite-rich sample containing hematite and goethite

A first example concerns a sample from a weathered boulder in a granite outcrop in Sungai Ringit (Malaysia), which is relatively rich in hematite. The spectra at RT and at 80 K are displayed in Fig. 3.38.

The RT spectrum is composed of a sextet with asymmetric lines having a relatively high hyperfine field and a negative quadrupole shift, which is typical for hematite. The hyperfine parameters are collected in Table 3.19. The center of the spectrum shows a doublet that corresponds to Fe^{3+}, but can in principle not directly be assigned to a particular mineral. Further, close inspection learns that the spectrum exhibits a slightly curved bag-like shape, which has been accounted for by including in the fit a *B*-distributed sextet component in the low hyperfine-field region (5–35 T). Although the latter adjustment is not always theoretically correct because of the comparable strength of the quadrupole and the magnetic interaction [268], it adequately describes the overall spectral shape. This collapsed spectrum can usually be considered as originating from that fraction of the goethite particles that exhibit the highest degree of crystallinity.

At 80 K the doublet has almost completely disappeared in favor of a sextet with strongly asymmetrical line shape. The hyperfine parameters of this sextet point to goethite. This change is clearly the effect of super paramagnetism in which the sextet increases at the expense of the doublet by lowering the temperature as a result of a distribution of particle sizes. Because the hyperfine fields in the derived goethite field distribution are tending to low values, it can be expected that the remaining doublet at 80 K is due to that part of the goethite with the poorest crystallinity. The moderate quadruple splitting of that doublet (0.57 mm/s) points indeed in that direction because ferrihydrite, the presence of which cannot be excluded a priori, has usually $\Delta \geq 0.6$ mm/s. The sextet lines of hematite at 80 K are sharp and only slightly asymmetric. However, the spectrum itself is asymmetric in the sense that the first line is significantly deeper than the sixth one, whereas the it is opposite is noticed for lines 2 and 4. This feature is typical for the presence of the two magnetic hematite phases (cfr. Fig. 3.9). Introducing a weak AF hematite component indeed improved the fit significantly.

Table 3.20 Hyperfine parameters for the goethite-hematite sample of example 1

T	B_{av} (T)	B_p (T)	2ε or Δ (mm/s)	δ_{Fe} (mm/s)	RA (%)	Assignment
RT	48.3	49.7	−0.20	0.36	63	Hematite (WF)
	(21)	–	−0.2	0.36	10	Goethite (coll.)
	–	–	0.57	0.35	27	Goethite (SP)
80 K	52.4	52.9	−0.20	0.47	52	Hematite (WF)
	53.5	53.9	0.20	0.47	6	Hematite (AF)
	39.7	48.0	−0.24	0.48	39	Goethite (AF)
	–	–	0.56	0.46	3	Goethite (SP)

The relative spectral areas RA (see Table 3.20) provide an indication of the amount of Fe species in the different components. However, the relative area of hematite derived from the RT spectrum (63 %) is not the same as that observed at 80 K (52 % + 6 %). This quite strong reduction (about 8 %) cannot be attributed to the relative change in the Mössbauer fraction of hematite with respect to that of goethite on decreasing the temperature from RT to 80 K. This difference is rather an artifact of the distribution fitting applied to sextets where there is strong overlap of the broad goethite sextet with the low-field tail of the hematite sextet. So, the relative area is most accurately determined from the RT spectrum in which the goethite appears as a doublet and consequently the sextet of hematite is well resolved.

In a second example it is demonstrated that Mössbauer spectroscopy is helpful in determining the relative change in the amounts of the different Fe phases present in samples taken at different depths from a so-called Griffin Farmhill soil profile in South Africa [269]. The RT spectra show a dominant doublet together with a hematite sextet of which the intensity increases in the sequence C1 to C6, i.e. with increasing depth along the profile (Fig. 3.39). The 80 K spectra reveal a similar increase of goethite, leaving only a small amount of doublet for C6. It was found that the remaining doublet at 80 K for sample C1 possessed a large quadrupole splitting of 0.68 mm/s (Table 3.21) pointing to ferrihydrite. In order to verify the latter, spectra of sample C1 have been taken at lower temperatures.

The spectrum at 4 K shows three sextets: one of hematite, one of goethite and one of ferrihydrite (Fig. 3.40). However, there is still a doublet present at 4 K. At 15 K the spectrum shows that the contribution of this doublet has increased at the expense of the ferrihydrite sextet. This means that the doublet arises from ferrihydrite species behaves superparamagnetically at temperatures as low as 4 K. This feature can be explained by the presence of so-called DOM ferrihydrite [73] in view of the high carbon content in the topsoil samples.

The evolution of the relative spectral areas for the different iron-bearing phases as a function of depth is represented in Fig. 3.41, which thus provides an idea of the transformation of ferrihydrite to goethite and hematite in the different horizons. From this picture is clear that in the deeper layers ferrihydrite is nearly completely transformed to goethite and hematite.

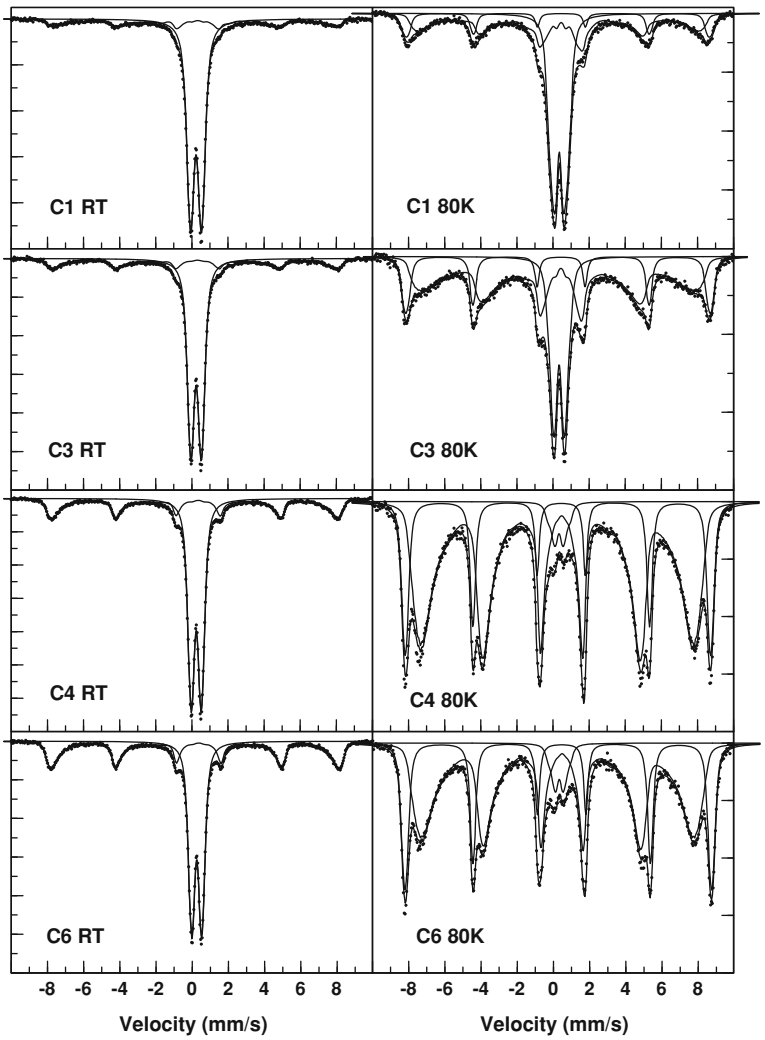

Fig. 3.39 Mössbauer spectra at RT and 80 K of samples from a Griffin Farmhill soil profile

3.7.2 Hidden Doublets

Relevant doublets of weak intensity are often largely hidden under other, more intense doublets or inner lines of sextet components and their presence will generally not be recognized although they have hyperfine parameters that deviate from the predominant doublets. In order to overcome this shortcoming to some extent, it is always advisable to throw a closer look at the central part of the spectrum.

Table 3.21 Hyperfine parameters of sample C1 at different temperatures

T (K)	B_{av} (T)	B_p (T)	$2\varepsilon/\Delta$ (mm/s)	δ_{Fe} (mm/s)	RA (%)	Assignment
300	37.0	49.1	−0.17	0.35	22	Hematite
	–	–	0.62	0.34	78	Goethite + Ferrihydrite
15	52.4	52.5	−0.17	0.47	23	Hematite (WF)
	47.9	49.1	−0.20	0.47	32	Goethite
	29.7	37.7	−0.06	0.46	19	Ferrihydrite
	–	–	0.69	0.44	26	Fe^{3+} doublet (Fh)
4	52.5	52.5	−0.17	0.47	27	Hematite (WF)
	48.6	49.3	−0.19	0.47	34	Goethite
	37.2	42.7	−0.06	0.42	32	Ferrihydrite
	–	–	0.67	0.41	7	Fe^{3+} doublet (Fh)

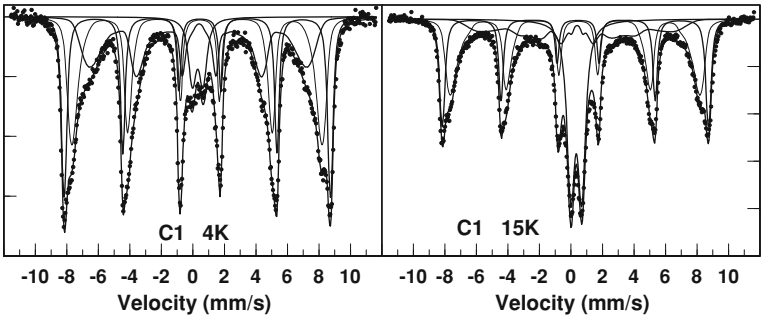

Fig. 3.40 Mössbauer spectra of C1 at 4 and 15 K

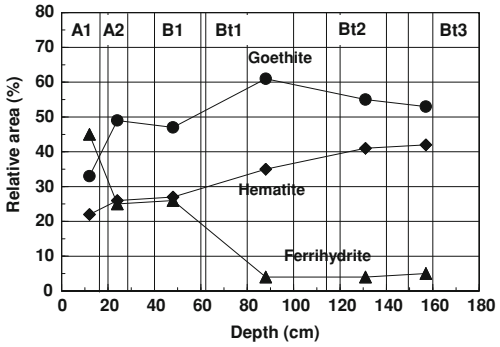

Fig. 3.41 Evolution of the relative spectral areas representing Fe in the different iron-bearing components as a function of depth

Figure 3.42a represents the full RT spectrum of one of the soil samples from Cameroun, which were investigated by MS in the framework of a soil mapping project. The spectrum shows the typical hematite sextet together with the

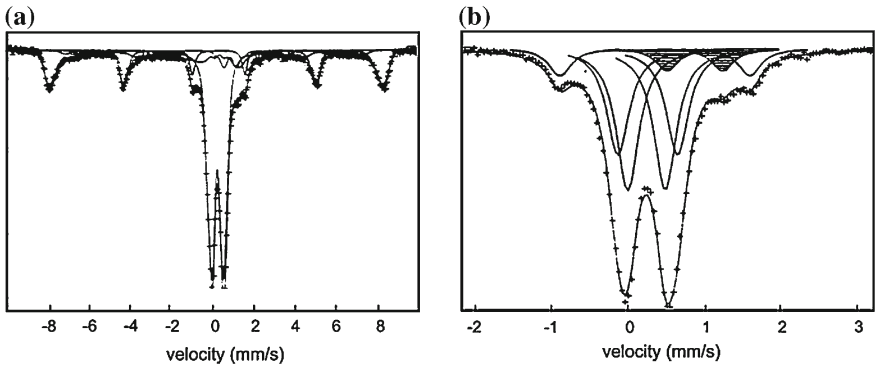

Fig. 3.42 RT Mössbauer spectrum of Cameroun soil sample (**a**) full spectrum, **b** central part—the shaded doublet represents the ilmenite subspectrum

non-resolved doublets of superparamagnetic goethite and ferrihydrite. However, the central part of that spectrum has been analyzed more carefully with conventional doublets (Fig. 3.42b). The overlapping long tails of the distributed lines of the goethite and hematite sextets can be considered as contributing to a constant non-resonant background in the central part. It was thus attempted to fit this part with two Lorentzian lines to account for the inner lines of the hematite sextet and two doublets for goethite. It was found, however, that an additional doublet was needed to obtain a reasonable fit. This extra doublet with $\delta_{Fe} = 1.02$ mm/s and $\Delta = 0.8$ mm/s corresponds to ilmenite which was not detected by any other technique. So, it clear that a closer inspection of the central part of the spectra might reveal the presence of some minor amounts of Fe-bearing minerals which would not have been found by a quick standard fit.

Another example concerns the Mössbauer measurement of iron-containing nodules in a planosol from the S–W Ethiopian highlands [270]. The RT Mössbauer spectrum of the nodules in the vertic horizon as well as that of the accumulated nodules consists of a single doublet at RT, which converts partly into a goethite sextet at 80 K (Fig. 3.43). The remaining Fe^{3+} doublet with a quadrupole splitting of 0.60 mm/s might be attributed to ferrihydrite.

At this point, one might conclude that no other iron-bearing phases are present unless another spectral component in addition to the one of goethite/ferrihydrite would be hidden in the Fe^{3+} doublet. However, if the doublet at RT is analyzed with a quadrupole-splitting distribution an extra maximum is found around 1.1 mm/s in addition to the expected one for goethite/ferrihydrite at about 0.5–0.6 mm/s (Fig. 3.44). The second sample showed the same features. The RT spectra were then accordingly reanalyzed with two doublets. The second doublet with $\delta_{Fe} = 0.37$ mm/s and $\Delta = 1.1$ mm/s appeared indeed in the fit (Fig. 3.44) and could be identified as the main doublet of bixbyite ($FeMnO_3$) [271, 272], the presence of which was detected by XRD. The other bixbyite doublet with a lower quadrupole splitting of 0.6 mm/s coincides with the main goethite/ferrihydrite doublet.

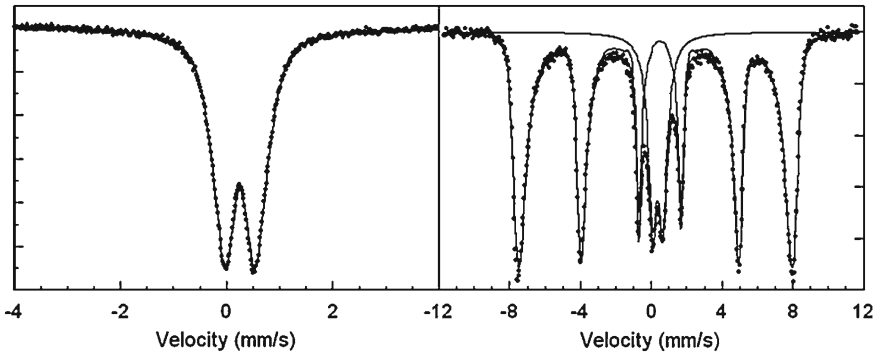

Fig. 3.43 Mössbauer spectrum at RT (*left*) and 80 K (*right*) of an iron nodule in a planosol

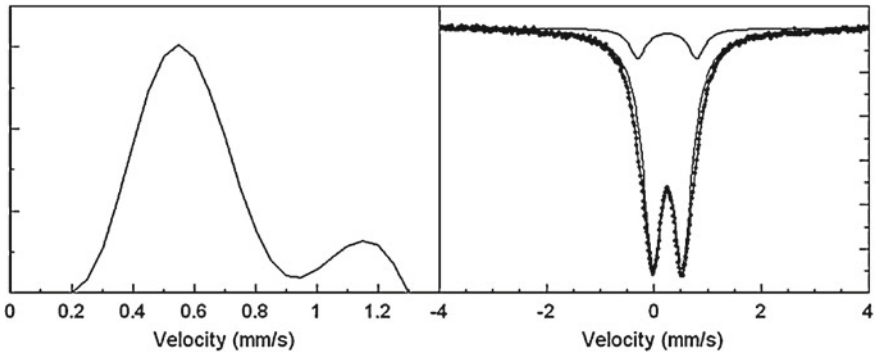

Fig. 3.44 Quadrupole distribution (*left*) from the RT spectrum of the nodule and the spectrum refitted with 2 doublets (*right*)

In conclusion, also the use of quadrupole-splitting distributions may reveal the presence of minor doublet fractions in multi-phase Mössbauer spectra.

3.7.3 Magnetic Mineralogy

Many soil or rock samples contain magnetic minerals other than hematite, such as magnetite, titanomagnetite and maghemite, which are often only present in small amounts. These magnetic compounds appear then as vague sextets in the Mössbauer spectra and as-such can hardly be analyzed. Magnetic separation is then the pre-eminently solution to bring this interesting magnetic mineralogy on the foreground. A strong hand magnet can already be used for that purpose, but a more sophisticated magnetic separator is obviously more efficient.

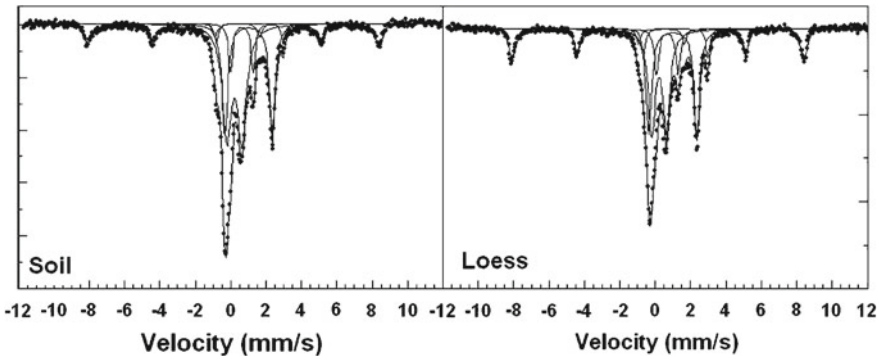

Fig. 3.45 RT spectra of topsoil and underlying loess

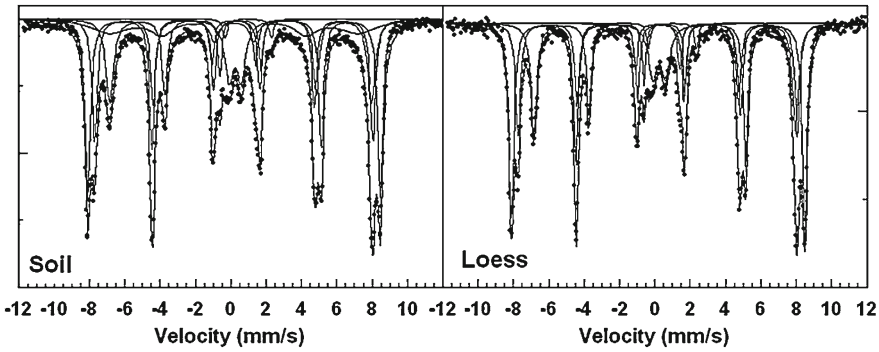

Fig. 3.46 RT spectra of magnetically separated topsoil and underlying loess

As a first example, a sample from the topsoil and one from an underlying loess of a paleosol-loess sequence at Xiadong in the Jixian loess section (China), will be considered. The RT Mössbauer spectra of soil and loess show a series of central doublets, which can be attributed to illite. Apart from these doublets the sextet typical for soil hematite is observed (Fig. 3.45).

However, it is well known that these soils, which possess an even higher magnetic susceptibility than the underlying loess, contain other magnetic components such as magnetite and maghemite. Apparently, their spectra fall below the detection or analyzing limit of MS. After the sample was submitted to a wet magnetic separation in a Franz isodynamic separator a totally different picture appeared in the Mössbauer spectra (Fig. 3.46). The sextets of magnetite, maghemite and of a more course-grained hematite could be adjusted to the spectrum of the soil, whereas for the loess sample only the sextets for magnetite and hematite were resolved. This was the first time that the magnetic components of loess and paleosol were visualized in a direct way [273, 274].

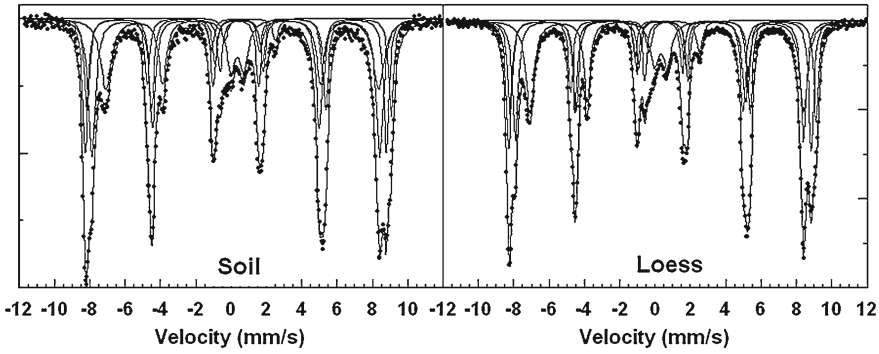

Fig. 3.47 Spectra at 130 K of magnetically separated topsoil and underlying loess

The samples were also measured at low temperature i.e. at 130 K in order to remain above the Verwey transition of magnetite (Fig. 3.47). In these spectra the AF and WF phase of hematite were simultaneously present demonstrating a better crystallinity for this hematite phase than for the hematite observed in the total soil and loess sample, for which at 80 K only the WF state was revealed.

This procedure of separation has also been applied to a series of samples from a paleosol-loess sequence section in Huangling (China). From the corresponding Mössbauer spectra and particularly from the relative spectral area ratios, interesting conclusions could be drawn with respect to the origin of the enhanced magnetic susceptibility of the soils in comparison with that of the loess [275]. A similar method was applied and concurrent results were obtained in a series of samples from a section in the north-eastern area of the Buenos Aires province [276].

A second example of magnetic separation concerns a study of fresh dolerite samples from Berg en Dal, 90 km north of Paramaribo in Suriname, in which MS was utilized as an additional characterization technique of the samples [277]. Apart from several doublets, the RT spectrum shows two weak sextets that can be assigned to magnetite. In order to study more carefully the magnetic components the sample has been subjected to a magnetic separation yielding a magnetic and a non-magnetic fraction. The RT spectra of both fractions are depicted in Fig. 3.48.

The spectrum of the magnetic fraction shows clearly the two sextets of magnetite and no other sextets were visible at first sight. In order to fit the spectrum adequately in the complex central part of the spectrum, those hyperfine parameters were used that were obtained from the fit of the spectrum of the non-magnetic fraction, which is not disturbed by inner sextet lines. The ratio of the relative areas for magnetite, $S(Fe^{2.5+})/S(Fe^{3+})$, turned out to be 2.2 which is by far larger than 1.8 as expected for pure magnetite. Because oxidation or substitution lowers the amount of $Fe^{2.5+}$ pairs and thus the relative area of the $Fe^{2.5+}$ sextet, there must be another sextet component present, which overlaps to some extent with the latter. This can hardly be another Fe^{3+} oxide component because this low field would correspond to a small particle morphology, which would lead to a rather bag-like

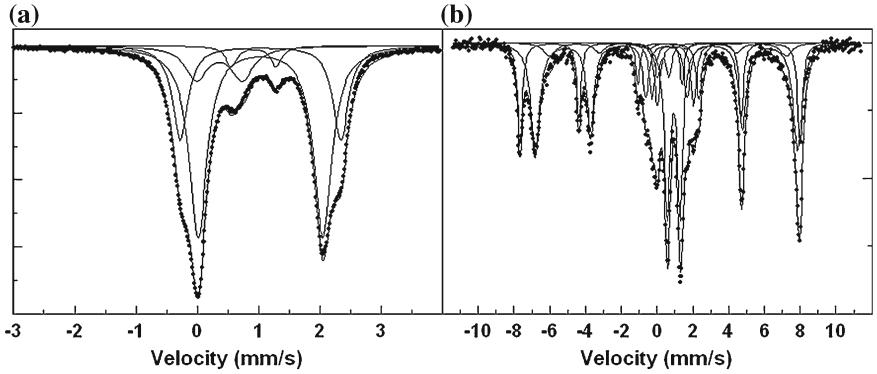

Fig. 3.48 RT spectrum of non-magnetic (**a**) and magnetic (**b**) fraction of a dolerite sample

shape of the spectrum. A sextet with low hyperfine field ($B = 42$ T) and high isomer shift ($\delta_{Fe} = 0.71$ mm/s) could be added pointing to a Fe^{2+} sextet as expected for a titanomagnetite (Fig. 3.48b).

3.7.4 The Strong Means: External Magnetic Fields

The question often arises to what extent one can resolve sextets in a Mössbauer spectrum. Of course there is no general answer. If sextets strongly overlap, it will be very difficult to resolve them in a correct way. Moreover, if they possess a hyperfine-field distribution, it will be practically impossible to discern the different components, even if other hyperfine parameters like the quadrupole shift or the isomer shift are significantly different. Only when the lines exhibit distinct shoulders one can expect another sextet component to be present because strong anomalies in hyperfine field distributions for the same iron species are rare.

In some cases, Mössbauer measurements with the sample in a high external field might be a welcome solution to improve the resolution of sextets. Ferrimagnetic compounds have the advantage that their magnetic moments align in a more or less strong external magnetic field. Consequently, the external field is added to the hyperfine field of the site with the smallest magnetic moment and subtracted from that of the site with the strongest magnetic moment because the hyperfine field is opposite to the magnetic moment.

A typical example is maghemite with its strongly overlapping sextets of *A* and *B* sites. This spectrum can be simply fitted with 2 sextets, but the resulting hyperfine parameters will depend on the initial values used in the fit. This ill-posed problem can only be solved by performing measurements in an external magnetic field, where the outer sextet from the A sites is well separated from that of the B sites (Fig. 3.49), yielding accurate values for both isomer shifts and hyperfine fields.

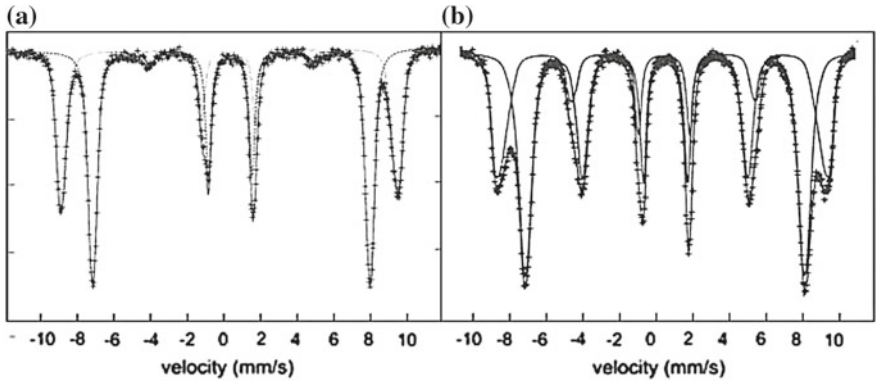

Fig. 3.49 External-field (6 T) spectra at RT of well-crystallized (**a**) and poorly crystallized (**b**) maghemite. Note the presence of lines 2 and 5 as an indication of spin canting

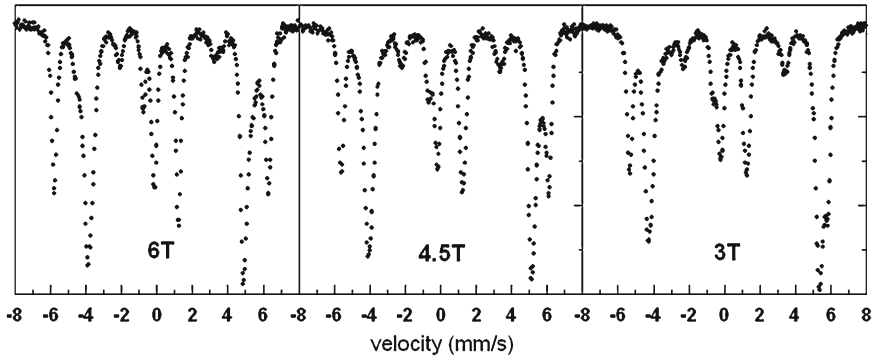

Fig. 3.50 Mössbauer spectra of the greigite-smythite sample at 80 K in different external magnetic fields showing the separation of the greigite lines

A mineral-related example was the use of external field measurements in the study of greigite [148]. The RT spectrum of a greigite-smythite sediment sample has been reproduced in Sect. 3.4.1 (Fig. 3.19). This spectrum has been fitted with two sextets from greigite, three sextets from smythite and a siderite doublet. As shown, the spectrum fit seems at first sight to be straightforward, but that was not at all the case. At that moment, the hyperfine fields on tetrahedral and octahedral sites of greigite were not well known and the purpose of that study was to determine the temperature behavior of the hyperfine fields. The only way to tackle the problem consisted of measuring the sample at 80 K in applied fields of various strengths. Because greigite is ferrimagnetic the external field separates its A- en B-site spectrum (Fig. 3.50), whereas the lines of smythite, being ferromagnetic shift more to center of the spectrum. Extrapolation for the different fields yielded the values of the hyperfine fields at 80 K and the respective isomer shifts.

Repeating this procedure for a few other temperatures and analyzing the zero-field spectra in a consistent way a complete picture of the hyperfine fields of greigite and smythite could be determined.

Other examples of the application of external-field MS to improve the spectral resolution in the characterization of soils are described by De Grave et al. [278].

3.7.5 Extraterrestrial Samples

Although the title of this chapter refers to applications of MS in earth sciences, one cannot exclude to mention briefly the MS investigations of soils and rock materials which are not strictly connected to the planet Earth.

First of all, a lot of extraterrestrial material has reached the Earth by means of meteorites. These meteorites are in 85 % of the cases so-called chondrites, which contain predominantly particles or chondrules that are composed of silicate minerals, such as olivine and pyroxene, and that are surrounded by some glassy or crystalline feldspathic material. Sulfides such as triolite are also present. However, the most interesting meteorites are the iron meteorites containing Fe–Ni alloys [279, 280]. In this kind of meteorite 1:1 crystallographically ordered Fe–Ni alloys (tetrataenite) have been discovered [281, 282], which has never been observed for terrestrial variants. In that respect, the Ni-rich Santa Catharina meteorite, which was found in Brazil in 1875, received special attention and has been thoroughly examined by MS [283, 284] and by MS in applied magnetic fields [285]. The central singlet, manifestly present in the RT spectrum, has been shown to exhibit a small hyperfine field at low temperatures (Fig. 3.51). It has in a later stage been assigned to a low-spin Fe–Ni phase as an intergrowth of low-spin γ-Fe(Ni) and tetrataenite and has been proposed as a new mineral, called antitaenite [286].

Secondly, different space programs for the exploration of the Moon were initiated in the sixties of the former century. During the American manned Apollo

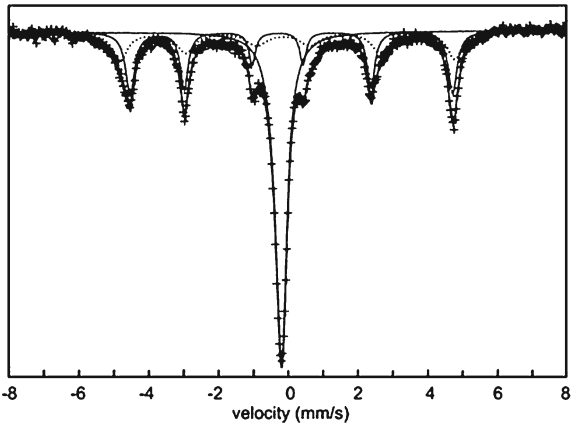

Fig. 3.51 RT spectrum of a sample of the Santa Catharina meteorite showing the sextets of ordered 50–50 Fe–Ni (*dash*) and disordered 50–50 Fe–Ni (*dots*) and the singlet of the paramagnetic 28 % Ni phase (adapted from [284])

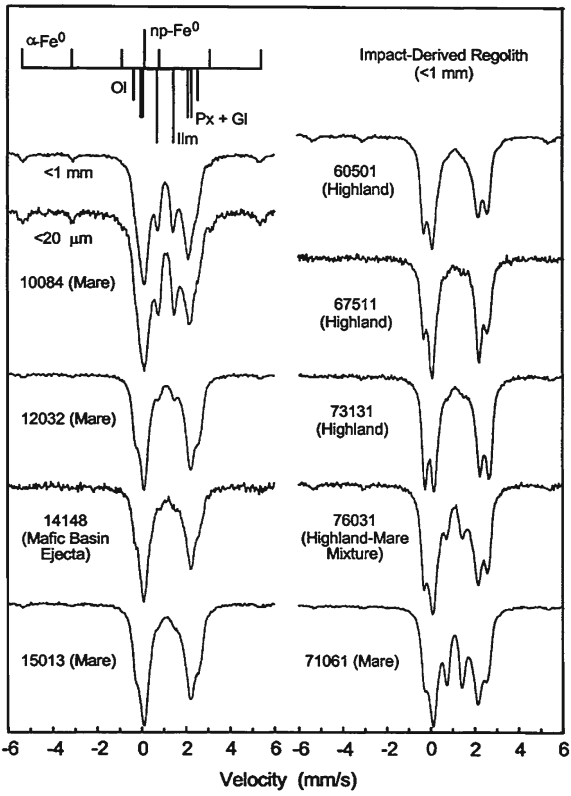

Fig. 3.52 RT spectra for impact-derived regolith samples at different lunar locations. Peak positions for the individual phases are indicated by the stick diagram (after Morris et al. [291])

lunar missions between 1969 and 1972 almost 400 kg of material have been brought to earth. Also, the Russian Luna program succeeded in 1970 in returning lunar samples to the Earth. All those regolith samples have been investigated by MS, showing the spectra of Fe-bearing phases, such as olivine, glass, pyroxene, ilmenite, triolite, iron metal and Fe–Ni alloys [287–291]. Figure 3.52 shows a collection of RT spectra of impact-derived regolith samples, i.e. surface dust less than 1 mm depth, collected at different lunar locations, illustrating ilmenite and pyroxene to be the dominant crystalline phases in mare samples, whereas pyroxene and olivine are the dominant crystalline phases in highland samples.

Two Mars exploration rovers (MER) both equipped with a miniaturized Mössbauer spectrometer (MIMOS), developed by Gustar Klingelhöfer and coworkers [292, 293], were launched in 2003. The first Mössbauer spectrum was transmitted to Earth in January 2004 and was undoubtedly the most exciting event for every Mössbauer spectroscopist. Since then both spectrometers have collected more than thousand spectra during 5 years. The spectrometer on the Opportunity (MER-B) is still operating in 2011, although the collecting time has increased considerably due to the weak source, whereas since March 2010 the other rover, the Spirit (MER-A), is not responding anymore.

All the Mössbauer spectra recorded on Mars have been publically released so that every research group could dispose of them freely. Together with each sampled spectrum, a spectrum of a reference absorber was collected and also the recorded error signal of the driver is provided. As expected, the spectra are not linear in the velocity scale, which causes some calibration difficulties. Agresti et al. [284] calibrated the spectra by considering the α-Fe lines in the reference target, combined with the error signal of the drive.

The many Mössbauer investigations of the spectra taken by the MERs on soils and rocks along their pathways showed olivines and pyroxenes as the main silicates [294–296]. Most interesting was the obvious observation of a jarosite spectrum, inferring the former presence of water on Mars [297]. This was also corroborated by the identification of goethite in the spectra from some locations [298].

Concerning the magnetic spectra, hematite and magnetite were found as the predominant iron oxides. Unfortunately, those spectra with relatively high hyperfine fields were not so well defined due to significant deviations from linearity experienced in the highest velocities, which are not covered by the sextet lines of metallic Fe in the calibration spectra. The direct use of the hematite and magnetite in the reference target for calibration was initially not simple because along with the strongly overlapping spectral lines, hematite showed the two magnetic phases in the temperature windows of the measurements. By determining the hyperfine parameters of the five sextets of Fe metal, hematite and magnetite in a laboratory sample consisting of the same reference target material measured at the appropriate temperature windows, the spectra of the reference target could be calibrated [299]. With this calibration method, several magnetic spectra recorded on Mars at different temperature windows could be accurately analyzed [299, 300] (Fig. 3.53).

For instance, magnetite could be fitted without parameter constraints. From the fit there was also a strong indication that goethite exhibits two maxima in the hyperfine field distribution inferring two different goethite formations. It was further demonstrated that the Mars hematite measured in different temperature windows between 210 and 260 K showed both the AF and WF phase giving an idea about its morphology. Some spectra are shown in Fig. 3.53. Similar results were recently obtained by Agresti et al. [301], using a simfit method consisting of the simultaneous analysis of 60 spectra with multi-spectrum constraints. However, the latter results were interpreted by the presence of two kinds of hematites, i.e. one showing the Morin transition and another remaining in the WF phase.

Finally, it is worth to mention that the Opportunity came across several meteorites on the surface of Mars [302]. The first one was found in Meridiani Planum [303]. The recorded Mössbauer spectra showed this meteorite to consist mainly of kamacite, having about 7 wt % Ni [304, 319]. No taenite spectrum was observed indicating that this iron-nickel phase probably occurs in the meteorite only in a very small amount below the detection limit of the spectrometer.

Further extraterrestrial Mössbauer measurements are planned using an improved version of the MIMOS [319]. Phobos, one of the moons of Mars, is the next target for Mössbauer investigations during the Phobos-Grunt mission by the

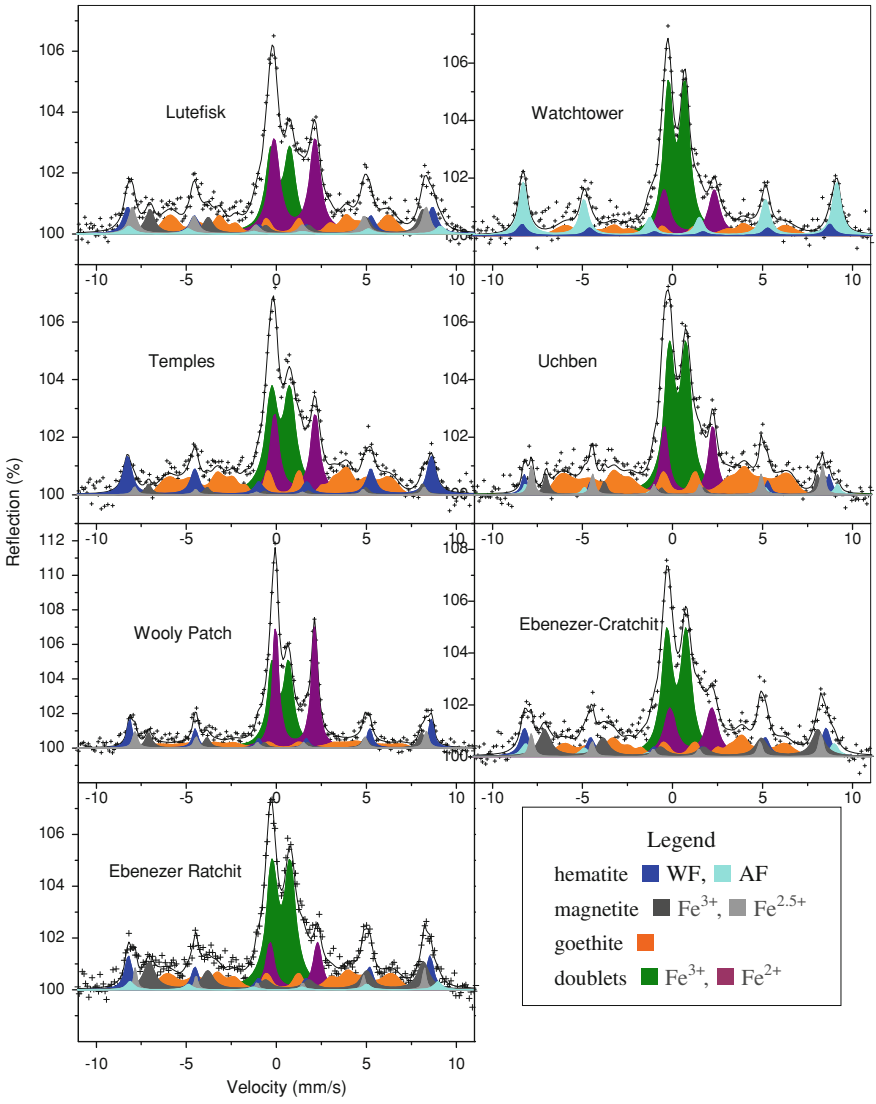

Fig. 3.53 Analyzed Mössbauer spectra taken on Mars by the Spirit at different spots in the temperature window 210–220 K (m 5) (adapted from Van Cromphaut et al. [299, 300])

Russian Space Agency. A joint ESA-NASA project aims to send two new rovers, both again equipped with a MIMOS, to Mars in 2018.

Acknowledgments We are grateful to Darby Dyar, Enver Murad and Jean-Marie Génin for providing precious information about some specific items. Darby Dyar, Richard Morris and Jean-Marie Génin are also acknowledged for giving the authorization of using some of their figures.

References

1. G.J. Long, T.E. Cranshaw, G. Longworth, The ideal Mössbauer effect absorber thicknesses. Mössbauer Eff. Ref. Data J. **6**, 42–49 (1983)
2. D.G. Rancourt, A.M. McDonald, A.E. Lalonde, J.Y. Ping, Mössbauer absorber thicknesses for accurate site populations in Fe-bearing minerals. Am. Mineral. **78**, 1–7 (1993)
3. G.M. Bancroft, *Mössbauer Spectroscopy. An Introduction for Inorganic Chemists and Geochemists* (McGraw-Hill, Maidenhead, 1973)
4. G. Lang, Interpretation of experimental Mössbauer spectrum areas. Nucl. Instrum. Meth. **24**, 425–428 (1963)
5. D.G. Rancourt, Accurate site populations from Mössbauer spectroscopy. Nucl. Instr. Meth. Phys. Res. B **44**, 199–210 (1989)
6. E. Murad, The characterization of goethite by Mössbauer spectroscopy. Am. Mineral. **67**, 1007–1011 (1982)
7. D.D. Amasiriwardena, E. De Grave, L.H. Bowen, S.B. Weed, Quantitative determination of aluminium-substituted goethite-hematite mixtures by Mössbauer spectroscopy. Clays Clay Miner. **34**, 250–256 (1986)
8. R.E. Vandenberghe, E. De Grave, G. De Geyter, C. Landuydt, Characterization of goethite and hematite in a Tunisian soil profile by Mössbauer spectroscopy. Clays Clay Miner. **34**, 275–280 (1986)
9. J. Hesse, A. Rübartsch, Model independent evaluation of overlapped Mössbauer spectra. J. Phys. E. Sci. Instrum. **7**, 526–532 (1974)
10. G. Le Caer, J.M. Dubois, Evaluation of hyperfine distributions from overlapped Mössbauer spectra of amorphous alloys. J. Phys. E. Sci. Instrum. **12**, 1083–1090 (1979)
11. C.O. Wivel, S. Morup, Improved compotutional procedure for evaluation of overlapping hyperfine parameter distributions in Mössbauer spectra. J. Phys. E. Sci. Instrum. **14**, 605–610 (1981)
12. R.E. Vandenberghe, E. De Grave, P.M.A. de Bakker, On the methodology of the analysis of Mössbauer spectra. Hyp. Interact. **83**, 29–49 (1994)
13. L.H. Bowen, S.B. Weed, Mössbauer spectroscopy of soils and sediments, in *Chemical Mössbauer Spectroscopy*, ed. by R.H. Herber (Plenum, New York, 1984), pp. 217–242
14. E. Murad, J.H. Johnston, Iron oxides and oxyhydroxides, in *Mössbauer Spectroscopy Applied to Inorganic Chemistry*, vol. 2, ed. by G.J. Long (Plenum, New York, 1987), pp. 507–582
15. R.L. Parfitt, C.W. Childs, Estimation of forms of Fe and Al—A review and analysis of contrasting soils by dissolution and Mössbauer methods. Aust. J. Soil Res. **26**, 121–144 (1988)
16. E. Murad, Application of ^{57}Fe Mössbauer spectroscopy to problems in clay mineralogy and Soil Science: possibilities and limitations, in *Advances in Soil Science*, vol. 12, ed. by B.A. Stewart (Springer, New York, 1990), pp. 125–157
17. R.E. Vandenberghe, E. De Grave, L.H. Bowen, C. Landuydt, Some aspects concerning the characterization of iron oxides and hydroxides in soils and clays. Hyp. Interact. **53**, 175–196 (1990)
18. L.H. Bowen, E. De Grave, R.E. Vandenberghe, Mössbauer effect studies of magnetic soils and sediments, in *Mössbauer Spectroscopy Applied to Magnetism and Material Science*, vol. 1, ed. by G.J. Long, F. Grandjean (Plenum, New York, 1993), pp. 115–159
19. E. Murad, Mössbauer spectroscopy of clays, soils and their mineral constituents. Clay Miner. **45**, 413–430 (2010)
20. J.B. Forsyth, I.G. Hedley, C.E. Johnson, The magnetic structure and hyperfine field of goethite (α-FeOOH). J. Phys. Chem. C **1**, 179–188 (1968)
21. E. De Grave, R.E. Vandenberghe, 57Fe Mössbauer effect study of well crystallized goethite (α-FeOOH). Hyp. Interact. **28**, 643 (1986)
22. D.C. Golden, L.H. Bowen, S.B. Weed, J.M. Bigham, Mössbauer studies of synthetic and soil-occuring aluminium-substituted goethites. Soil Sci. Soc. Am. J. **43**, 802–808 (1979)

23. B.A. Goodman, D.G. Lewis, Mössbauer spectra of aluminous goethites (α—FeOOH). J. Soil Sci. **32**, 351–364 (1981)
24. S.A. Fysh, P.E. Clark, Aluminium goethite: A Mössbauer study. Phys. Chem. Miner. **8**, 180–187 (1982)
25. E. Murad, U. Schwertmann, The influence of aluminum substitution and crystallinity on the Mössbauer spectra of goethite. Clay Miner. **18**, 301–312 (1983)
26. J. Fleisch, R. Grimm, J. Grübler, P. Gütlich, Determination of the aluminum content in natural and synthetic alumo-goethites using Mössbauer spectroscopy. J. Phys. Colloq. **C1**(41), 169–170 (1980)
27. T. Ericsson, A. Krishnamurthy, B. Srivastava, Morin-transition in Ti-substituted hematite: A Mössbauer study. Phys. Scr. **33**, 88–90 (1986)
28. J.H. Johnston, K. Norrish, ^{57}Fe Mössbauer spectroscopic study of a selection of Australian and other goethites. Aust. J. Soil Res. **19**, 231–237 (1981)
29. J. Friedl, U. Schwertmann, Aluminium influence on iron oxides: XVIII. The effect of Al substitution and crystal size on magnetic hyperfine fields of natural goethites. Clay Miner. **31**, 455–464 (1996)
30. D.G. Schulze, U. Schwertmann, The influence of aluminum on iron oxides. X. Properties of Al substituted goethites. Clay Miner. **19**, 521–539 (1984)
31. E. Wolska, U. Schwertmann, The mechanism of solid solution formation between goethite and diaspore. N Jb. Miner. Mh. **5**, 213–223 (1993)
32. C.A. Barrero, R.E. Vandenberghe, E. De Grave, G.M. Da Costa, A qualitative analysis of the Mössbauer spectra of aluminous goethites based on existing models, in ed. by I. Ortali. Conference Proceedings, vol 50 "ICAME 95″ (Editrice Compositoir, Bologna, 1996)
33. C.A. Barrero, R.E. Vandenberghe, E. De Grave, The electrical hyperfine parameters in synthetic aluminogoethites. Czech J. Phys. **47**, 533–536 (1997)
34. C.A. Barrero, R.E. Vandenberghe, E. De Grave, A.L. Morales, The influence of the sample properties on the electrical hyperfine parameters in synthetic aluminogoethites. Hyp. Interact. **C2**, 209–212 (1997)
35. R.E. Vandenberghe, C.A. Barrero, G.M. Da Costa, E. Van San, E. De Grave, Mössbauer characterization of iron oxides and (oxy) hydroxides: The present state of the art. Hyp. Interact. **126**, 247–259 (2000)
36. C.A. Barrero, R.E. Vandenberghe, E. De Grave, A.L. Morales, H. Perez, The experimental nuclear quadrupole interaction in synthetic Al-goethites of various crystallinity. Hyp. Interact. **148/149**, 337–344 (2003)
37. J.A.M. Gómez, V.G. de Resende, J. Antonissen, E. De Grave, Influence of Mn-for-Fe substitution on structural properties of synthetic goethite. Hyp. Interact. **189**, 143–149 (2009)
38. R.E. Vandenberghe, A.E. Verbeeck, E. De Grave, W. Stiers, ^{57}Fe Mössbauer effect Study of Mn-substituted goethite and hematite. Hyperfine Interact. **29**, 1157–1160 (1986)
39. R.M. Cornell, R. Giovanoli, P.W. Schindler, Clays Clay Miner. **35**, 21–28 (1987)
40. T.G. Quin, G.J. Long, C.G. Benson, S. Mann, R.J. Williams, Influence of silicon and phosphorus on structural and magnetic properties of synthetic goethite and related oxides. Clays Clay Miner. **36**, 165–175 (1988)
41. S.K. Kwon, K. Kimijima, K. Kanie, S. Suzuki, A. Muramatsu, M. Saito, K. Shinoda, Y. Waseda, Influence of silicate ions on the formation of goethite from green rust in aqueous solution. Corros. Sci. **49**, 2946–2961 (2007)
42. D. Chambaere, E. De Grave, On the Néel temperature of β-FeOOH: structural dependence and its implications. J. Magn. Magn. Mater. **42**, 263–268 (1984)
43. C.W. Childs, B.A. Goodman, E. Paterson, F.W.D. Woodhams, Nature of iron in akaganeite (ϑ-FeOOH). Aust. J. Chem. **33**, 15–26 (1980)
44. D. Chambaere, E. De Grave, R.L. Vanleerberghe, R.E. Vandenberghe, The electric field gradient at the iron sites in β-FeOOH. Hyp. Interact. **20**, 249–262 (1984)
45. D. Chambaere, E. De Grave, On the influence of the double iron co-ordination on the hyperfine field in β-FeOOH. J. Magn. Magn. Mater. **44**, 349–352 (1984)

46. C.E. Johnson, Antiferromagnetism of γ-FeOOH: A Mössbauer effect study. J. Phys. C: Solid State Phys. **2**, 1996–2002 (1969)
47. E. Murad, U. Schwertmann, The influence of crystallinity on the Mössbauer spectrum of lepidocrocite. Mineral. Mag. **48**, 507–511 (1984)
48. E. De Grave, R.M. Persoons, D.G. Chambaere, R.E. Vandenberghe, L.H. Bowen, An ^{57}Fe Mössbauer effect study of poorly crystalline γ-FeOOH. Phys. Chem. Miner. **13**, 61–67 (1986)
49. U. Schwertmann, E. Wolska, The influence of aluminum on iron oxides. XV. Al-for-Fe substitution in synthetic lepidocrocite. Clays Clay Miner. **38**, 209–212 (1990)
50. E. De Grave, G.M. da Costa, L.H. Bowen, U. Schwertmann, R.E. Vandenberghe, ^{57}Fe Mössbauer-effect study of Al-substituted lepidocrocites. Clays Clays Miner. **44**, 214–219 (1996)
51. F.V. Chukhrov, B.B. Zvyagin, A.I. Gorshkov, L.P. Ermilova, V.V. Korovushkin, E.S. Rudnitskaya, N. Yu Yakubovskaya, Ferroxyhyte, a new modification of FeOOH. Izvest. Akad. Nauk. SSSR. Ser. Geol. **5**, 5–24 (1976)
52. Y.N. Vodyanitskii, A.V. Sivtsov, Formation of ferrihydrite, ferroxyhyte, and vernadite in soil. Eurasian Soil Sci. **37**, 863–875 (2004)
53. L. Carlson, U. Schwertmann, Natural occurrence of feroxyhite (δ'-FeOOH). Clays Clay Miner. **28**, 272–280 (1980)
54. M.B. Madsen, S. Mørup, C. Bender Koch, A study of microcrystals of synthetic feroxyhite (Ω'-FeOOH). Surf. Sci. **156**, 328–334 (1985)
55. K.M. Towe, W.F. Bradley, Mineralogical constitution of colloidal 'hydrous ferric oxides'. J. Colloid Interface Sci. **24**, 384–392 (1967)
56. R.A. Eggleton, R.W. Fitzpatrick, New data and a revised structural model for ferrihydrite. Clays Clay Miner. **36**, 111–124 (1988)
57. C.W. Childs, Ferrihydrite: A review of structure, properties and occurrence in relation to soils. Z. Pflanzenernähr. Bodenk. **155**, 441–448 (1992)
58. R.L. Parfitt, C.W. Childs, A structural model for natural siliceous ferrihydrite. Clays Clay Miner. **40**, 675–681 (1992)
59. V.A. Drits, B.A. Sakhorov, A.L. Salyn, A. Manceau, Structural model for ferrihydrite. Clay Miner. **28**, 185–207 (1993)
60. E. Jansen, A. Kyek, W. Schäfer, U. Schwertmann, The structure of six-line ferrihydrite. Appl. Phys. A **74**, 04–06 (2002)
61. F.M. Michel, L. Ehm, S.M. Antao, P.L. Lee, P.J. Chupas, L. Gang, D.R. Strongin, M.A.A. Schoonen, B.L. Phillips, J.B. Parise, The structure of ferrihydrite, a nanocrystalline material. Science **316**, 1726–1729 (2007)
62. R. Harrington, M. Michel, J. Parise, D. Hausner, D. Strongin, Powder neutron diffraction studies of ferrihydrite, a nanocrystalline material. Geochim. Cosmochim. Acta **74**(Suppl 1), A383–A383 (2010)
63. E. Murad, L.H. Bowen, G.J. Long, G.J. Quin, The influence of crystallinity on magnetic ordering in natural ferrihidrites. Clay Miner. **23**, 161–173 (1988)
64. C. Gilles, P. Bonville, K.K.W. Wong, S. Mann, Non-Langevin behaviour of the uncompensated magnetization in nanoparticles of artificial ferritin. Eur. Phys. J. B **17**, 417–427 (2000)
65. Y. Guyodo, S.K. Banerjee, R.L. Penn, D. Burleson, T.S. Berquó, T. Seda, P. Solheid, Magnetic properties of synthetic six-line ferrihydrite nanoparticles. Phys. Earth Plant. Int. **157**, 222–233 (2006)
66. G. De Geyter, R.E. Vandenberghe, L. Verdonck, G. Stoops, Mineralogy of Holocene bog iron ore in northern Belgium. Neues Jahrb. Miner. Abh. **153**, 1–17 (1985)
67. U. Schwertmann, J. Friedl, A. Kyek, Formation and properties of a crystallinity series of synthetic ferrihydrites (2- to 6-line) and their relation to FeOOH forms. Clays Clay Miner. **52**, 221–226 (2004)
68. E. Murad, The Mössbauer spectrum of "well"-crystallized ferrihydrite. J. Magn. Magn. Mater. **74**, 153–157 (1988)

69. J. Chadwick, D.H. Jones, M.F. Thomas, G.J. Tatlock, R.W. Devenish, A Mössbauer study of ferrihydrite and aluminium substituted ferrihydrites. J. Magn. Magn. Mater. **61**, 88–100 (1986)
70. L. Carlson, U. Schwertmann, Natural ferrihydrites in surface deposits from Finland and their association with silica: Geochim. Cosmochim. Acta **45**, 421–429 (1981)
71. A.S. Campbell, U. Schwertmann, H. Stanjek, J. Friedl, A. Kyek, P.A. Campbell, Si incorporation into hematite by heating Si-ferrihydrite. Langmuir **18**, 7804–7809 (2002)
72. T.S. Berquó, S.K. Banerjee, R.G. Ford, R.L. Pichler, T. Penn, High crystallinity Si-ferrihydrite: An insight into its Néel temperature and size dependence of magnetic properties. J. Geophys. Res. **112**, B02102 (2007). doi:10.1029/2006JB004583
73. U. Schwertmann, F. Wagner, H. Knicker, Ferrihydrite–humic associations: magnetic hyperfine interactions. Soil Sci. Soc. Am. J. **69**, 1009–1015 (2005)
74. U. Schwertmann, Differenzierung der Eisenoxide des Bodens durch Extraktion mit Ammoniumoxalat-Lösung Z. Pflanzenernähr. Düng. Bodenk. **195**, 194–202 (1964)
75. U. Schwertmann, D.G. Schulze, E. Murad, Identification of ferrihydrite in soils by dissolution kinetics, differential X-ray-diffraction, and Mössbauer-spectroscopy. Soil Sci. Am. J. **46**, 869–875 (1982)
76. J.A. McKeague, J.H. Day, Dithionite- and oxalate-extractable Fe and Al as aids in differentiating various classes of soils. Can. J. Soil Sci. **46**, 13–22 (1966)
77. U. Schwertmann, Use of oxalate for Fe extraction from soils. Can. J. Soil Sci. **53**, 244–246 (1973)
78. A.L. Walker, The effects of magnetite on oxalate-and dithionite-extractable iron. Soil Sci. Soc. Am. J. **47**, 1022–1026 (1983)
79. A.S. Campbell, U. Schwertmann, Evaluation of selective dissolution extractants in soil chemistry and mineralogy by differential X-ray diffraction. Clay Miner. **20**, 515–519 (1985)
80. J. Arocena, G. De Geyter, C. Landuydt, U. Schwertmann, Dissolution of soil iron oxides with ammonium oxalate: Comparison between bulk samples and thin sections. Pedologie **XXXIX-3**, 275–297 (1989)
81. F. van der Woude, Mössbauer Effect in α-Fe_2O_3. Phys. Status Solidi **17**, 417–432 (1966)
82. W. Kündig, H. Bömmel, G. Constabaris, R.H. Linquist, Some properties of supported small α-Fe_2O_3 particles determined with the Mössbauer effect. Phys. Rev. **142**, 327–333 (1966)
83. A.M. van der Kraan, Mössbauer effect studies of surface ions of ultrafine α-Fe_2O_3 particles. Phys. Status Solidi (a) **18**, 215–226 (1973)
84. T. Shinjo, M. Kiyama, N. Sugita, K. Watanabe, K. Takada, Surface magnetism of α- Fe_2O_3 by the Mössbauer spectroscopy. J. Magn. Magn. Mater. **35**, 133–135 (1983)
85. T. Yang, A. Krishnan, N. Benczer-Koller, G. Bayreuther, Surface magnetic hyperfine interactions in Fe_2O_3 determined by energy-resolved conversion-electron. Phys. Rev. Lett. **48**, 1292–1295 (1982)
86. C. Van Cromphaut, V.G. de Resende, E. De Grave, R.E. Vandenberghe, Surface effects in α-Fe_2O_3 nanoparticles studied by ILEEMS and TMS. Hyp. Interact. **191**, 167–171 (2009)
87. D.G. Rancourt, S.R. Julian, J.M. Daniels, Mössbauer characterization of very small superparamagnetic particles: Application to intra-zeolitic Fe_2O_3. J. Magn. Magn. **49**, 305–316 (1985)
88. R.C. Nininger Jr, D. Schroeer, Mössbauer studies of the Morin transition in bulk and microcrystalline α-Fe_2O_3. J. Phys. Chem. Solids **39**, 137–144 (1978)
89. A.E. Verbeeck, E. De Grave, R.E. Vandenberghe, Effect of the particle morphology on the Mössbauer effect in α-Fe_2O_3. Hyp. Interact. **28**, 639–642 (1986)
90. E. De Grave, R.E. Vandenberghe, Mössbauer effect study of the spin structure in natural hematites. Phys. Chem. Miner. **17**, 344–352 (1990)
91. N. Amin, S. Arajs, Morin temperature of annealed submicronic α-F_2O_3 particles. Phys. Rev. B **35**, 4810–4811 (1987)
92. E. De Grave, L.H. Bowen, D.D. Amarasiriwardena, R.E. Vandenberghe, ^{57}Fe Mössbauer effect study of highly substituted aluminum hematites: determination of the magnetic hyperfine field distributions. J. Magn. Magn. Mater. **72**, 129–140 (1988)

93. M.-Z. Dang, D.G. Rancourt, J.E. Dutrizac, G. Lamarche, R. Provencher, Interplay of surface conditions, particle size, stoichiometry, cell parameters, and magnetism in synthetic hematite-like materials. Hyp. Interact. **117**, 271–319 (1998)
94. J.F. Bengoa, M.S. Moreno, S.G. Marchetti, R.E. Vandenberghe, R.C. Mercader, Study of the Morin transition in pseudocubic α-Fe_2O_3 particles. Hyp. Interact. **161**, 177–183 (2005)
95. P.M.A. de Bakker, E. Grave, R.E. Vandenberghe, L.H. Bowen, R.J. Pollard, R.M. Persoons, Mössbauer study of the thermal decomposition of lepidocrocite and characterization of the decomposition products. Phys. Chem. Miner. **18**, 131–143 (1991)
96. E. Van San, E. De Grave, R.E. Vandenberghe, H.O. Desseyn, L. Datas, V. Barrón, A. Rousset, Study of Al-substituted hematites, prepared from thermal treatment of lepidocrocite. Phys. Chem. Miner. **28**, 488–497 (2001)
97. R.E. Vandenberghe, E. Van San, E. De Grave, G.M. Da Costa, About the Morin transition in hematite in relation with particle size and aluminium substitution. Czech J. Phys. **51**, 663–675 (2001)
98. U. Schwertmann, R.W. Fitzpatrick, R.M. Taylor, D.G. Lewis, The influence of aluminum on iron oxides: II. Preparation and properties of aluminum-substituted hematites. Clays Clay Miner. **27**, 105–112 (1979)
99. S.A. Fysh, P.E. Clark, Aluminium hematite: a Mössbauer study. Phys. Chem. Miner. **8**, 257–267 (1982)
100. E. De Grave, L.H. Bowen, S.B. Weed, Mössbauer study of aluminum-substituted hematites. J. Magn. Magn. Mater. **27**, 98–108 (1982)
101. E. De Grave, D. Chambaere, L.H. Bowen, Nature of the Morin transition in Al-substituted hematite. J. Magn. Magn. Mater. **30**, 349–354 (1983)
102. E. Murad, U. Schwertmann, Influence of Al substitution and crystal size on the room-temperature Mössbauer spectra of hematite. Clays Clay Miner. **34**, 1–6 (1986)
103. G.M. da Costa, E. Van San, E. De Grave, R.E. Vandenberghe, V. Barrón, L. Datas, Al hematites prepared by homogeneous precipitation of oxinates: material characterization and determination of the Morin transition. Phys. Chem. Miner. **29**, 122–131 (2002)
104. V. Baron, J. Gutzmer, H. Rundlof, R. Tellgren, Neutron powder diffraction study of Mn-bearing hematite, α-$Fe_2 - {}_xMn_xO_3$, in the range $0 \leq x \leq 0.176$. Solid State Sci. **7**, 753–759 (2005)
105. R.M. Cornell, R. Giovanoli, Effect of manganese on the transformation of ferrihydrite into goethite and jacobsite in alkaline media. Clays Clay Miner. **35**, 11–20 (1987)
106. R.E. Vandenberghe, A.E. Verbeeck, E. De Grave, On the Morin transition in Mn-substituted hematite. J. Magn. Magn. Mater. **54–57**, 898–900 (1986)
107. G. Shirane, D.E. Cox, W.J. Takei, S.L. Ruby, A study of the magnetic properties of the $FeTiO_3$-αFe_2O_3 system by neutron diffraction and the Mössbauer effect. J. Phys. Soc. Jpn. **17**, 1598–1611 (1962)
108. A.H. Muir Jr, R.M. Housley, R.W. Grant, M. Abdel-Gawad, M. Blander, Mössbauer spectroscopy of Moon samples. Science **167**, 688–690 (1970)
109. R.W. Grant, R.M. Housley, S. Geller, Hyperfine interactions of Fe^{2+} in ilmenite. Phys. Rev. B **5**, 1700–1703 (1972)
110. W. Kim, I.I.J. Park, C.S. Kim, Mössbauer study of magnetic structure of cation-deficient iron sulfide $Fe_{0.92}S$. J. Appl. Phys. **105**, 07D535–07D535-3 (2009)
111. W.Q. Guo, S. Malus, D.H. Ryan, Z. Altounian, Crystal structure and cation distributions in the $FeTi_2O_5$–Fe_2TiO_5 solid solution series. J. Phys. Condens. Matter. **11**, 6337–6346 (1999)
112. L. Häggström, H. Annersten, T. Ericsson, R. Wäppling, W. Karner, S. Bjarman, Magnetic dipolar and electric quadrupolar effects on the Mössbauer spectra of magnetite above the Verwey transition. Hyp. Interact. **5**, 201–214 (1978)
113. H. Annersten, S.S. Hafner, Vacancy distribution in synthetic spinels of the series Fe_3O_4–γ-Fe_2O_3. Z. Kristallogr. **137**, 321–340 (1973)
114. A. Ramdani, J. Steinmetz, C. Gleitzer, J.M.D. Coey, J.M. Friedt, Perturbation de l'échange electronique rapide par des lacunes cationiques dans $Fe_{3-x}O_4$ ($x \leq 0.09$). J. Phys. Chem. Solids **48**, 217–228 (1987)

115. C.I. Pearce, C.M.B. Henderson, N.D. Teiling, R.A.D. Pattrick, D.J. Vaughan, J.M. Charnock, E. Arenholz, F. Tuna, V.S. Coker, G. van der Laan, Iron site occupancies in magnetite-ulvöspinel solid solution: a new approach using X-ray magnetic circular dichroism. Am. Mineral. **95**, 425–439 (2010)
116. H. Tanaka, M. Kono, Mössbauer spectra of titanomagnetite: A reappraisal. J. Geomag. Geoelectr. **39**, 463–475 (1987)
117. H.H. Hamdeh, K. Barghout, J.O. Ho, P.M. Shand, L.L. Miller, A Môssbauer evaluation of cation distribution in titanomagnetites. J. Magn. Magn. Mater. **191**, 72–78 (1999)
118. R.S. Hargrove, W. Kündig, Mössbauer measurements of magnetite below the Verwey transition. Solid State Commun. **8**, 303–308 (1970)
119. Y. Miyahara, Impurity effects on the transition temperature of magnetite. J Phys. Soc. Jpn. **32**, 629–634 (1972)
120. V.A.M. Brabers, F. Waltz, H. Kronmuller, Impurity effects upon the Verwey transition in magnetite. Phys. Rev. B **58**, 14163–14166 (1998)
121. M.M. Hanzlik, N. Petersen, R. Keller, E. Schmidbauer, Electron microscopy and ^{57}Fe Mössbauer spectra of 10 nm particles, intermediate in composition between Fe_3O_4–γ-Fe_2O_3, produced by bacteria. Geophys. Res. Lett. **23**, 479–482 (1996)
122. G.M. da Costa, E. De Grave, L.H. Bowen, P.M.A. de Bakker, R.E. Vandenberghe, The center shift in Mössbauer spectra of maghemite and aluminum maghemites. Clays Clay Miner. **42**, 628–633 (1994)
123. J.M.D. Coey, D. Khalafalla, Superparamagnetic γ-Fe_2O_3. Phys. Status Solidi (a) **11**, 229–242 (1972)
124. U. Schwertmann, Occurrence and formation of iron in various pedenvironments, in *Iron in Soils and Clay Minerals*, vol. 217, NATO ASI Series, Series C: Math. and Phys. Sci., ed. by J.W. Stucki, B.A. Goodman, U. Schwertmann (D.Reidel Publication, Dordrecht, 1988), pp. 267–308
125. G.M. da Costa, C.H. Laurent, E. De Grave, R.E. Vandenberghe, A comprehensive Mössbauer study of highly-substituted aluminium maghemite. eds. by M.D. Dyar, C. McCammon, M.W. Schaefer, Mineral Spectroscopy: A Tribute to Roger G. Burns, The Geochemical Society (Special Publication 5, 1996) pp. 93–104
126. G.M. da Costa, E. De Grave, R.E. Vandenberghe, Mössbauer studies of maghemites and Al-substituted maghemites. Hyp. Interact. **117**, 207–243 (1998)
127. J.E.M. Allan, J.M.D. Coey, I.S. Sanders, U. Schwertmann, G. Friedrich, A. Wiechowski, An occurrence of a fully-oxidized natural titanomaghemite in basalt. Miner. Mag. **53**, 299–304 (1989)
128. W. Xu, D.R. Peacor, W.A. Dollase, R. Van Der Voo, R. Beaubouef, Transformation of titanomagnetite to titanomaghemite: A slow-step oxidation ordering process in MORB. Am. Mineral. **82**, 1101–1110 (1997)
129. S. Collyer, N.W. Grimes, D.J. Vaughan, G. Longworth, Studies of the crystal structure and crystal chemistry of titanomaghemite. Am. Mineral. **73**, 153–160 (1988)
130. E. Murad, R.M. Taylor, The Mössbauer spectra of hydroxycarbonate green rusts. Clay Miner. **19**, 77–83 (1984)
131. J.M.R. Génin, Ph Bauer, A.A. Olowe, D. Rézel, Mössbauer study of the kinetics of simulated corrosion process of iron in chlorinated aqueous solution around room temperature: the hyperfine structure of ferrous hydroxides and green rust I. Hyp. Interact. **29**, 1355–1360 (1986)
132. A.A. Olowe, J.M.R. Génin, Ph Bauer, Hyperfine interactions and structures of ferrous hydroxide and green rust II in sulfated aqueous media. Hyp. Interact. **41**, 501–504 (1988)
133. S.H. Drissi, Ph Refait, M. Abdelmoula, J.-M.R. Génin, Preparation and thermodynamic properties of Fe(II)-Fe(III) hydroxycarbonate (green rust 1), Pourbaix diagram of iron in carbonate-containing aqueous media. Corros. Sci. **37**, 2025–2041 (1995)
134. C. Ruby, M. Abdelmoula, S. Naille, A. Renard, V. Khare, G. Ona-Nguema, G. Morin, J.M.R. Génin, Oxidation modes and thermodynamics of Fe^{II-III} oxyhydroxycarbonate green

rust: dissolution-precipitation versus in situ deprotonation. Geochim. Cosmochim. Acta **74**, 953–966 (2009)
135. F. Trolard, J.M.R. Génin, M. Abdelmoula, G. Bourrié, B. Humbert, A.J. Herbillon, Identification of a green rust mineral in a reductomorphic soil by Mössbauer and Raman spectroscopies. Geochim. Cosmochim. Acta **61**, 1107 (1997)
136. M. Abdelmoula, F. Trolard, G. Bourrié, J.M.R. Génin, Evidence of Fe(II)-Fe(III) Green rust "Fougerite" mineral occurrence in hydromorphic soil and its transformation with depth. Hyp. Interact. **112**, 235–238 (1998)
137. F. Féder, F. Trolard, G. Klingelhöfer, G. Bourrié, In situ Mössbauer spectroscopy evidence for green rust (fougerite) in a gleysol and its mineralogical transformations with time and depth. Geochim. Cosmochim. Acta **69**, 4463–4483 (2005)
138. J.-M.R. Génin, O. Guérin, A.J. Herbillon, E. Kuzmann, S.J. Mills, G. Morin, G. Ona-Nguema, C. Ruby, C. Upadhyay, Redox topotactic reactions in Fe^{II-III} oxyhydroxycarbonate new minerals related to fougèrite in gleysols: "trébeurdenite and mössbauerite". Hyp. Interact. **204**(1–3), 71–81 (2012)
139. B. Rusch, J.M.R. Génin, C. Ruby, M. Abdelmoula, P. Bonville, Ferrimagnetic properties of Fe(II-III) (oxy)hydoxycarbonate green rust. Solid State Sci. **10**, 40 (2008)
140. S. Hafner, M. Kalvius, The Mössbauer resonance of Fe in troilite and pyrrhotite. Z. Krist. **123**, 443–458 (1966)
141. L.F. Power, H.A. Fine, The iron-sulphur system. Part l. The structures and physical properties of the compounds of the low-temperature phase fields. Miner. Sci. Eng. **8**, 106–128 (1976)
142. A.D. Elliot, Structure of pyrrhotite 5*C* (Fe_9S_{10}). Acta Cryst. **B66**, 271–279 (2010)
143. R. Gosselin, M.G. Townsend, R.J. Tremblay, A.H. Webster, Mössbauer effect in single-crystal $Fe_{1-x}S$. J. Solid State Chem. **17**, 43–48 (1976)
144. M.G. Townsend, A.H. Webster, J.L. Harwood, H. Roux-Buisson, Ferrimagnetic transition in $Fe_{0.9}S$—Magnetic, thermodynamic and kinetic aspects. J. Phys. Chem. Solids **40**, 183–189 (1979)
145. V.P. Gupta, A.K. Singh, K. Chandra, S.K. Jaireth, Investigations of pyrrhotites of Indian ore deposits. in *ED Proceedings of the Indian Science Academy*, International Conferences on the Application of the Mössbauer Effect, Jaipur 1981, (Indian Nat Science Academy, New Delhi, 1982), pp. 863–865
146. M. Saporoschenko, C.C. Hinckley, H. Twardowska, G.V. Smith, O. Zahraa, R.H. Shiley, K.L. Konopka, Mössbauer study of synthetic pyrrhotite. in *ED Proceedings of the Indian Science Academy*, *International Conference on the Application of the Mössbauer Effect*, *Jaipur 1981*, (Indian National Science Academy, New Delhi, 1982), pp. 869–871
147. C. Jeandey, J.L. Oddou, J.L. Mattei, G. Fillion, Mössbauer investigation of the pyrrhotite at low temperature. Solid State Commun. **78**, 195–198 (1991)
148. R.E. Vandenberghe, E. De Grave, P.M.A. de Bakker, M. Krs, J.J. Hus, Mössbauer study of natural greigite. Hyp. Interact. **68**, 319–322 (1991)
149. V. Hoffmann, H. Stanjek, E. Murad, Mineralogical, magnetic and Mössbauer data of smythite (Fe_9S_{11}). Studia Geophys. Geod. **37**, 366–380 (1993)
150. J.M.D. Coey, M.R. Spender, A.H. Morrish, Magnetic structure of spinel Fe_3S_4. Solid State Commun. **8**, 1605–1608 (1970)
151. L. Chang, B.D. Rainford, J.R. Stewart, C. Ritter, A.P. Roberts, Y. Tang, Q. Chen, Magnetic structure of greigite (Fe_3S_4) probed by neutron powder diffraction and polarized neutron diffraction. J. Geophys. Res. **114**, B07101 (2009). doi:10.1029/2008JB006260
152. A.P. Roberts, L. Chang, C.J. Rowan, C.-S. Horng, F. Florindo, Magnetic properties of sedimentary greigite (Fe_3S_4): An update. Rev. Geophys. **49**, RG1002 (2011). doi:10.1029/2010RG000336
153. J.A. Morice, L.V.C. Rees, D.T. Rickard, Mössbauer studies of iron sulphides. J. Inorg. Nucl. Chem. **31**, 3797–3802 (1969)
154. D.J. Vaughan, M.S. Ridout, Mössbauer studies of some sulphide minerals. J. Inorg. Nucl. Chem. **33**, 741–746 (1971)

155. O. Knop, C.-H. Huang, F.W.D. Woodhams, Chalcogenides of the transition elements. VII. A Mössbauer study of pentlandite. Am. Mineral. **55**, 115–1130 (1970)
156. P.L. Wincott, D.J. Vaughan, Spectroscopic studies of sulfides. Rev. Mineral. **61**, 181–229 (2006)
157. F.C. Hawthorne, S.V. Krivovichev, P.C. Burns, The crystal chemistry of sulfate minerals. Rev. Mineral. Geochem. **40**, 1–112 (2000)
158. J.G. Stevens, A.M. Khasanov, J.W. Miller, H. Pollak, Z. Li (eds.), *Mössbauer Minerals Handbook* (Mössbauer Effect Data Center, Asheville, 1998)
159. V.A. O'Connor, Comparative crystal chemistry of hydrous iron sulfates from different terrestrial environments. Ph.D thesis, Mount Holyoke College, South Hadley, (2005)
160. M.D. Dyar, D.G. Agresti, M.W. Schaefer, C.A. Grant, E.C. Sklute, Mössbauer spectroscopy of earth and planetary materials. An. Rev. Earth Planetary Sci. **34**, 83–125 (2006)
161. A. Ertl, M.D. Dyar, J.M. Hughes, F. Brandstätter, M.E.M. Gunther, R.C. Peterson, Pertlikite, a new tetragonal Mg-rich member of the voltaite group from Madeni Zakh. Iran. Can. Mineral. **46**, 661–669 (2008)
162. A. Van Alboom, V.G. De Resende, E. De Grave, J.A.M. Gómez, Hyperfine interactions in szomolnokite ($FeSO_4 \cdot H_2O$). J. Molec. Struct. **924–926**, 448–456 (2009)
163. P.P. Gil, A. Pesquera, F. Velasco, X-ray diffraction, infrared and Mössbauer studies of Fe-rich carbonates. Eur. J. Miner. **4**, 521–526 (1992)
164. V.I. Goldanskii, E.F. Makarov, I.P. Suzdalev, I.A. Vinogradov, Quantitative test of the vibrational anisotropy origin of the asymmetry of quadrupole Mössbauer doublets. Phys. Rev. Lett. **20**, 137–140 (1968)
165. T. Ericsson, R. Wäppling, Texture effects in 3/2-1/2 Mössbauer spectra. J. Phys. **C6**(37), 719–726 (1976)
166. K.K.P. Srivastava, A Mössbauer study of slow spin relaxation of paramagnetic Fe^{2+} in $MgCO_3$. J. Phys. C. Solid State Phys. **16**, 1137–1139 (1983)
167. E. De Grave, R. Vochten, An ^{57}Fe mössbauer effect study of ankerite. Phys. Chem. Miner. **12**, 108–113 (1985)
168. E. De Grave, ^{57}Fe Mössbauer effect in ankerite: Study of the electronic relaxation. Solid State Commun. **60**, 541–544 (1986)
169. G. Hilscher, P. Rogl, J. Zemann, T. Ntaflos, Low-temperature magnetic investigation of ankerite. Eur. J. Miner. **17**, 103–105 (2005)
170. R.J. Reeder, W.A. Dollase, Structural variation in the dolomite-ankerite solid-solution series: An X-ray, Mössbauer, and TEM study. Am Miner. **74**, 1159–1167 (1989)
171. M.W. Schaefer, Measurements of iron(Ill)-rich fayalites. Nature **303**, 325–327 (1983)
172. J.F. Duncan, J.H. Johnston, The determination of the cation distribution in olivine from single crystal Mössbauer studies. Aust. J. Chem. **26**, 231–239 (1973)
173. R. Santoro, R. Newnham, S. Nomura, Magnetic properties of Mn_2SiO_4 and Fe_2SiO_4. J. Phys. Chem. Solids **27**, 655–666 (1966)
174. W. Lottermoser, K. Forcher, G. Amthauer, H. Fuess, Powder- and single crystal Mössbauer spectroscopy on synthetic fayalite. J. Phys. Chem. Miner. **22**, 259–267 (1995)
175. F. Belley, E.C. Ferré, F. Martín-Hernández, M.J. Jackson, M.D. Dyar, E.J. Catlos, The magnetic properties of natural and synthetic $(Fe_x, Mg_{1-x})_2SiO_4$ olivines. Earth and Planet. Sci. Lett. **284**, 516–526 (2009)
176. W. Kündig, J.A. Cape, R.H. Lindquist, G. Constabaris, Some magnetic properties of Fe_2SiO_4 from 4 K to 300 K. J. Appl. Phys. **38**, 947–948 (1967)
177. S.S. Hafner, J. Stanek, M. Stanek, ^{57}Fe hyperfine interactions in the magnetic phase of fayalite, Fe_2SiO_4. J. Phys. Chem. Solids **51**, 203–208 (1990)
178. X. Kan, J.M.D. Coey, Mössbauer spectra, magnetic and electrical properties of laihunite, a mixed-valence iron olivine mineral. Am. Mineral. **70**, 567–580 (1985)
179. M.W. Schaefer, Site occupancy and two-phase character of "ferrifayalite". Am. Mineral. **70**, 729–736 (1985)
180. G. Amthauer, H. Annersten, S.S. Hafner, The Mössbauer spectrum of ^{57}Fe in silicate garnets. Zeit. Kristallogr. **143**, 14–55 (1976)

181. E. Murad, F.E. Wagner, The Mössbauer spectrum of almandine. Phys. Chem. Miner. **14**, 264–269 (1987)
182. E. Murad, Magnetic ordering in andradite. Am. Mineral. **69**, 722–724 (1984)
183. K.B. Schwartz, D.A. Nolet, R.G. Burns, Mössbauer spectroscopy and crystal chemistry of natural Fe-Ti garnets. Am. Mineral. **65**, 142–153 (1980)
184. G.M. Bancroft, A.G. Maddock, R.G. Burns, Application of the Mössbauer effect of silicate mineralogy: I. Iron silicates of known crystal structure. Geochim. Cosmochim. Acta **31**, 831–834 (1967)
185. W.A. Dollase, Mössbauer spectra and iron distribution in the epidote-group minerals. Z. Krist. **138**, 41–63 (1973)
186. K.T. Fehr, S. Heuss-Assbichler, Intracrystalline equilibria and immiscibility along the join clinozoisite-epidote. An experimental and ^{57}Fe Mössbauer study. N. Jb. Min. Abh. **172**, 43–67 (1997)
187. M. Grodzicki, S. Heuss-Assbichler, G. Amthauer, Mössbauer investigations and molecular orbital calculations. Phys. Chem. Miner. **28**, 675–681 (2001)
188. A.K. Dzhemai, Distribution of cations in structures of iron magnesia silicates. Staurolites. V.A. Glebovitskii, ed. by in *Raspred Kationov Termodin Zhelezo-Magrez Tverd Rastvorov Silik*. (Izv. Nauka, Leningrad Old, Leningrad 1978), pp. 136–152
189. M.D. Dyar, C.L. Perry, C.R. Rebbert, B.L. Dutrow, M.J. Holdway, H.M. Lang, Mössbauer spectroscopy of synthetic and naturally occurring staurolite. Am. Mineral. **76**, 27–41 (1991)
190. M. Akasaka, M. Nagashima, K. Makino, H. Ohashi, Distribution of Fe_3 + in a synthetic $(Ca, Na)_2(Mg, Fe^{3+})Si_2O_7$–melilite: ^{57}Fe Mössbauer and X-ray Rietveld studies. J. Mineral. Petrol. Sci. **100**, 229–236 (2005)
191. B. Ghazi-Bayat, M. Behruzi, F.J. Litterst, W. Lottermoser, G. Amthauer, Crystallographic phase transition and valence fluctuation in synthetic Mn-bearing ilvaite CaFe2+2–xMnxFe3+[Si2O7/O/(OH)]. Phys. Chem. Miner. **18** 491–496 (1992)
192. F.J. Litterst, G. Amthauer, Electron delocalization in ilvaite, a reinterpretation of its ^{57}Fe Mössbauer spectrum. Phys. Chem. Miner. **10**, 250–255 (1984)
193. C.R. Dotson, B.J. Evans, The effects of chemical composition on electron delocalization and magnetic ordering in ilvaite, $Ca[Fe^{2+},Fe^{3+}][Fe^{2+}]Si_2O_7O(OH)$. J. Appl. Phys. **85**, 5235–5236 (1999)
194. D.A. Nolet, Electron delocalization observed in the Mössbauer spectrum of ilvaite. Solid State Commun. **28**, 719–722 (1978)
195. D.A. Nolet, R.G. Burns, Ilvaite: A study of temperature dependent electron delocalization by the Mössbauer effect. Phys. Chem. Miner. **4**, 221–234 (1979)
196. N. Zotov, W. Kockelman, S.D. Jacobsen, I. Mitov, D. Paneva, R.D. Vassileva, I.K. Bonev, Structure and cation ordering in manganilvaite: a combined X-ray diffraction, neutron diffraction, and Mössbauer study. Can. Mineral. **43**, 1043–1053 (2005)
197. G. Amthauer, W. Lottermoser, G. Redhammer, G. Tippelt, Mössbauer studies of selected synthetic silicates. Hyp. Interact. **113**, 219–248 (1998)
198. D.C. Price, E.R. Vance, G. Smith, A. Edgar, B.L. Dickson, Mössbauer effect studies on beryl. J. Phys. **C6**(37), 811–816 (1976)
199. R.R. Viana, G.M. da Costa, E. De Grave, H. Jordt-Evangelista, W.B. Stern, Characterization of beryl (aquamarine variety) by Mössbauer spectroscopy. Phys. Chem. Miner. **29**, 78–86 (2002)
200. J.F. Duncan, J.H. Johnston, Single crystal ^{57}Fe Mössbauer studies of the site positions in cordierite. Aust. J. Chem. **27**, 249–258 (1974)
201. C.A. Geiger, T. Armbruster, V. Khomenko, S. Quartieri, Cordierite I: The coordination of Fe^{2+}. Am. Mineral. **85**, 1255–1264 (2000)
202. R.G. Burns, Mixed valencies and site occupancies of iron in silicate minerals from Mössbauer spectroscopy. Can. J. Spectr. **17**, 51–59 (1972)
203. Y. Fuchs, M. Lagache, J. Linares, R. Maury, F. Varret, Mössbauer and optical spectrometry of selected schorl-dravite tourmalines. Hyperfine Interact. **96**, 245–258 (1995)

204. A. Pieczka, J. Kraczka, W. Zabinski, Mössbauer spectra of Fe^{3+}-poor schorls: reinterpretation on the basis of the ordered structure model. J. Czech Geol. Soc. **43**, 69–74 (1998)
205. G.M. da Costa, C. Casteneda, N.S. Gomes, N.S. Pedrosa-Soares, C.M. Santana, On the analysis of the Mössbauer spectra of tourmalines. Hyp. Interact. **2**, 29–34 (1997)
206. M.D. Dyar, M.E. Taylor, T.M. Lutz, C.A. Francis, C.V. Guidotti, M. Wise, Inclusive chemical characterization of tourmaline: Mössbauer study of Fe valence site occupancy. Am. Mineral. **83**, 848–864 (1998)
207. S.G. Eeckhout, C. Corteel, E. Van Coster, E. De Grave, P. De Paepe, Crystal-chemical characterization of tourmalines from the English Lake District: Electron-microprobe analyses and Mössbauer spectroscopy. Am. Mineral. **89**, 1743–1751 (2004)
208. B.J. Evans, S. Ghose, S.S. Hafner, Hyperfine splitting of ^{57}Fe and Mg-Fe order-disorder in orthopyroxenes ($MgSiO_3$–$FeSiO_3$ solid solution). J. Geol. **75**, 306–322 (1967)
209. M.D. Dyar, R.L. Klima, D. Lindsley, C.M. Pieters, Effects of differential recoil-free fraction on ordering and site occupancies in Mössbauer spectroscopy of orthopyroxenes. Am. Mineral. **92**, 424–428 (2007)
210. S.G. Eeckhout, E. De Grave, C.A. McCammon, R. Vochten, Temperature dependence of the hyperfine parameters in synthetic *P*21/*c* Mg-Fe pyroxenes along the $MgSiO_3$-$FeSiO_3$ join. Am. Mineral. **85**, 943–952 (2000)
211. G.M. Bancroft, P.G.L. Williams, R.G. Burns, Mössbauer spectra of minerals along the diopside—hedenbergite tie line. Am. Mineral. **56**, 1617–1625 (1971)
212. S.G. Eeckhout, E. De Grave, ^{57}Fe Mössbauer-effect studies of Ca-rich, Fe-bearing clinopyroxenes: Part I. Paramagnetic spectra of magnesian hedenbergite. Am. Mineral. **88**, 1128–1137 (2003)
213. E. De Grave, S.G. Eeckhout, ^{57}Fe Mössbauer-effect studies of Ca-rich, Fe-bearing clinopyroxenes: Part III Diopside. Am. Mineral. **88**, 1145–1152 (2003)
214. E. Dowty, D.H. Lindslay, Mössbauer spectra of synthetic hedenbergite-ferrosilite pyroxenes. Am. Mineral. **58**, 850–868 (1973)
215. L.P. Aldridge, G.M. Bancroft, M.E. Fleet, C.T. Herzberg, Omphacite studies; II, Mössbauer spectra of C2/c and P2/n omphacites. Am. Mineral. **63**, 1107–1115 (1978)
216. E. De Grave, A. Van Alboom, S.G. Eeckhout, Electronic and magnetic properties of a natural aegirine as observed from its Mössbauer spectra. Phys. Chem. Miner. **25**, 378–388 (1998)
217. W.R. Nelson, D.T. Griffen, Crystal chemistry of Zn-rich rhodonite ("fowlerite"). Am. Mineral. **90**, 969–983 (2005)
218. D.T. Griffen, W.R. Nelson, Mössbauer spectroscopy of Zn-poor and Zn-rich rhodonite. Am. Mineral. **92**, 1486–1491 (2007)
219. F.A. Seifert, D. Virgo, Kinetics of the Fe^{2+}-Mg, order-disorder reaction in anthophyllites: quantitative cooling rates. Science **188**, 1107–1109 (1975)
220. G.M. Bancroft, R.G. Burns, A.G. Maddock, Determination of cation distribution in the cummingtonite-grunerite series by Mössbauer spectra. Am. Mineral. **52**, 1009–1026 (1967)
221. G.M. Bancroft, A.G. Maddock, Cation distribution in anthophyllite from Mössbauer and infra-red spectroscopy. Nature **212**, 913–915 (1966)
222. M. Schindler, E. Sokolova, Y. Abdu, F.C. Hawthorne, B.W. Evans, K. Ishida, The crystal chemistry of the gedrite-group amphiboles. I. Crystal structure and site populations. Miner. Mag. **72**, 703–730 (2008)
223. F.S. Spears, The gedrite-anthophyllite solvus and the composition limits of orthoamphibole from the Post Pond Volcanics, Vermont. Am. Mineral. **65**, 1103–1118 (1980)
224. A.D. Law, E.J.W. Whittaker, Studies of the orthoamphiboles.1. The Mössbauer and infrared spectra of holmquistite. Bull. Mineral. **104**, 381–386 (1981)
225. R.G. Burns, C. Greaves, Correlations of infrared and Mössbauer site population measurements of actinolites. Am. Mineral. **56**, 2010–2033 (1971)
226. D.S. Goldman, A reevaluation of the Mössbauer spectroscopy of calcic amphiboles. Am. Mineral. **64**, 109–118 (1979)

227. G.M. Bancroft, R.G. Burns, A.J. Stone, Applications of the Mössbauer effect to silicate mineralogy. II. Iron silicates of unknown and complex crystal structures. Geochim. Cosmochim. Acta **32**, 547–559 (1968)
228. G.M. Bancroft, R.G. Burns, Mössbauer and absorption spectral study of alkali amphiboles. Mineral. Soc. Am. Spec. Pap. **2**, 137–148 (1969)
229. D.G. Rancourt, Mössbauer spectroscopy of minerals: I. Inadequacy of Lorentzian-line doublets in fitting spectra arising from quadrupole distributions. Phys. Chem. Miner. **21**, 244–249 (1994)
230. J. De Grave, P. De Paepe, E. De Grave, R. Vochten, S.G. Eeckhout, Mineralogical and Mössbauer spectroscopic study of a diopside occurring in the marbles of Andranondamo, southern Madagascar. Am. Mineral. **87**, 132–141 (2002)
231. A. Van Alboom, E. De Grave, Temperature dependence of the ^{57}Fe Mössbauer parameters in riebeckite. Phys. Chem. Miner. **23**, 377–386 (1996)
232. R.G. Burns, M.D. Dyar, Crystal chemistry and Mössbauer spectra of babingtonite. Am. Mineral. **76**, 892–899 (1991)
233. G. Amthauer, K. Langer, M. Schliestedt, Thermally activated electron delocalization in deerite. Phys. Chem. Miner. **6**, 19–30 (1980)
234. E. Murad, U. Wagner, Mössbauer spectra of kaolinite, halloysite and the firing products of kaolinite: new results and a reappraisal of published work. N. Jb Miner. Abh. **162**, 281–309 (1991)
235. I. Rozenson, E.R. Bauminger, L. Heller-Kallai, Mössbauer spectra of iron in 1:1 phyllosilicates. Am. Mineral. **64**, 893–901 (1979)
236. D.S. O'Hanley, M.D. Dyar, The composition of lizardite 1 T and the formation of magnetite in serpentinite. Am. Mineral. **78**, 391–404 (1993)
237. J.M.D. Coey, A. Moukarika, C.M. McDonagh, Electron hopping in cronstedtite. Solid State Commun. **41**, 797–800 (1982)
238. O. Ballet, J.M.D. Coey, Greenalite—A clay showing two-dimensional magnetic order. J. Phys. **C6**(39), 765–766 (1978)
239. K.J.D. Mackenzie, R.M. Berezowski, Thermal and Mössbauer studies of iron-containing hydrous silicates. V. Berthierine. Thermochimica Acta **74**, 291–312 (1984)
240. J.M.D. Coey, Mössbauer spectroscopy of silicate minerals, in *Mössbauer Spectroscopy Applied to Inorganic Chemistry*, vol. 1, ed. by G.J. Long (Plenum, New York, 1984), pp. 443–509
241. J.H. Johnston, C.M. Cardile, Iron substitution in montmorillonite, illite and glauconite by ^{57}Fe Mössbauer spectroscopy. Clays Clay Miner. **35**, 170–176 (1987)
242. E. Murad, J. Cashion, *Mössbauer spectroscopy of environmental materials and their industrial utilization* (Kluwer, Boston, 2004)
243. E. Murad, U. Wagner, Mössbauer spectrum of illite. Clay Miner. **29**, 1–10 (1994)
244. E. De Grave, J. Vandenbruwaene, E. Elewaut, An ^{57}Fe Mössbauer effect study on glauconites from different locations in Belgium and northern France. Clay Miner. **20**, 171–179 (1985)
245. L.H. Bowen, E. De Grave, D.A. Reid, R.C. Graham, S.B. Edinger, Mössbauer study of a California desert celadonite and its pedogenically-related smectite. Phys. Chem. Miner. **16**, 697–703 (1989)
246. J.M.D. Coey, T. Bakas, S. Guggenheim, Mössbauer spectra of minnesotaite and ferrous talc. Am. Mineral. **76**, 1905–1909 (1991)
247. O. Ballet, J.M.D. Coey, Magnetic properties of sheet silicates; 2:1layer minerals. Phys. Chem. Miner. **8**, 218–229 (1982)
248. C. Blaauw, G. Stroink, W. Leiper, Mössbauer analysis of talc and chlorite. J. Phys. **C141**, 411–412 (1980)
249. M.D. Dyar, R.G. Burns, Mössbauer spectral study of ferriginous one-layer trioctahedral micas. Am. Mineral. **71**, 955–965 (1986)
250. M.D. Dyar, A review of Mössbauer data on trioctahdral micas: Evidence of tetrahedral Fe^{3+} and cation ordering. Am. Mineral. **72**, 102–112 (1987)

251. E. De Grave, J. Vandenbruwaene, M. Van Bockstael, Mössbauer spectroscopic analysis of chlorite. Phys. Chem. Miner. **15**, 173–180 (1987)
252. S.G. Eeckhout, E. De Grave, R. Vochten, N.M. Blaton, Mössbauer effect study of anapaite, $Ca_2Fe^{2+}(PO_4)_2.4H_2O$, and of its oxidation products. Phys. Chem. Minerals **26**, 506–512 (1999)
253. G.M. da Costa, R. Scholz, J. Karfunkel, V. Bermanec, M.L.S.C. Chavez, ^{57}Fe-Mössbauer spectroscopy on natural eosphorite-childrenite-ernstite samples. Phys. Chem. Miner. **31**, 714–720 (2005)
254. R. Vochten, E. De Grave, Mössbauer- and infrared spectroscopic characterization of ferristrunzite from Blaton, Belgium. N. Jb. Miner. Mh. 176–190 (1990)
255. R. Vochten, E. De Grave, K. Van Springel, L. Van Haverbeke, Mineralogical and Mössbauer spectroscopic study of some strunzite varieties of the Silbergrube, Waidhaus, Oberpfalz, Germany. N. Jb. Mineral. Mh. 11–25 (1995)
256. R. Van Tassel, E. De Grave, Ferrostrunzite from Arnsberg, Sauerland, Germany. N. Jb. Miner. Mh. 207–212 (1992)
257. U. Gonser, R.W. Grant, Determination of spin directions and electric field gradient axis in vivianite by polarized recoil-free γ-rays. Phys. Stat. Sol. **21**, 331–342 (1967)
258. J.R. Forsyth, C.E. Johnston, C. Wilkinson, The magnetic structure of vivianite, $Fe_3(PO_4)_2.8H_2O$. J. Phys. C: Solid State Phys. **3**, 1127–1139 (1970)
259. E. De Grave, ^{57}Fe-Mössbauerspectroscopie: fundamentele bijdragen en praktische toepassingen in de fysika, de mineralogie en de technologie. (Thesis Hoger Aggregaat, University of Gent) 1983
260. E. De Grave, R. Vochten, M. Desseyn, D. Chambaere, Analysis of some oxidized vivianites. J. Phys. (Paris) Colloq. **41**, 407–408 (1980)
261. C.A. McCammon, R.G. Burns, The oxidation mechanism of vivianite as studied by Mössbauer spectroscopy. Am. Mineral. **65**, 361–366 (1980)
262. J.L. Dormann, M. Gaspérin, J.F. Poullen, Etude structural de la séquence d'oxydation de la vivianite $Fe_3(PO_4)_2.8H_2O$. Bull. Minér. **105**, 147–160 (1982)
263. L. Aldon, A. Perea, M. Womes, C.M. Ionica-Bousquet, J.-C. Jumas, Determination of the Lamb-Mössbauer fractions of of $LiFePO_4$ and $FePO_4$ for electrochemical in situ and operando measurements in Li-ion batteries. J. Solid State Chem. **183**, 218–222 (2010)
264. A. Van Alboom, E. De Grave, M. Wolfahrt-Mehrens, Temperature dependence of the Fe^{2+} Mössbauer parameters in triphylite ($LiFePO_4$). Am. Mineral. **96**, 408–416 (2011)
265. A. Yamada, S. Chung, Crystal chemistry of the olivine-type $Li(Mn_yFe_{1-y})PO_4$ and $(Mn_yFe_{1-y})PO_4$ as possible 4 V cathode materials for lithium batteries. J. Electrochem. Soc. **148**, A960–A967 (2001)
266. T.H. Fehr, R. Hochleitner, A. Laumann, E. Schmidbauer, J. Schneider, Mineralogy, Mössbauer spectroscopy and electrical conductivity of heterosite $(Fe^{3+},Mn^{3+})PO_4$. Phys. Chem. Miner. **37**, 179–189 (2010)
267. V.G. de Resende, G.M. da Costa, E. De Grave, A. Van Alboom, Mössbauer spectroscopic study of synthetic leucophosphite, $KFe_2(PO_4)_2(OH).2H_2O$. Am. Mineral. **93**, 483–498 (2008)
268. G. Le Caër, J.M. Dubois, H. Fisher, U. Gonser, H.G. Wagner, On the validity of ^{57}Fe hyperfine field distribution calculations from Mössbauer spectra of magnetic amorphous alloys. Nucl. Instrum. Meth. Phys. Res. B **5**, 25–33 (1984)
269. R.E. Vandenberghe, E. Van Ranst, E. De Grave, Mössbauer study of a South African Griffin Farmhill soil profile. ICAME 2005, Montpellier, Book of Abstracts (2005)
270. E. Van Ranst, M. Dumon, A.R. Tolossa, J-Th Cornelis, G. Stoops, R.E. Vandenberghe, R.J. Deckers, Revisiting ferrolysis processes in the formation of Planosols for rationalizing the soils with stagnic properties in WRB. Geoderma **163**, 265–274 (2011)
271. E. Banks, E. Kostiner, G.K. Wertheim, Mössbauer effect in $MnFeO_3$. J. Chem. Phys. **45**, 1189–1191 (1966)
272. S.N. de Medeiros, A. Luciano, L.F. Cótica, I.A. Santos, A. Paesano Jr, J.B.M. da Cunha, Structural and magnetic characterization of the ball-milled α-Fe_2O_3 –Mn_2O_3 and α-Fe–Mn_2O_3 systems. J. Magn. Magn. Mater. **281**, 227–233 (2004)

273. J.M. Han, J.J. Hus, R. Paepe, R.E. Vandenberghe, T.S. Liu, The rock magnetic properties of the Malan and Lishi formations in the loess plateau of China, in *Loess, Environment and Global Change*, ed. by Liu Tungsheng (Science Press, Beijing, 1991), pp. 30–47
274. R.E. Vandenberghe, E. De Grave, J.J. Hus, J. Han, Characterization of Chinese loess and associated palaeosol by Mössbauer spectroscopy. Hyp. Interact. **70**, 977–980 (1992)
275. R.E. Vandenberghe, J.J. Hus, E. De Grave, Evidence from Mössbauer spectroscopy of neo-formation of magnetite/maghemite in the soils of loess/palaeosol sequences in China. Hyp. Interact. **117**, 359–369 (1998)
276. R.C. Mercader, F.R. Sives, P.A. Imbellone, R.E. Vandenberghe, Magnetic and Mössbauer studies of quaternary Argentine loessic soils and paleosols. Hyp. Interact. **161**, 43–53 (2005)
277. C. Algoe, G. Stoops, R.E. Vandenberghe, E. Van Ranst, Selective dissolution of Fe-Ti oxides—Extractable iron as a criterion for andic properties revisited. Catena **92**, 49–54 (2011)
278. E. De Grave, G.M. Da Costa, L.H. Bowen, C.A. Barrero, R.E. Vandenberghe, Characterization of soil-related analogs by applied-field ^{57}Mössbauer spectroscopy. Hyp. Interact. **117**, 245–270 (1998)
279. R.B. Scorzelli, Application of the Mössbauer effect to the study of meteorites—A review. Hyp. Interact. **66**, 249–257 (1991)
280. R.B. Scorzelli, Meteorites: Messengers from the outer space. J. Braz. Chem. Soc. **19**, 226–231 (2008)
281. J. Danon, R.B. Scorzelli, I. Souza-Azevedo, J. Laugier, A. Chamberod, Santa Catharina meteorite and phase composition of irradiated Fe–Ni Invar alloys. Nature **284**, 537–538 (1980)
282. R.B. Scorzelli, I.S. Azevedo, J. Danon, M.A. Meyers, Mössbauer study of shock-induced effects in the ordered alloy $Fe_{50}Ni_{50}$ in meteorites. J. Phys. F. Met. Phys. **17**, 1993–1997 (1987)
283. R.B. Scorzelli, J. Danon, Mössbauer spectroscopy and X-ray diffraction studies of Fe–Ni order-disorder processes in a 35 % Ni meteorite (Santa Catharina). Phys. Scr. **32**, 143–148 (1985)
284. E. De Grave, R.E. Vandenberghe, P.M.A. De Bakker, A. Van Alboom, R. Vochten, R. Van Tassel, Temperature dependence of the Mössbauer parameters of the FeNi phases in the Santha Catharina meteorite. Hyp. Interact. **70**, 1009–1012 (1992)
285. E. De Grave, R.J. Pollard, R.E. Vandenberghe, P.M.A. De Bakker, The effect of high external magnetic fields on the hyperfine interactions in the Fe-Ni phases of the Santa Catharina meteorite. Hyp. Interact. **94**, 2349–2353 (1992)
286. D.G. Rancourt, R.B. Scorzelli, Low spin γ-Fe-Ni (γLS) proposed as a new mineral in Fe-Ni-bearing meteorites: epitaxial intergrowth of γLS and tetrataenite as possible equilibrium state at $\sim$20–40 at % Ni. J. Magn. Magn. Mat. **150**, 30–36 (1995)
287. C.L. Herzenberg, D.L. Riley, Mössbauer spectrometry of lunar samples. Science **167**, 683–686 (1970)
288. P. Gay, G.M. Bancroft, M.G. Bown, Diffraction and Mössbauer studies of minerals from lunar soils and rocks. Science **167**, 626–628 (1970)
289. J. Duchesne, J. Depireux, A. Gérard, F. Grandjean, M. Read, Study with Mössbauer spectrometry on iron distribution in mineralogical fractions separated by lunar rocks reported by Apollo-12. Bull. Cl. Sci. Acad. R. Belg. **57**, 1204–1211 (1971)
290. T.C. Gibb, R. Greatrex, N.N. Greenwood, An assessment of results obtained from Mössbauer spectra of lunar samples. Phil. Trans. R. Soc. Lond. A **285**, 235–240 (1977)
291. R.V. Morris, G. Klingelhöfer, R.L. Korotev, T.D. Shelfer, Mössbauer mineralogy on the Moon: The lunar regolith. Hyp. Interact. **117**, 405–432 (1998)
292. G. Klingelhöfer, In situ analysis of planetary surfaces by Mössbauer spectroscopy. Hyp. Interact. **113**, 369–374 (1998)
293. G. Klingelhöfer, R.V. Morris, B. Bernhardt, D. Rodionov, P.A. de Souza, S.W. Squyres, J. Foh, E. Kankeleit, R. Gellert, C. Schröder, S. Linkin, E. Evlanov, B. Zubkov, O. Prilutski, Athena MIMOS II Mössbauer spectrometer investigation. J. Geophys. Res. Planets **108**, 8067 (2003)

294. R.V. Morris, G. Klingelhöfer, B. Bernhardt, C. Schröder, D.S. Rodionov, P.A. De Souza Jr, A. Yen, R. Gellert, E.N. Evlanov, J. Foh, E. Kankeleit, P. Gütlich, D.W. Ming, F. Renz, T. Wdowiak, S.W. Squyres, R.E. Arvidson, Mineralogy at Gusev Crater from the Mössbauer spectrometer on the Spirit Rover. Science **305**, 833–836 (2004)
295. R.V. Morris, G. Klingelhöfer, C. Schröder, D.S. Rodionov, A. Yen, D.W. Ming, P.A. De Souza Jr, I. Fleischer, T. Wdowiak, R. Gellert, B. Bernhardt, E.N. Evlanov, B. Zubkov, J. Foh, E. Kankeleit, U. Bonnes, P. Gütlich, F. Renz, S.W. Squyres, R.E. Arvidson, Mössbauer mineralogy of rock, soil, and dust at Gusev Crater, Mars: Spirit's journey through weakly altered olivine basalt on the Plains and pervasively altered basalt in the Columbia Hills. J. Geophys. Res. **111**, E02S13 (2006)
296. R.V. Morris, G. Klingelhöfer, C. Schröder, D.S. Rodionov, A. Yen, D.W. Ming, P.A. De Souza Jr, T. Wdowiak, I. Fleischer, R. Gellert, B. Bernhardt, U. Bonnes, B.A. Cohen, E.N. Evlanov, J. Foh, P. Gütlich, E. Kankeleit, T. McCoy, D.W. Mittlefehldt, F. Renz, M.E. Schmidt, B. Zubkov, S.W. Squyres, R.E. Arvidson, Mössbauer mineralogy of rock, soil, and dust at Meridiani Planum, Mars: Opportunity's journey across sulfate-rich outcrop, basaltic sand and dust, and hematite lag deposits. J. Geophys. Res. **111**, E12S15 (2006)
297. G. Klingelhöfer, R.V. Morris, B. Bernhardt, C. Schröder, D.S. Rodionov, P.A. de Souza, A. Yen, R. Gellert, E.N. Evlanov, E. Kankeleit, P. Gütlich, D.W. Ming, F. Renz, T. Wdowiak, S.W. Squyres, R.E. Arvidson, Jarosite and hematite at Meridiani Planum from Opportunity's Mössbauer spectrometer. Science **306**, 1740–1745 (2004)
298. G. Klingelhöfer, E. De Grave, R.V. Morris, A. Van Alboom, V.G. de Resende, P.A. De Souza, D. Rodionov, C. Schröder, D.W. Ming, A. Yen, Mössbauer spectroscopy on Mars: goethite in the Columbia Hills at Gusev crater. Hyp. Interact. **166**, 549–554 (2006)
299. C. Van Cromphaut, V.G. de Resende, E. De Grave, A. van Alboom, R.E. Vandenberghe, G. Klingelhöfer, Characterisation of the magnetic iron phases in Clovis Class rocks in Gusev crater from the MER Spirit Mössbauer spectrometer. Geochim. Cosmochim. Acta **71**, 4814–4822 (2007)
300. C. Van Cromphaut, V.G. de Resende, E. De Grave, R.E. Vandenberghe, Temperature dependence of the hyperfine parameters of the iron bearing phases in the Mössbauer spectra collected by the Mars Exploration Rover Spirit. Hyp. Interact. **190**, 143–148 (2009)
301. D.G. Agresti, I. Fleischer, G. Klingelhöfer, R.V. Morris, On simfitting MER Mössbauer data to characterize Martian hematite. J. Phys. Conf. Ser. **217**, 012063 (2010)
302. C. Schröder, D.S. Rodionov, T.J. McCoy, B.L. Jolliff, R. Gellert, L.R. Nittler, W.H. Farrand, J.R. Johnson, S.W. Ruff, J.W. Ashley, D.W. Mittlefehldt, K.E. Herkenhoff, I. Fleischer, A.F.S. Haldemann, G. Klingelhöfer, D.W. Ming, R.V. Morris, P.A. De Souza Jr, S.W. Squyres, C. Weitz, A.S. Yen, J. Zipfel, T. Economou, Meteorites on Mars observed with the Mars Exploration Rovers. J. Geophys. Res. **113**, 06 (2007)
303. D. Rodionov, C. Schröder, G. Klingelhöfer, R.V. Morris, T. Wdowiak, P.A. de Souza Jr, A. Yen, T. Wdowiak, S.W. Squyres, And the Athena Science Team: Mössbauer investigation of "Bounce Rock" at Meridiani Planum on Mars—Indications for the first shergottite on Mars. Meteorit. Planet. Sci. **39**, A91 (2004)
304. C. Schröder, R. Gellert, B.L. Jolliff, G. Klingelhöfer, T.J. McCoy, R.V. Morris, D.S. Rodionov, P.A. De Souza Jr, A.S. Yen, J. Zipfel, And the Athena Science team: A stony meteorite discovered by the Mars Exploration Rover Opportunity on Meridiani Planum. Mars. Meteorit. Planet. Sci. **41**, 5285 (2006)
305. M. Blumers, B. Bernhardt, P. Lechner, G. Klingelhöfer, C. d'Uston, H. Soltau, L. Strüder, R. Eckhardt, J. Brückner, H. Henkel, J.G. Lopez, J. Maul, The miniaturized Mössbauer spectrometer MIMOS IIA: Increased sensitivity and new capability for elemental analysis. Nucl. Instrum. Methods: Phys. Res. A **624**, 277–281 (2010)
306. D. Chambaere, Studie van de strukturele en magnetische eigenschappen van β-FeOOH en van zijn fasetransformatie naar αFe_2O_3. Ph.D. thesis, (Ghent University, 1983)
307. B.J. Evans, R.G. Johnson, F.E. Senftle, C.B. Cecil, F. Dulong, The ^{57}Fe Mössbauer parameters of pyrite and marcasite with different provenances. Geochim. Cosmochim. Acta **46**, 761–775 (1982)

308. S.G. Eeckhout, C. Casteñeda, A.C.M. Ferreira, A. Sabioni, E. De Grave, D.C.L. Vasconcelos, Spectroscopic studies of spessartine from Brazilian pegmatites. Am. Mineral. **87**, 1297–1306 (2002)
309. E. De Grave, S. Geets, ^{57} Fe Mössbauermetingen aan Belgische Glauconieten. Bull. Soc. Belge Géol. **88**, 237–251 (1979)
310. E. De Grave, A. Van Alboom, Evaluation of ferrous and ferric Mössbauer fractions. Phys. Chem. Miner. **18**, 337–342 (1991)
311. W. Stiers, U. Schwertmann, Evidence for manganese substitution in synthetic goethite. Geochim. Cosmochim. Acta **49**, 1909–1911 (1985)
312. D.J. Vaughan, M.S. Ridout, Mössbauer study of pyrrhotite (Fe_7S_8). Solid State Commun. **8**, 2165–2167 (1970)
313. H.V. Varma, J. Varma, Mössbauer effect study of natural staurolite. Phys. Stat. Solidi (a) **97**, 275–278 (1986)
314. F. Seifert, A note on the Mössbauer spectrum of ^{57}Fe in ferrocarpholite. Mineral. Mag. **43**, 313–315 (1979)
315. Y. Fuchs, M. Mellini, I. Memmi, Crystal-chemistry of magnesiocarpholite: controversial X-ray diffraction, Mössbauer, FTIR and Raman results. Eur. J. Mineral. **13**, 533–543 (2001)
316. L.G. Dainyak, V.A. Drits, Interpretation of the Mössbauer spectra of nontronite, celadonite and glauconite. Clays Clay Miner. **35**, 363–372 (1987)
317. H. Kodoma, G. Longworth, M.G. Townsend, A Mössbauer investigation of some chlorites and their oxidation products. Can. Mineral. **20**, 585–590 (1982)
318. D.G. Agresti, M.D. Dyar, M.W. Schaefer, Velocity calibration for in situ Mössbauer data from Mars. Hyp. Interact. **167**, 845–850 (2006)
319. C. Van Cromphaut, V.G. de Resende, E. De Grave, R.E. Vandenberghe, Mössbauer study of Meridiani Planum, the first iron-nickel meteorite found on the surface of Mars by the MER Opportunity. Meteorit. Planet. Sci. **42**, 2119–2123 (2007)

Author Biographies

Robert E. Vandenberghe Robert Vandenberghe (°1945) is Professor Emeritus at the Department of Physics and Astronomy (formerly Subatomic and Radiation Physics) of the Ghent University in Belgium. As an experimental physicist, his research started in the field of structural and magnetic properties of magnetic oxides using magnetic measurements and neutron diffraction. At the end of the seventies of the former century, he began to perform Mössbauer spectroscopy on nanoferrite systems. Using this technique, he further investigated a large variety of materials in which his interest was often focused on the methodology of Mössbauer spectral analysis. All the work was based on ^{57}Fe MS, but, he made some studies of magnetic materials using ^{61}Ni Mössbauer spectroscopy as well.

During the nineties he continued with fundamental studies on goethite and hematite. His application of Mössbauer spectroscopy went particularly to the characterization of Fe-bearing compounds in soils and sediments. In that respect, he cooperated with many laboratories of geology and soil sciences. His is author or co-author of more than 150 papers and several chapters in books. He was several times invited as plenary speaker at international conferences.

Eddy De Grave Eddy De Grave (°1951) is Professor at the Department of Physics and Astronomy (formerly Subatomic and Radiation Physics) of the Ghent University in Belgium. He was the first researcher doing Mössbauer spectroscopy at Ghent University in 1972. His PhD treated an ^{57}Fe MS study magnesium titanoferrites for which he stayed for several months in Marburg (Germany) with Prof. S. Hafner in order to perform external-field measurements. Apart from the study of magnetic oxides, he further dedicated a considerable time to the fundamental study soil-related oxides and oxyhydroxides, together with the late Prof. L. Bowen of the North Carolina State University (USA), were he stayed for one year and subsequently several times for a few months. He also cooperated with Dr. Chr. Laurent from the Paul Sabatier University in Toulouse (France) in relation with MS studies on the precursor materials in the synthesis of carbon nanotubes. However, the main connecting thread in his work is undoubtedly the Mössbauer study of a large amount of minerals in which phosphate-based minerals take a great part. In recognition of his significant contributions in the field of mineralogy, he was elected in 2006 "A Fellow" the Mineralogical Society of America. Eddy De Grave is author or co-author of more than 250 papers and several chapters in books.

As a consequence of their experience in magnetic oxides and soil materials, both authors were invited to write a chapter about "Mössbauer effect studies of oxidic spinels" in the series Mössbauer Spectroscopy Applied to Inorganic Chemistry, edited by G. Long and F. Grandjean, and together with H. Bowen about "Mössbauer effect studies of magnetic soils and sediments" in the series Mössbauer Spectroscopy Applied to Magnetism and Materials Science, also edited by G. Long and F. Grandjean.

Our message to the next generation is: *It will still give you great scientific possibilities when you, as a Mössbauer spectroscopist, cooperate with laboratories related to earth sciences, and have an eye for reliable spectral analyses*.